IMPLEMENTATION OF WIND ENERGY SYSTEMS TO THE EXISTING POWER GRID

A Thesis

Presented to

the Faculty of the Department of Electrical and Computer Engineering

University of Houston

In Partial Fulfillment

of the Requirements for the Degree

Master of Science

in Electrical Engineering

by

Jalaja Gogineni

May 2012

I would like to dedicate this work to my wonderful parents, brother, husband and adviser.

ACKNOWLEDGEMENTS

First of all, I would like to sincerely thank my advisor, Dr.Ovidiu Crisan for his remarkable guidance, constant support and valuable time throughout my Masters program at the University of Houston. The completion of this thesis work would not have been possible without his efforts and encouragement, and I will always be thankful to him for that. Working with him has been a great learning experience and it is something I will cherish for life.

I would also like to thank Dr. Leang-San Shieh and Dr. Richard B. Bannerot for agreeing to serve on my thesis committee and their suggestions and valuable time spent in reviewing this document. And also, would like to thank Mr. Robert Spiewak, Lecturer, University of Houston for the ideas discussed and help with the research material.

I finally thank all my family members in India and my husband, for their moral support, because without them this would not have happened. I would also like to thank all my friends in the U.S and back in India for being supportive and helpful in every way possible.

IMPLEMENTATION OF WIND ENERGY SYSTEMS TO THE EXISTING POWER GRID

An Abstract

of a

Thesis

Presented to

the Faculty of the Department of Electrical and Computer Engineering

University of Houston

In Partial Fulfillment

of the Requirements for the Degree

Master of Science

in Electrical Engineering

by

Jalaja Gogineni

May 2012

ABSTRACT

Steady state and transient analysis of a Doubly Fed Induction Generator (DFIG) belonging to a Wind Power Generator is performed. Firstly, the steady state model of the DFIG is derived, and based on the DFIG characteristics, its steady state operating condition is determined. Also, the control strategies that determine the gating signals to the Back to Back Converter (BBC) are described. Secondly, the transient model of the DFIG is derived, and its transient characteristics are analyzed and simulated for a three phase metallic fault. The results of the transient analysis are obtained using both the analytical model and DFIG wind turbine model in Matlab/Simulink software. The study shows the significance of protecting the Back to Back converter during the occurrence of a fault.

TABLE OF CONTENTS

LIST OF FIGURES

LIST OF TABLES

CHAPTER 1

Introduction

1.1. Need for Renewable Energy

It is known that the primary sources of energy, namely coal, petroleum and natural gas that are currently being used for power generation all over the world are not sustainable, i.e., these resources across the globe will perish within a finite amount of time and cannot be replaced. Thus there is a clear need for alternative resources that not only meet the rise in energy consumption but also are renewable, i.e., can be replaced by natural processes with the passage of time. Solar radiation, wind, tides, geothermal and biomass are a few of these resources. Also the environmental impacts associated with the conventional energy production - global climate change, acid rain, large fresh water usage, hazardous air pollution and radioactive waste - can be reduced with the effective usage of renewable energy resources. The renewable energy utilization also helps to create local jobs and plays a key role in improving the nation's energy security by providing a distributed and diversified energy infrastructure.

1.2. Statistics of the U.S. Total and Renewable Energy Consumption

U.S. statistics show that in 2010 the renewable energy sources provided 8% of the nation's energy consumption (Figure 1.1), and by 2030 it is expected to provide about 14% of it (Figure 1.2) [1].

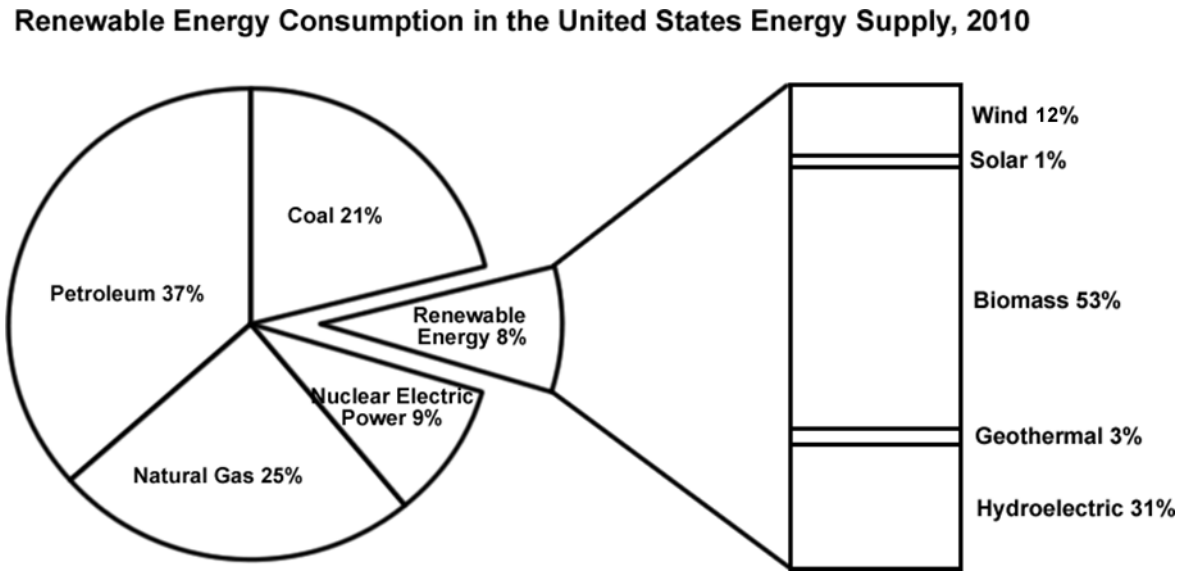

Figure 1.1. United States Total and Renewable Energy Consumption in 2010 [1]

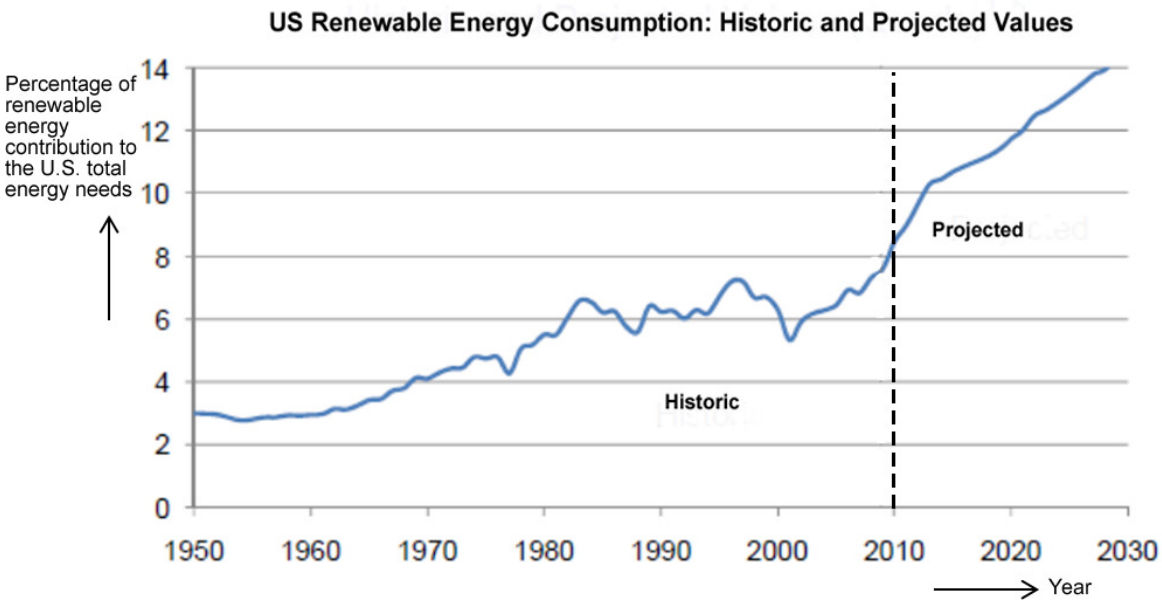

Figure 1.2. Historic and Projected Percentage Values of Renewable Energy Contribution to the U.S. Total Energy Needs [1]

1.3. Types of Renewable Energy

1.3.1. Solar Energy

Photovoltaic (PV) or solar energy is harnessing the sun's energy to produce electricity directly. Solar energy initially has been used to power small and medium-sized applications, from the calculator powered by a single solar cell to off-grid homes powered by photovoltaic arrays. Solar cells are becoming more efficient, transportable and flexible allowing for easy installation. The main drawback of solar energy is the cost of the equipment required to convert the direct current output to an alternating current for use in a house. Electricity generated from solar cells is still more than twice as expensive as electricity from fossil fuels. Solar PV modules produce no emissions during operation, but toxic substances, e.g., cadmium and arsenic, are used in their manufacture.

From Figure 1.1, it is seen that in 2010 solar energy accounted for 1% of the total U.S. renewable energy consumption. Even though there was a 50% increase in solar energy since 2000, it still accounts for only 0.08% of the U.S. total energy consumption. The sunny state of California is the leading U.S state in installed solar energy with a capacity of over 500 |MW|. It also houses the largest solar power plant in the world, namely the 354 |MW| SEGS thermal power plant [2].

1.3.2. Hydroelectric Energy

Hydroelectricity uses the gravitational force of falling or flowing water for power generation. Small scale hydro energy has been an increasingly popular alternative energy source, especially in remote areas where other energy sources are not viable. While electricity generated from hydropower is virtually emission free, biological plants that are flooded by the dam water emit methane and CO_2 at a level that some have claimed causes more damage than a conventional power plant [2]. Other environmental concerns include

fish injury and mortality, habitat degradation, and water quality impairment. “Fish-friendly” turbines and smaller dams help mitigate some of these problems. Besides generating electricity, hydroelectric energy has some important benefits in irrigation, recreation, and water supply.

From Figure 1.1, it is seen that in 2010, hydroelectric energy accounted for 31% of the U.S. total renewable energy consumption, i.e., 2.5% of the U.S. total energy consumption. Net electricity generation from hydro-energy peaked in 1997 at 356 billion kWh, and then steadily declined through 2001, thereafter being relatively stable. In 2009 the hydroelectricity generation was 272 billion kWh, 24% lower than in 1997 [2]. For the next 25 years the hydroelectric generation is projected to stabilize at just less than 300 billion kWh per year.

1.3.3. Wind Energy

Wind energy is the conversion of kinetic energy in the wind by wind turbines into electrical energy. Wind energy does not produce CO_2 or greenhouse gases and hence is considered clean. A Wind turbine once installed, can start producing energy very quickly compared to the conventional energy systems. Wind energy has proved that it can compete on price with conventional energy systems of oil and gas. But, there are a few environmental and social concerns such as bat and bird kills, noise pollution and aesthetics associated with the usage of wind energy. Recently, the noise problem has mostly been eliminated through improved engineering.

From Figure 1.1, it is seen that in 2010 wind energy accounted for only 12% the U.S. total renewable energy consumption, i.e., less than 1% of the U.S. total energy consumption. Areas with good wind resources have the capability to supply up to 20% of U.S. electricity consumption. Based on the average U.S. utility fuel mix, a 1 |MW| wind turbine annually

displaces 1800 tons of CO_2 emissions [2]. In 2010, the emission of nearly 44 million tons of CO_2 was avoided.

By 2030, the estimate of the total wind energy installed capacity in the U.S. is projected to be 300 |GW|, and if achieved would avoid 800 million metric tons of CO_2 emissions annually. This target is achievable due to the availability of good wind resources in the U.S.

1.3.4. Geothermal Energy

Geothermal plants use hydrothermal fluids, e.g., hot water or steam from underground to produce heat or electricity. There are three geothermal technologies currently in use in the U.S: the direct-use system, deep reservoirs, and geothermal heat pumps. Hydrothermal resources are available only in the western U.S., Alaska and Hawaii. Heat pumps are to be used at other places to extract the heat from the soil or air. Geothermal electricity currently displaces 4.1 million metric tons of CO_2 per year [2]. Few byproducts of geothermal plants can be recovered and recycled, but others produce solid waste such as salts and minerals that must be disposed of in approved sites.

The United States is the world leader in both installed capacity and generating electricity from geothermal energy. The largest group of geothermal power plants in the world is located at The Geysers, a geothermal field in California. As seen in Figure 1.1, 2010 geothermal energy provided 3% of the U.S. total renewable energy consumption that represents 0.24% of the U.S. total energy consumption. Electricity generated from geothermal power plants is expected to increase from 17 billion kWh in 2008 to 26 billion kWh in 2030 [2].

1.3.5. Biomass Energy

Biomass energy is the energy obtained from plants and plant-derived materials such as food crops, grassy and woody plants, residues from agricultures or forestry, and the organic

component of municipal and industrial wastes. Biomass energy is also considered as a vital part of the U.S waste management infrastructure. Biomass energy has low net CO_2 emissions. It only releases the CO_2 it previously removed from the atmosphere, plus emissions from processing. But it requires 124 acres of land to generate one GWh of energy per year. Currently, the New Hope Energy Partnership located in Florida is the largest biomass power plant in North America. This facility reduces dependence on oil by more than one million barrels per year.

As seen in Figure 1.1, biomass energy contributes to about 53% of the U.S. total renewable energy consumption, i.e., 4.24% of the U.S. total energy consumption. Ethanol production is expected to reach 1.82 million gallons per day by 2035.

1.4. Comparison of Environmental Impacts of Different Renewable Energy Sources

A study conducted by Mark Z. Jacobson reviews and ranks major proposed energy-related solutions to global warming, air pollution mortality, and energy security, while considering other impacts of the proposed solutions, such as on water supply, land use, wildlife, resource availability, thermal pollution, water chemical pollution, nuclear proliferation, and under nutrition [3]. Nine different energy sources and two liquid fuel options were considered. The energy sources include solar-photovoltaic (PV), concentrated solar power (CSP), wind, geothermal, hydroelectric, wave, tidal, nuclear, and coal with carbon capture, and storage (CCS) technology. The liquid fuel options include corn-ethanol (E85) and cellulosic-E85. In order to compare the energy sources and liquid fuel options on a common base, they were assumed to be used to power Electric Battery Vehicles (BEVs), hydrogen fuel cell vehicles (HFCVs). Flex-fuel vehicles run on E85. Twelve different energy source-vehicle options were considered, weighed and compared based on eleven impact categories.

Few of the eleven impact categories that were considered individually are C02 equivalent emissions, air pollution mortality, footprint on ground, water consumption, effects on wildlife, and operating reliability. Figure 1.3 shows the ranking of the renewable energy source – vehicle options based on their environmental impact. As seen in Figure 1.3, wind-BEVs were ranked first, which implies that wind energy has the lowest environmental impact of all the energy sources. Hence, a lot of research is going on to implement the wind energy to the fullest extent.

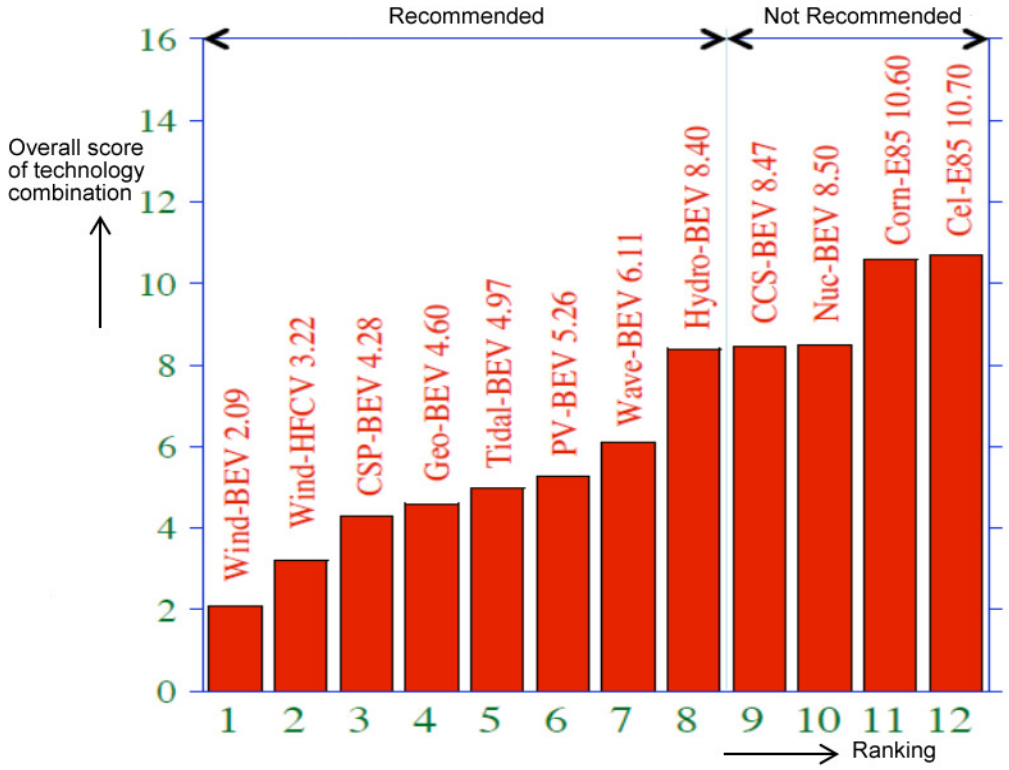

Figure 1.3. Ranking of Different Renewable Energies [3]

1.5. Wind Energy in the US

At the end of 2010, the worldwide nameplate capacity of wind-powered generators was around 197 |GW|, which was about 2.5% of the world wide electricity usage, and it has grown rapidly, having doubled in three years between 2005 and 2008. By the end of December 2010 the total installed wind power capacity in the United States was 40,180

|MW|, making it second in the world behind China [4]. States like Texas, Iowa and California are the main reason why the United States is the global leader, with just over 35,000 megawatts |MW| of installed wind power capacity. Texas is also the home to the world's largest wind farm, namely the Roscoe Wind Farm, with a capacity of 780 |MW|. Appendix A shows the total installed wind capacity across the United States by the end of the year 2010 [5].

1.6. Wind Turbines

A wind turbine is a device that converts the kinetic energy of the wind into mechanical energy. If the mechanical energy is used to produce electricity, the device may be called a wind generator or wind charger. If the mechanical energy is used to drive machinery, such as for grinding grain or pumping water, the device is called a windmill or wind pump.

1.6.1. Components of a Wind Turbine

The wind turbine consists of many components and some of the basic components shown on Figure 1.4 are briefly described below [6].

Tower: The tower on which the wind turbine is mounted is not only a support structure, but also raises the wind turbine to a height that its blades safely clear the ground and also helps to reach for stronger winds that are available at higher elevations. The tower height can be optimized based on the cost of taller towers versus the increase in energy production resulting from their use. Large wind turbines are usually mounted on towers ranging from 40 to 70 meters tall.

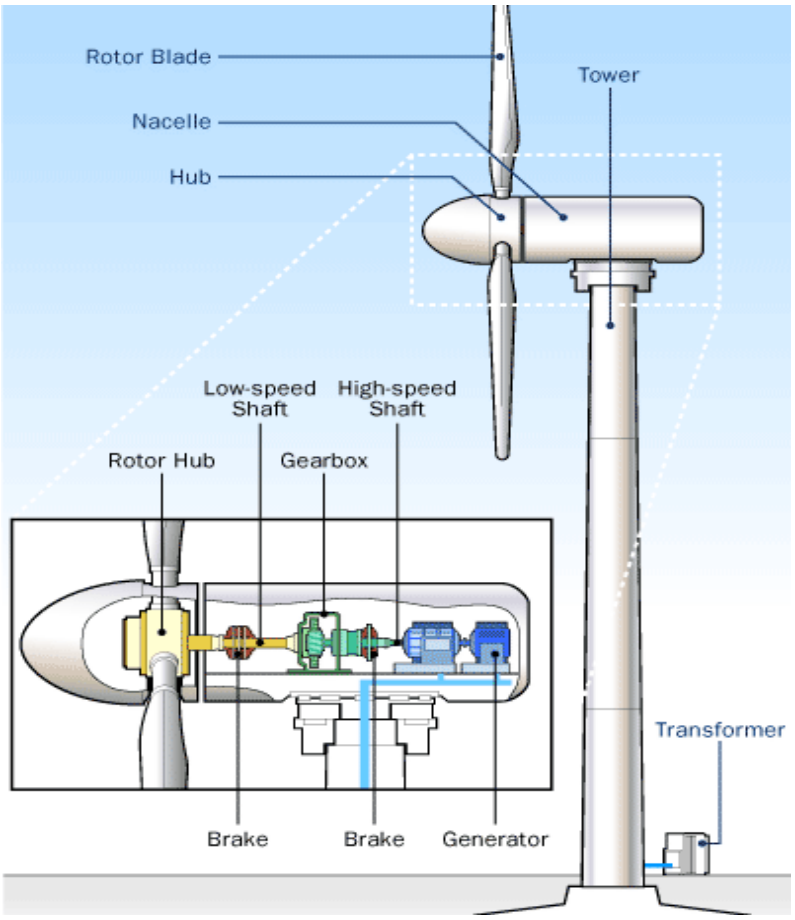

Figure 1.4. Basic Components of a Wind Turbine [6]

Rotor: The rotor is the portion of the wind turbine that collects the energy from the wind. The rotor usually consists of two or more wooden, fiber glass or metal blades which rotate around an axis at a rate determined by the wind speed and shape of the blades. These rotor blades are attached to the hub, which in turn is attached to the main shaft.

Nacelle: The nacelle houses the main shaft which consists of low-speed shaft, gearbox, brakes, high-speed shaft and electrical generator.

Transformers and cables are used to transfer the generated electric energy to the substation for distribution purposes.

1.6.2. Wind Turbine Energy Generation Principle

As mentioned, a wind generator uses the power of wind to drive an electrical generator. Wind passes over the blades, generating lift and exerting a turning force. The rotating blades turn the shaft inside the nacelle, which goes into a gearbox. The gearbox increases the rotational speed so that it is appropriate for the electrical generator, which uses magnetic fields to convert the rotational energy into electrical energy. The electric power output goes to a transformer, which converts the electricity from the generator terminal voltage at around 1000 |V| to the appropriate voltage for the power collection system, typically 33 |KV|.

The power in the airflow is given by [7]

$$P_{air} = \frac{1}{2} \rho \pi r^2 V^3, \quad (1.1)$$

where

P_{air} = Output power |watts|,

r = Radius of the wind turbine rotor |m|,

V = Velocity of wind |m/s|, and

ρ = Density of air |kg/m^3|.

Equation (1.1) gives the power available in the wind, but the power transferred to the wind turbine rotor is reduced by the power coefficient C_P, defined as

$C_P = \frac{P_{windturbine}}{P_{air}}$ = Coefficient of performance.

A maximum value of C_P is defined by the Betz limit, which states that a wind turbine can never extract more than 59.3% of the power from an air stream. Practically, wind turbine rotors have maximum C_P values in the range of 25-45% [7].

1.6.3. Wind Turbine Power Curve

The power output of a wind turbine at various wind speeds is described by its power curve. Power curves of existing wind turbines are normally obtained from the turbine manufacturer. Figure 1.5 shows an example of a power curve of Vestas V90 wind turbine. As seen in Figure 1.5, the power curve has three key points:

1) Cut-in speed – the minimum speed at which the machine will deliver useful power
2) Rated wind speed – the wind speed at which rated power (maximum output power) is obtained
3) Cut-out speed – the maximum wind speed at which the turbine is allowed to deliver power.

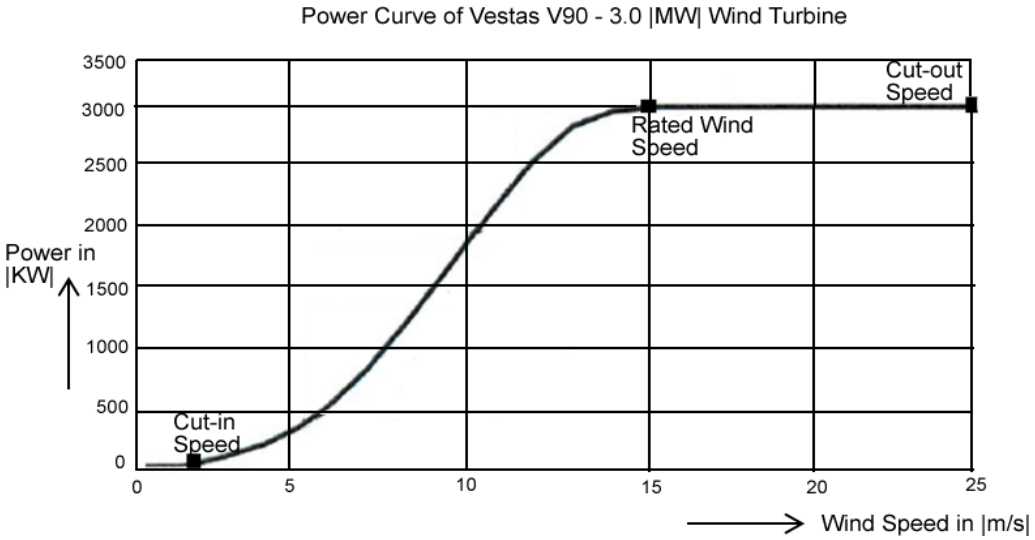

Figure 1.5. Vestas V90 Power Curve [8]

Below the cut-in speed, the wind turbine remains shut down as the wind speed is too low for useful energy production. Then once in operation, the power output increases following a cubic relation with wind speed (as in equation 1.1) until rated wind speed is reached. Above the rated wind speed, the aerodynamic rotor is arranged to limit the mechanical power extracted from the wind. At very high wind speeds the wind turbine will be shut down.

1.7. Classification of Wind Turbines

1.7.1. Based on Axis of Rotation

Wind turbines can rotate around a horizontal or a vertical axis and are classified as such.

Horizontal Axis Wind Turbine

Horizontal axis wind turbines (HAWT) have the main rotor shaft and the electrical generator installed on the top of the tower and must be pointed into the wind. The turbine should be positioned upwind of its supporting tower as the tower produces turbulence behind it [9]. Turbine blades are made stiff to prevent the blades from being pushed into the tower by high winds.

Vertical Axis Wind Turbine

Vertical axis wind turbines (VAWT) have the main rotor shaft arranged vertically. This type of wind turbine need not be pointed into the wind to be effective and its advantageous on sites where wind is highly variable. The electrical generator and gearbox can be placed near the ground which improves the accessibility for maintenance. VAWT can capture the wind from all directions and at a lower wind speeds than HAWT. VAWT have low rotational speed, and require high cost of the drive train. In VAWT, it is difficult to model the wind flow accurately due to the 360 degree rotation of the aero foil. It would be challenging to analyze and design the rotor prior to fabrication, due to high dynamic loading on the blade.

1.7.2. Based on Rating

Based on the rating, wind turbines are classified as 1) utility scale – corresponds to large turbines (900 |kW| and above) that generate bulk power for sale in the power markets, 2) industrial scale - corresponds to medium sized turbines (50 |kW| - 250 |kW|) intended for remote grid operation, and 3) residential scale – corresponds to micro and small turbines (400W – 50kW) intended for remote power, battery charging, or net metering type

generation [10]. Utility scale electric power is generated from the so classically called "wind farm", that consists of a group of wind turbines of which electrical outputs are connected together and cover an area of hundreds of square miles. The resulting output power is connected to the grid.

1.7.3. Based on the type of Electrical Generator used

There are different types of electrical generators that can be used with a wind turbine to convert the available mechanical energy on the low-speed shaft into electrical energy. Based on this, wind turbines can be classified as fixed-speed and variable-speed wind turbines. Based on the type of the electrical generator used, different control schemes are implemented to produce grid-quality electricity. Every control scheme has its own advantages and disadvantages [11]. Below are shown a few different configurations and their control schemes used for the wind power generation.

1.7.3.1. Fixed-Speed Wind Turbine

Figure 1.6 illustrates the configuration of a fixed-speed wind turbine. It consists of a Squirrel Cage Induction Generator (SCIG) connected to the grid through a transformer. As the power level changes, the operating slip of the SCIG installed in the wind turbine nacelle varies only around 1% of the synchronous speed. Hence this type of wind generation is referred to as fixed-speed. For a fixed-speed wind turbine any fluctuation in the wind speed causes the mechanical power at the wind turbine rotor to vary, and since the rotational speed is fixed, the wind turbine rotor torque varies accordingly. The power output of the wind turbine changes as the rotor torque changes. This is a disadvantage, and it is considered as a source of instability to the power system network to which it is connected. When a wind gust occurs, there will be a sudden increase in the wind turbine rotor torque, and the mechanical components of the wind turbine (notably the gear box), will be stressed

[12]. Another disadvantage of the SCIG being used with the wind turbines is that it consumes reactive power, and such power factor correction capacitors, as shown in Figure 1.6, must be provided at each wind turbine [13]. Pwt and Qwt shown in Figure 1.6 are the total active and reactive powers delivered by the wind turbine electrical generator to the grid.

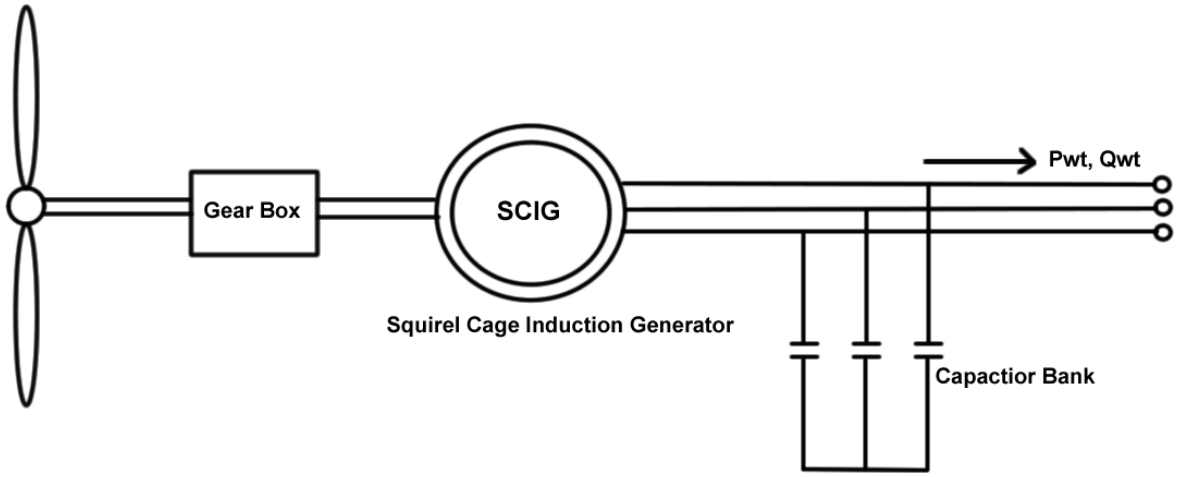

Figure 1.6. Configuration of Fixed-Speed Wind Turbine

1.7.3.2. Variable-Speed Wind Turbine

Currently, the most common variable-speed wind turbine configurations are 1) the Doubly Fed Induction Generator (DFIG) and, 2) the Fully Rated Converter (FRC).

1.7.3.2.1. Doubly Fed Induction Generator Wind Turbine

A typical configuration of the DFIG wind turbine is shown schematically in Figure 1.7. It uses a wound-rotor induction generator with slip rings to take the current into or out of the rotor winding, and variable-speed operation is obtained by injecting a controllable voltage into the rotor at slip frequency. The stator windings of the DFIG are directly connected to the grid. The rotor winding is fed through a variable-frequency power converter, typically based on two AC/DC IGBT based voltage source converters (VSCs) linked by a DC bus [13]. The power converter decouples the network electrical frequency from the rotor mechanical

frequency, enabling variable-speed operation of the wind turbine. The generator and converters are protected by voltage limits and an over-current 'crowbar.'

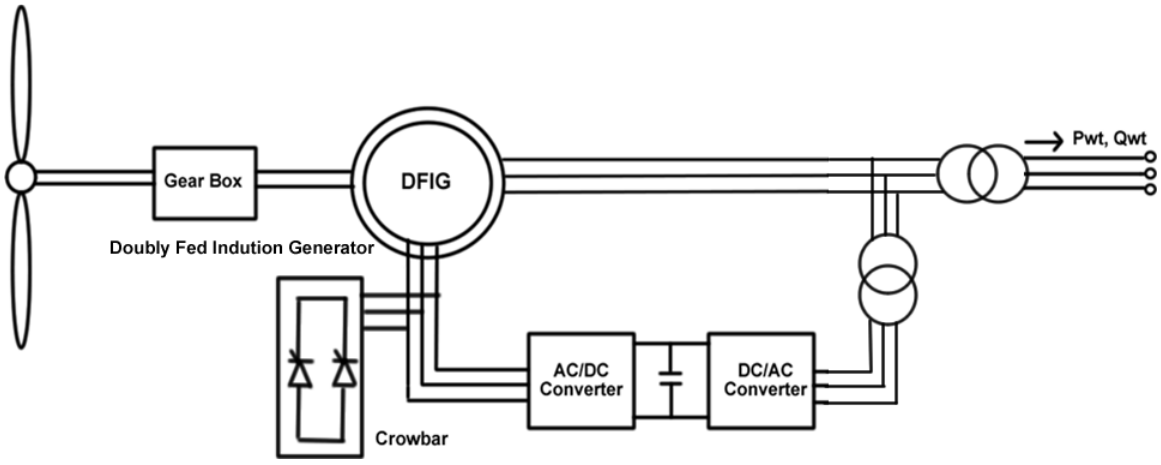

Figure 1.7. Configuration of DFIG Wind Turbine

For variable-speed wind turbines, the rotation speed of the rotor is allowed to vary as the wind speed varies. Hence the DFIG wind turbine allows operation without sudden torque variations at the wind turbine rotor, thereby decreasing the stress imposed on mechanical components of the wind turbine.

In the case of DFIG wind turbines, the generator output voltage and frequency can be maintained constant, irrespective of the generator rotor speed (and thus, irrespective of the wind speed). This is explained in detail in 'DFIG Principle of Operation' in Chapter 2 of this thesis.

In DFIG wind turbines it is possible to adjust the amount of reactive power exchanged between the generator and the AC power network. This allows the power factor of the system to be maintained at unity. DIFG wind turbines allow electrical power generation at lower wind speeds than fixed-speed wind turbines. Moreover, the power electronic devices used with DFIG wind turbines need to process only a fraction of the generator output power, i.e., the power supplied to or from the generator rotor windings, is typically about

30% of the generator rated power. This reduces the cost and size of the power electronic equipment and the associated losses. Disadvantages include regular maintenance of the slip rings, and protection of the power electronic equipment from fault currents.

1.7.3.2.2 Fully Rated Converter Wind Turbine

The typical configuration of a Fully Rated Converter (FRC) wind turbine is shown in Figure 1.8. It may or may not include a gearbox and a wide range of electrical generators (wound-rotor induction, synchronous or permanent magnet synchronous) can be employed with this configuration. With this arrangement, the power converters isolate the dynamic operation of the electrical generator from the power grid [14]. The electrical frequency of the generator may vary as the wind speed changes, while the grid frequency remains unchanged, thus allowing variable-speed operation of the wind turbine.

The generator-side converter can be a diode rectifier or a PWM voltage source converter (VSC) and the network-side converter is typically a PWM VSC [14]. Since the grid side DC-AC converter is always connected to the grid, it limits the range of variable speed operation. In the case of the FRC wind turbine, both converters can be made to generate or absorb reactive power independently.

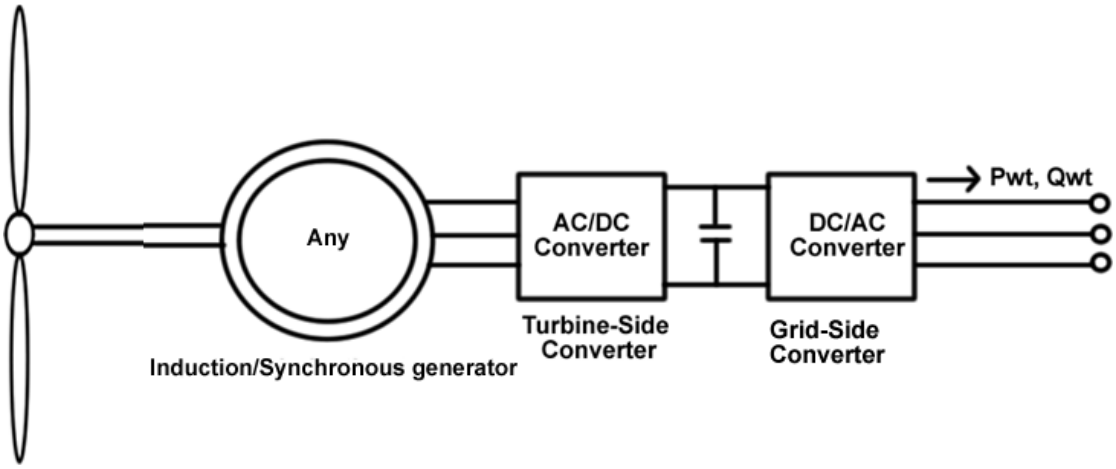

Figure 1.8. Configuration of FRC Wind Turbine

For FRC wind turbines the strategy to control the operation of the generator and the power flows to the network depends very much on the type of the power converter arrangement employed. A Grid-side converter can be used to control the DC bus voltage constant or torque applied to the generator. The main disadvantage of this method is the cost of the converter equipment involved, as it should be rated to withstand 100% of the generator output power.

1.8. Local and System Wide Impacts of the Wind Energy Generation on Operation of the Power System

There are a lot of differences between the conventional power plants and the wind generation power plants**.** A few of them are listed as:

1) Wind turbine power plants employ different, often converter-based generating systems compared to those used in conventional power plants.

2) As different from the conventional power plants, the prime mover of the wind turbine, the wind, is not controllable and fluctuates stochastically.

3) The typical size of an individual wind turbine is much smaller than that of a conventional utility synchronous generator.

Due to the above mentioned differences, wind generation may have both local and system-wide impacts on the operation of the power system. Local impacts occur in the electrical vicinity of a wind turbine power plant or wind farm, and can be attributed to a specific turbine or farm. On the other hand, system-wide impacts affect the behavior of the power system as a whole [15]. They are an inherent consequence of the utilization of wind power and cannot be attributed to an individual turbine or wind farm.

1.8.1. Local Impacts of Wind Generation

Locally, the wind power plants operation has an impact on the following characteristics of the power system: a) Circuit power flows and busbar voltages b) Protection schemes, fault currents and switch gear rating and c) Power quality [15].

The first two impacts are always considered when connecting any new generator to the power system and are not specific to wind generation. Harmonic voltage distortion is of major concern when power electronic converters are employed to interface the wind generation to the power system network. Voltage flicker is more significant when large fixed-speed wind turbines are connected to a non-infinite bus, i.e., the magnitude and phase values of voltages at the bus are not constant values.

Circuit Power Flows and Busbar Voltages

The local impacts of wind turbines on circuit power flows and busbar voltages depend on the type of the wind turbine used for wind power generation. The operating condition of a squirrel-cage induction generator used in fixed-speed turbines depends largely on the mechanical input power and the voltage at the generator terminals. Hence, fixed-speed wind turbines cannot control the reactive power exchange between the wind turbine and the power system network, and hence cannot control the busbar voltages by themselves. Additional reactive power compensation equipment such as shunt-connected capacitors is employed with the fixed-speed wind turbines.

On the other hand, variable-speed wind turbines which use a doubly-fed induction generator as shown in Figure 1.7 have the capability to control the reactive power flow between the wind turbine and the grid to affect their terminal voltage. But, the extent to which the variable-speed wind turbines can control the circuit power flows and busbar

voltages depends largely on the rating of the power electronic equipment and the type of controllers used to control those power electronic converters.

Protection Schemes, Fault Currents and Switchgear Rating

The extent to which the wind turbines contribute to the network fault depends on the type of generator technology employed. Since fixed-speed wind turbines use induction generators, they contribute only during the sub-transient fault current for a balanced three-phase fault, but they can also supply sustained fault current for unbalanced faults [15].

Variable-speed DFIG wind turbines also contribute to network fault currents. Due to the sensitivity of the power electronics to over-currents, this type of wind turbine is disconnected from the grid quickly and crowbar resistor is activated to protect the power electronic converters. The behavior of the variable-speed DFIG during network faults depends on the design of the power converters and the setting of their controllers to meet the grid code requirement for Fault Ride Through Capability (FRTC).

The capability of the DFIG to stay connected to the grid during a fault is called Low Voltage Ride Through (LVRT) or Fault Ride Through (FRT) capability. The severity of the voltage dip is defined by the voltage level during the dip which may go down to zero, and the duration of the dip. Depending on the application of the wind turbine, during and after the dip, it may be required to (1) disconnect temporarily from the grid, but reconnect and continue operation after the dip, or (2) stay operational and not disconnect from the grid or stay connected and support the grid with reactive power.

Fully rated converter wind turbines do not contribute significantly to the network fault current. The grid-side converter as shown in Figure 1.8 is not sized to supply sustained over-currents. In case of a fault, the FRC wind turbines disconnect quickly, unless there is a grid code requirement for FRTC of the wind turbine.

Power quality

Voltage harmonic distortion and flicker are considered as the two local effects of wind power on power quality. Harmonic distortion is mostly associated with the power converter based wind turbines (such as variable-speed DFIG and FRC wind turbines), as power electronic equipment are sources of high-frequency harmonic currents [15]. In fixed-speed wind turbines the wind fluctuations are directly translated into output power fluctuations. The output power fluctuations will result in grid voltage fluctuations and are referred to as flicker. Hence, voltage flicker problems occur only in fixed-speed wind turbines.

1.8.2. System-wide Impacts of Wind Generation

Wind generation has a system-wide impact on the following aspects of the power system:
a) Power system dynamics and stability, b) Reactive power and voltage support, and c) Frequency support. The impact of wind generation in the three areas mentioned depend on the type of the electrical generator used.

Power System Dynamics and Stability

During a fault, squirrel-cage induction generators used in fixed-speed wind turbines accelerate due to the imbalance between the mechanical power from the wind and the electrical power that can be supplied to the grid. When the fault is cleared, they absorb reactive power depressing the network voltage. If voltage does not recover quickly enough, the fixed-speed wind turbines continue to accelerate and to consume large amounts of reactive power leading to voltage and rotor speed instability [15]. Squirrel-cage induction generators tend to impede voltage recovery. In the case of Synchronous generators used in FRC wind turbine, the exciters of generators increase the reactive power output during low network voltages and support voltage recovery after a fault.

For the variable-speed Doubly Fed Induction Generator (DFIG) wind turbines, the sensitivity of the power electronics to over-currents might disconnect the turbines very quickly resulting in serious stability issues. The risk of disconnecting the DFIG at relatively small voltage reductions increases with their level of penetration into the power system network. In order to withstand voltage drops of certain magnitudes and durations, the DFIG wind turbines are required to be equipped with FRTC.

Reactive Power and Voltage Support

Voltage on a transmission network is mainly determined by the reactive power flow in the network. As fixed-speed electrical generators absorb reactive power to maintain their magnetic field, shunt compensators must be used to provide voltage support to the network. Whereas, variable-speed electrical generators have the capability of reactive power control and are able to provide voltage support to the power system network [15]. Reactive power and voltage control at the point of connection of the wind farm is achieved by using reactive power compensation equipment such as static var compensators (SVCs) or static synchronous compensators (STATCOMs).

Frequency Support

To provide frequency support from the generation unit, the generator power must increase or decrease as the system frequency changes. Both fixed-speed and variable-speed electric generators can provide frequency support to the power system network. In response to low network frequency, the output active power of the wind turbines electrical generators needs to be decreased, i.e., they are to be de-loaded. Fixed-speed wind turbines use pitch angle control to de-load the wind turbine such that a fraction of the power extracted from the wind is 'spilled'. Variable-speed wind turbines de-load the wind turbine by operating it away from the maximum power extraction curve.

1.9. Grid Code Requirements in the U.S.

Since the disconnection of the significant percentage of wind turbines has a profound effect on the stability of the power grid, the United States Federal Energy Regulatory Commission (FERC) proposed a rule for Low Voltage Ride Through (LVRT) according to article No.661 [16]. During a low-voltage event down to 15% of nominal voltage, an applicable wind turbine generator would be required to be online for up to 0.625 seconds (37.5 cycles at 60 Hz). This requirement is shown as a solid line on the Figure 1.9. The North American Reliability Council (NERC) together with the American Wind Energy Association (AWEA) proposed the LVRT requirement to be modified, such that the wind turbines need to remain online for low-voltage conditions down to zero volts for a period of not more than 0.15 sec (9 cycles). The dashed line on Figure 1.9 shows the requirement of NERC and AWEA.

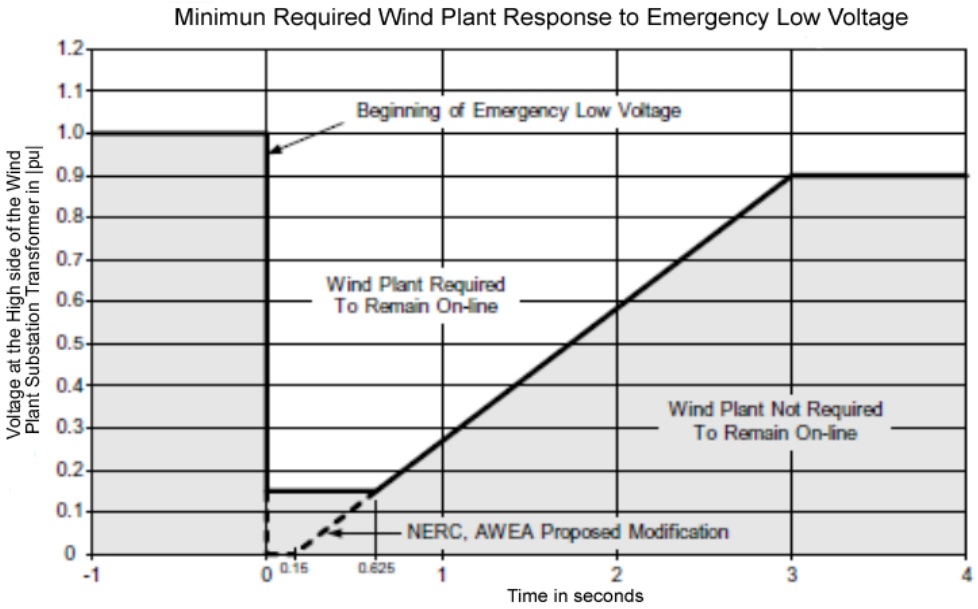

Figure 1.9. Graph Showing Grid Code Requirements in the U.S. [16]

CHAPTER 2

Doubly Fed Induction Generator Machine Model

2.1. DFIG Principle of Operation

In a Doubly Fed Induction Generator (DFIG) the mechanical power at the machine shaft is converted into electrical power and is supplied to the AC power network via the stator windings. The DFIG machine operates like a synchronous generator. In a three-phase synchronous generator the mechanical power supplied by the prime mover causes the rotor of the generator to rotate. The DC current fed into the generator rotor windings creates a static magnetic field that rotates at the same speed as the rotor (n_{rotor}). As the rotor magnetic field rotates, a continually changing magnetic flux passes through the stator windings inducing an alternative voltage across the stator windings [17]. For a DFIG generator, the speed at which the generator shaft must rotate to generate power at the power network frequency ($f_{network}$) can be varied by adjusting the frequency of the AC voltage fed into the generator rotor windings.

In a conventional singly-fed induction generator, the generator rotor is rotated by an external means to a speed greater than synchronous speed, and the stator magnetizing flux induces voltages that result in currents flowing through the rotor windings. These currents produce a rotor magnetomotive force that rotates in the opposite direction to the rotor movement. The resultant magnetic flux generated by the stator and rotor rotating magnetomotive forces will induce an alternative voltage across the stator windings at the synchronous frequency. Hence induction generators require electric supply to produce the stator magnetizing flux (often an induction generator will self start due to residual magnetism); the initial required electric power can be supplied from the grid or from the induction generator itself once it starts producing electric power.

The relationship between the frequency of the AC voltages induced across the stator windings (f_{stator}) of the generator and the rotor speed (n_{rotor}) is defined by using the following equation:

$$f_{stator} = \frac{n_{rotor} * N_{poles}}{120},$$

where

f_{stator} = the frequency of the ac voltages induced across the stator windings in |Hz| [17],

n_{rotor} = the speed of the rotor in |rpm|, and

N_{poles} = the number of poles per phase of the machine.

DFIG has the same operating principles applied to a conventional synchronous generator. The only difference is that the magnetomotive force created in the rotor due to the three phase AC currents flowing in the rotor is not static, but with respect to the rotor body, it rotates at a speed ($n_{\phi,rotor}$) proportional to the frequency of the AC currents flowing through the generator rotor windings. Therefore, in a DFIG both the rotation speed of the rotor (n_{rotor}) and the frequency of the AC currents in the rotor windings (f_{rotor}) determine the speed of the rotor rotating magnetomotive force ($n_{\phi,stator}$), and thus the frequency of the alternating voltage induced across the stator windings (f_{stator}).

When the magnetomotive force of the rotor rotates in the same direction as the generator rotor, the rotor speed (n_{rotor}) and the speed of the rotor rotating magnetomotive force ($n_{\phi,rotor}$), that is proportional to (f_{rotor}), will add up as shown in Figure 2.1a. Therefore, the frequency of the voltag**es** induced across the stator windings is given by

$$f_{stator} = \frac{n_{rotor} * N_{poles}}{120} + f_{rotor},$$

where

f_{rotor}= the frequency of the ac currents flowing through the DFIG rotor windings.

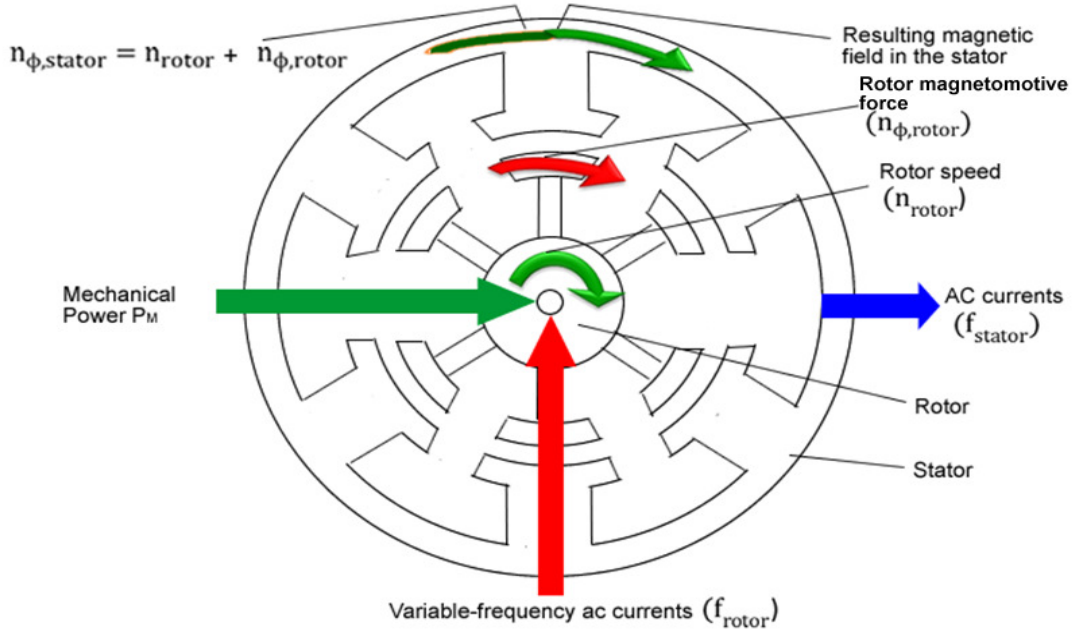

Figure 2.1a. When stator and rotor magnetomotive forces rotate in the same direction [17]

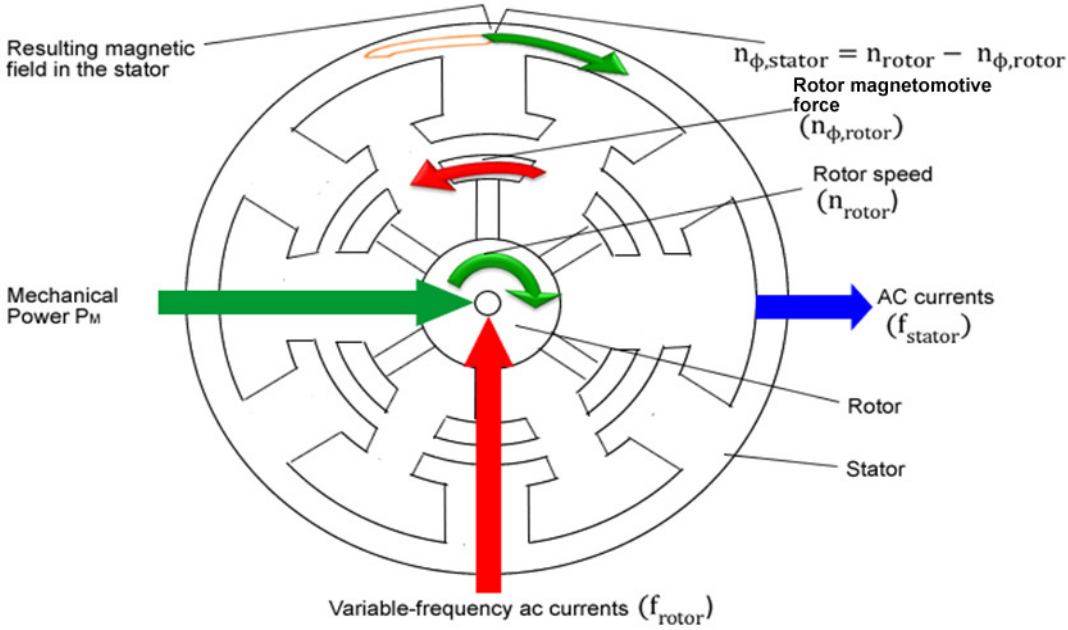

Figure 2.1b. When stator and rotor magnetomotive forces rotate in the opposite direction [17]

Figure 2.1. Interaction between the rotor speed and the frequency of the rotor rotating magnetomotive force of a DFIG [17]

Conversely, if the magnetomotive force of the rotor rotates in the opposite direction to the generator rotor movement, the rotor speed and the speed of the rotor rotating magnetomotive force will be subtracted as shown in Figure 2.1b. The frequency of the voltages induced across the stator windings is given by

$$f_{stator} = \frac{n_{rotor} * N_{poles}}{120} - f_{rotor}.$$

2.1.1. Using DFIG to Produce Fixed-Frequency Voltages

The primary reason for using a doubly-fed induction generator is to produce three-phase stator voltages of which frequency (f_{stator}) is constant, i.e., frequency f_{stator} to remain equal to the frequency of the ac power network ($f_{network}$) to which the generator is connected. This must be satisfied despite variations in the generator rotor speed (n_{rotor}), caused by fluctuations of the mechanical power provided by the prime mover (e.g., the wind turbine rotor) driving the generator. To achieve this purpose, the frequency of the AC currents in the rotor windings (f_{rotor}) must be continuously adjusted to counteract any variation in the rotor speed (n_{rotor}) caused by fluctuations of the mechanical power provided by the prime mover driving the generator [17].

The frequency of the AC currents that need to be flowing through the generator rotor windings (f_{rotor}) can be calculated by using the following equation:

$$f_{rotor} = f_{network} - \frac{n_{rotor} * N_{poles}}{120},$$

where

$f_{network}$ = the frequency of the ac power network to which the doubly-fed induction generator is connected, expressed in Hertz (Hz).

By using the above equation it can be stated that, if the generator rotor rotates at the nominal synchronous speed (n_s), the frequency of the AC currents flowing through the generator rotor windings (f_{rotor}) must be equal to 0 Hz. Then the DFIG would operate as a conventional three-phase synchronous machine.

When the generator rotor speed (n_{rotor}) decreases below the nominal synchronous speed (n_s), the frequency of the AC currents flowing through the generator rotor windings (f_{rotor}) increases accordingly and is of a positive sequence. The positive sequence of the rotor frequency (f_{rotor}) indicates that the phase sequence of the three-phase ac currents fed into the rotor windings will make the rotor magnetomotive force to rotate in the same direction as the generator rotor, as it is illustrated in Figure 2.1a.

Similarly, when the generator rotor speed (n_{rotor}) increases above the nominal synchronous speed (n_s), the frequency of the ac currents flowing through the generator rotor windings (f_{rotor}) increases accordingly and is of negative sequence. The negative sequence of the rotor frequency (f_{rotor}) indicates that the phase sequence of the three-phase AC currents fed into the rotor windings will make the rotor magnetomotive force rotate in the direction opposite to that of the generator rotor, as it is illustrated in Figure 2.2b.

For example, consider a doubly-fed induction generator having 4 magnetic poles per phase. The generator supplies power to a 60 Hz ac power network. Considering that the prime mover causes the generator rotor to rotate at a speed of 1980 |rpm|, the frequency of the AC currents that need to be fed into the generator rotor windings (f_{rotor}) can be calculated as

$$f_{rotor} = f_{network} - \frac{n_{rotor} * N_{poles}}{120} = 60\ \text{Hz} - \frac{1980\ \text{r/min} \times 4\ \text{poles}}{120} = -6\ \text{Hz}.$$

Such, to have the frequency of the generator output voltage (f_{stator}) equal to the frequency of the AC power network ($f_{network}$) it results that the frequency of the AC currents to be fed into the generator rotor windings (f_{rotor}), which must be 6 |Hz|. The negative sign of the rotor frequency (f_{rotor}) indicates that the magnetomotive force created by the rotor windings must rotate in the direction opposite to the direction of the rotor movement.

2.1.2. V/f Control

When a doubly-fed induction generator is used to produce power at the ac power network voltage and frequency, any deviation of the generator rotor speed (n_{rotor}) from the synchronous speed (n_s) is compensated by adjusting the frequency of the ac currents flowing through the generator rotor windings (f_{rotor}), such that the frequency of the voltage at the stator terminals (f_{stator}) remains equal to the AC power network frequency ($f_{network}$) [16]. In other words, the frequency f_{rotor} is adjusted such that the speed of the rotating magnetomotive force ($n_{\phi,stator}$) remains constant. Consequently, to maintain the voltage at the stator terminals equal to the AC power network voltage, a specific magnetic flux value must be maintained in the machine. This can be achieved by applying a voltage to the generator rotor windings that is proportional to the frequency of the voltages applied to the rotor windings (this maintains the V/f ratio constant and ensures a constant magnetic flux value in the machine). The value of the V/f ratio is generally set such that the reactive power delivered by the stator, Q_{delbys}, equals zero.

2.2. DFIG Modes of Operation

The DFIG machine can operate in two different modes, over-synchronous mode and under-synchronous mode, depending on the slip of the machine. The slip of the DFIG is defined as the ratio of the difference between the rotating speeds of the stator magnetomotive force and the rotor mechanical speed to the speed of the stator magnetomotive force.

The analytical equation for the slip of the DFIG is

$$s = \frac{n_s{}^{|rpm|} - n_{rotor}{}^{|rpm|}}{n_s{}^{|rpm|}}$$

$$= \frac{\omega_{del}{}^{|el.rad/s|} - \omega_{rel}{}^{|el.rad/s|}}{\omega_{del}{}^{|el.rad/s|}},$$

where

n_{rotor} = mechanical speed of the rotor in |rpm|,

n_s = speed of the stator magnetomotive force in |rpm|

= synchronous speed defined by $n_s = \frac{60 * f_s}{p_p}$,

f_s = frequency of the stator voltages and currents,

p_p = no of pair of poles per phase,

ω_{del} = angular frequency of the stator magnetomotive force in |el. rad/s|, and

ω_{rel} = angular frequency of the rotor in |el. rad/s|.

DFIG can deliver active power to the grid during both modes of operation. DFIG is said to operate in over-synchronous mode for negative values of the slip and under-synchronous mode for positive values of the slip. During over-synchronous mode the DFIG can deliver more than the rated power of the machine. During the sub-synchronous mode and for a particular range of rotor voltages, DFIG can still deliver power to the grid, but it will be below the rating of the DFIG [18]. Detailed DFIG characteristics are studied in Chapter 3. If P_{deltot} is the total active power delivered to the grid, P_{delbys} and P_{absbyr} are the corresponding active powers delivered by the stator to the grid and absorbed by the rotor of the DFIG from the grid, then they are related as $P_{deltot} = P_{delbys} - P_{absbyr}$, which is valid for the both over synchronous and under-synchronous modes of operation. Figure 2.3 shows the active power flow in the DFIG during over-synchronous and sub-synchronous modes of operation.

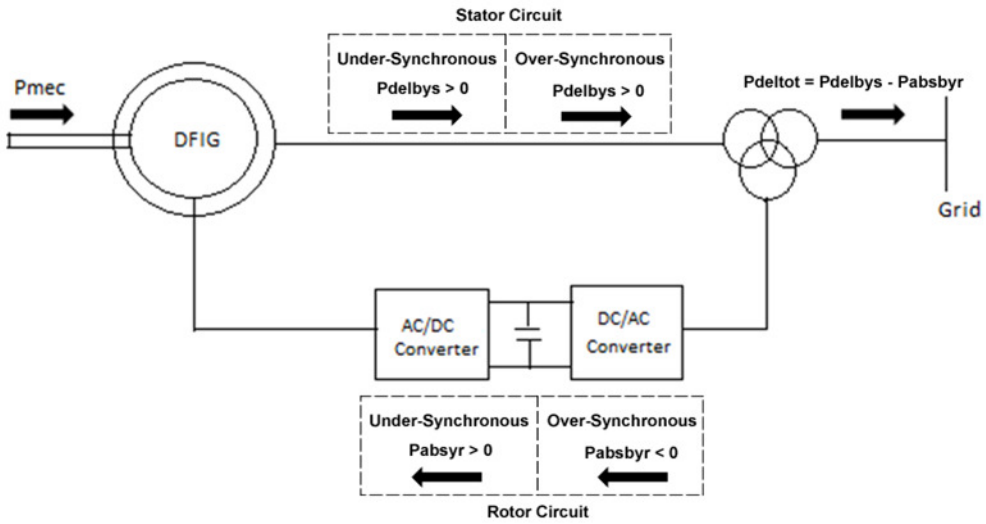

Figure 2.2. Active Power Flow during Different Modes of the DFIG Operation

2.3. DFIG Machine Model

2.3.1. Model Description

A three phase doubly fed induction generator shown in Figure 2.3 is considered for modeling. Both the stator and rotor cores are considered to be cylindrical. They host three distributed AC windings with axes radial from the rotor rotational axis, and with a relative angle of 120 electrical degrees between any two of them. These windings are represented as concentrated windings a, b, c on the stator side and a', b', c' on the rotor side, as shown in Figure 2.3. The stator and rotor winding axes are also represented as a, b, c and a', b', c', corresponding to the windings they house. The stator winding axis is radial with respect to, diverging from the rotor rotational axis and aligned with the windings maximum air-gap magnetomotive force. The rotor winding axis is radial with respect to, converging to the rotor rotational axis and aligned with the windings maximum air-gap magnetomotive force. For example, the stator winding axis "a" is aligned with $\mathcal{F}_{\mathrm{msa}}$ vector as seen in Figure 2.3. The phase sequence of the DFIG in operation is a-b-c.

The rotor movement is considered to be clockwise, defined by the angular frequency ω_{rel} in electrical radians/second. Longitudinal, or direct, or d-axis diverges from the rotor rotational shaft axis and has the same movement direction as the rotor positive movement. Transversal, or quadrature, or q-axis also diverges from the rotor rotational shaft axis and leads the d-axis with $\pi/2$ electrical radians towards the rotor positive movement. Both d and q-axes rotate at rated angular frequency of the stator and are introduced to have inductances that are independent of time [19]. As seen in Figure 2.3, the axis of the stator phase "a" winding (represented as a) is taken as a reference for both θ_{rel} and θ_{del}, where θ_{rel} is the angle between the rotor phase "a' " axis and stator phase "a" axis, and θ_{del} is the angle between the d-axis and stator phase "a" axis. Windings magnetomotive force and magnetic flux positive reference is the same as the positive reference of the winding axis, represented as $\mathcal{F}_{\text{m}}$ vectors in Figure 2.3. The positive polarity of the voltages applied to the machine windings is indicated clearly in Figure 2.3. The current polarity follows the load convention for the rotor windings i.e., positive current flows into the positive terminal of the winding, and the source convention for the stator windings. The torques of the DFIG are defined as positive in the same direction as the rotor positive movement.

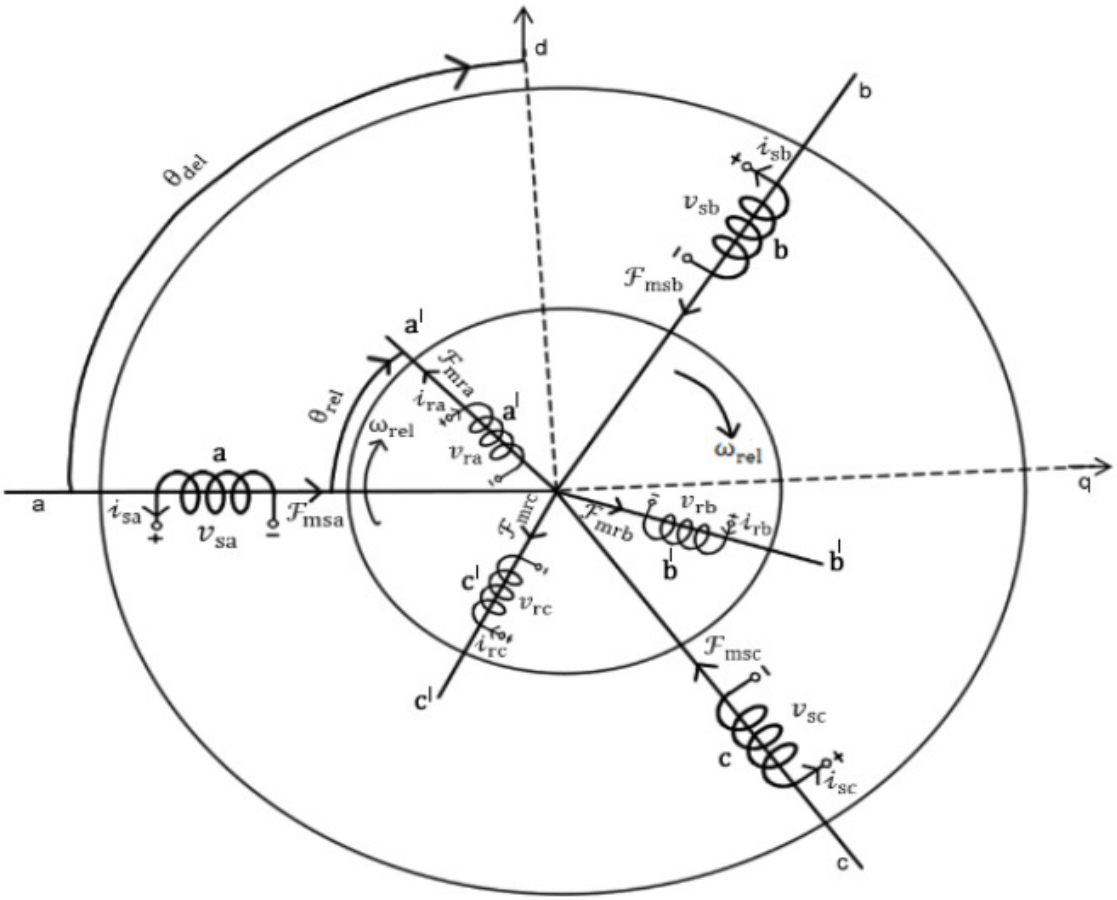

Figure 2.3. Components of DFIG

2.3.2. Assumptions

-- The stator windings (a, b, c) are assumed identical and with the same parameters

-- The rotor windings (a', b', c') are assumed identical and with the same parameters

-- Constructively, the DFIG machine is symmetrical as with respect to the rotor shaft rotational axis

-- The hysteresis phenomenon is disregarded

-- The winding capacitance is not taken into consideration

-- The slots and end effects are not distinctively considered. They are included on the corresponding permeance value

-- For modeling, the dependence of inductance with saturation, and of the windings

resistance with temperature and frequency are disregarded. Such a linear model of the DFIG is obtained, where the superposition principle applies:

-- For every winding the self-magnetomotive force produced in the air-gap is cosinusoidally distributed as with respect to the winding axis,

-- Both stator and rotor windings are considered to be Y connected,

-- All the lower case letters used as a notation in this thesis refer to instantaneous quantities of the DFIG,

-- Subscripts used for notations are described as follows:

s, r, g denote the quantities corresponding to the stator, rotor and grid, respectively

a, b, c denote the quantities corresponding to phases a, b and c, respectively

d, q, o denote the quantities corresponding to d, q and o axes, respectively

rec, inv denote the quantities corresponding to rectifier and inverter respectively

ph denotes quantities defined on the phase reference frame

dq denotes quantities defined on the dqo reference frame

-- Description of the notation of letters used:

i , v, Ψ denote instantaneous currents, voltages, and flux linkages, respectively

R, L, N denote resistance, inductance and number of turns of the windings, respectively

$\mathcal{P}$ denotes the magnetic permeance of a path and

p_P denotes number of pair of poles per phase.

For example N_{sd} denotes the number of turns of the stator winding on d-axis.

2.3.3. Windings Terminal Voltage and Flux Linkage Equations in Phase Reference

Winding terminal voltage and flux linkage equations that determine the electrical characteristics of the stator windings a, b, c, and rotor windings a', b', c', as shown in Figure 2.3, are defined in a matricial form as

$$[v]_{\text{sph}}^{|\text{V}|} = -[\text{R}]_{\text{sph}}^{|\frac{\text{V}}{\text{A}}|} * [i]_{\text{sph}}^{|\text{A}|} - \frac{\text{d}}{\text{dt}^{|\text{s}|}}[\Psi]_{\text{sph}}^{|\text{Vs}|}, \tag{2.1}$$

$$[v]_{\text{rph}}^{|\text{V}|} = [\text{R}]_{\text{rph}}^{|\frac{\text{V}}{\text{A}}|} * [i]_{\text{rph}}^{|\text{A}|} + \frac{\text{d}}{\text{dt}^{|\text{s}|}}[\Psi]_{\text{rph}}^{|\text{Vs}|}, \tag{2.2}$$

$$[\Psi]_{\text{sph}}^{|\text{Vs}|} = [\text{L}]_{\text{ssph}}^{|\frac{\text{Vs}}{\text{A}}|} * [i]_{\text{sph}}^{|\text{A}|} + [\text{L}]_{\text{srph}}^{|\frac{\text{Vs}}{\text{A}}|} * [i]_{\text{rph}}^{|\text{A}|}, \text{ and} \tag{2.3}$$

$$[\Psi]_{\text{rph}}^{|\text{Vs}|} = [\text{L}]_{\text{rsph}}^{|\frac{\text{Vs}}{\text{A}}|} * [i]_{\text{sph}}^{|\text{A}|} + [\text{L}]_{\text{rrph}}^{|\frac{\text{Vs}}{\text{A}}|} * [i]_{\text{rph}}^{|\text{A}|}. \tag{2.4}$$

The voltage, current, flux linkage, resistance and inductance matrices defined in the above equations are shown in detail in Appendix B.1.

2.3.4. Phase to dqo Reference Transformation

The dqo transformation results in constant inductance matrices, which make the analysis of the DFIG much simpler. In other words, this dqo transformation converts the three phase AC quantities into three simple DC quantities. The chosen direct-quadrature-zero (dqo) reference frame rotates at a rated angular frequency of the stator. The angle between the stator "a" axis and direct axis is θ_{del}, as indicated in Figure 2.3. The transformation is done based on the conditions that the DFIG should have the same instantaneous terminal power, the same magnetic energy and the same air gap magnetomotive force before and after the transformation. The detailed derivations of the stator and rotor transformation matrices $[\text{T}]_{\text{s}}$ and $[\text{T}]_{\text{r}}$ are presented in Appendix B.2, and they are defined as

$$[\text{T}]_{\text{s}} = \sqrt{\frac{2}{3}} * \begin{bmatrix} \cos\theta_{\text{del}}{}^{0} & \cos(\theta_{\text{del}} - 120)^{0} & \cos(\theta_{\text{del}} - 240)^{0} \\ -\sin\theta_{\text{del}}{}^{0} & -\sin(\theta_{\text{del}} - 120)^{0} & -\sin(\theta_{\text{del}} - 240)^{0} \\ \frac{1}{\sqrt{2}} & \frac{1}{\sqrt{2}} & \frac{1}{\sqrt{2}} \end{bmatrix}, \text{ and}$$

$$[\mathrm{T}]_{\mathrm{r}} =$$

$$\sqrt{\frac{2}{3}} * \begin{bmatrix} \cos(\theta_{\mathrm{del}} - \theta_{\mathrm{rel}})^0 & \cos(\theta_{\mathrm{del}} - \theta_{\mathrm{rel}} - 120)^0 & \cos(\theta_{\mathrm{del}} - \theta_{\mathrm{rel}} - 240)^0 \\ -\sin(\theta_{\mathrm{del}} - \theta_{\mathrm{rel}})^0 & -\sin(\theta_{\mathrm{del}} - \theta_{\mathrm{rel}} - 120)^0 & -\sin(\theta_{\mathrm{del}} - \theta_{\mathrm{rel}} - 240)^0 \\ \frac{1}{\sqrt{2}} & \frac{1}{\sqrt{2}} & \frac{1}{\sqrt{2}} \end{bmatrix}.$$

By using the above transformation matrices, DFIG Machine equations in the dqo reference frame are obtained as shown in Appendix B.2, and they are

$$[v]_{\mathrm{sdq}}^{|\mathrm{V}|} = -[\mathrm{R}]_{\mathrm{sdq}}^{|\Omega|}[i]_{\mathrm{sdq}}^{|\mathrm{A}|} - \frac{\mathrm{d}}{\mathrm{dt}^{|\mathrm{s}|}}[\Psi]_{\mathrm{sdq}}^{|\mathrm{Vs}|} - [\mathrm{T}]_{\mathrm{sw}}^{|\frac{1}{\mathrm{s}}|}[\Psi]_{\mathrm{sdq}}^{|\mathrm{Vs}|}, \tag{2.5}$$

$$[v]_{\mathrm{rdq}}^{|\mathrm{V}|} = [\mathrm{R}]_{\mathrm{rdq}}^{|\Omega|}[i]_{\mathrm{rdq}}^{|\mathrm{A}|} + \frac{\mathrm{d}}{\mathrm{dt}^{|\mathrm{s}|}}[\Psi]_{\mathrm{rdq}}^{|\mathrm{Vs}|} + [\mathrm{T}]_{\mathrm{rw}}^{|\frac{1}{\mathrm{s}}|}[\Psi]_{\mathrm{rdq}}^{|\mathrm{Vs}|}, \tag{2.6}$$

$$[\Psi]_{\mathrm{sdq}}^{|\mathrm{Vs}|} = [\mathrm{L}]_{\mathrm{ssdq}}^{|\frac{\mathrm{Vs}}{\mathrm{A}}|} * [i]_{\mathrm{sdq}}^{|\mathrm{A}|} + [\mathrm{L}]_{\mathrm{srdq}}^{|\frac{\mathrm{Vs}}{\mathrm{A}}|} * [i]_{\mathrm{rdq}}^{|\mathrm{A}|}, \text{ and} \tag{2.7}$$

$$[\Psi]_{\mathrm{rdq}}^{|\mathrm{Vs}|} = [\mathrm{L}]_{\mathrm{rsdq}}^{|\frac{\mathrm{Vs}}{\mathrm{A}}|} * [i]_{\mathrm{sdq}}^{|\mathrm{A}|} + [\mathrm{L}]_{\mathrm{rrdq}}^{|\frac{\mathrm{Vs}}{\mathrm{A}}|} * [i]_{\mathrm{rdq}}^{|\mathrm{A}|}. \tag{2.8}$$

A detailed explanation of the voltage, current, flux linkage, resistance, inductance and transformation matrices that are presented above are shown in Appendix B.2.

2.3.5. Windings Terminal Voltage and Flux Linkage Equations with Rotor Quantities Referred to the Stator

In order to interpret the per unit values using a single base, any machine modeling the rotor side quantities is referred to as the stator side. Rotor quantities on the rotor dqo axes are referred to as the stator dqo axes by satisfying the following requirements: magnetomotive force (mmf) at the stator windings level of the new rotor currents to be the same as the actual mmf; the rotor's terminal instantaneous power to remain unchanged; and the rotor windings magnetic energy to remain the same. The derivation involved for referring the rotor quantities to the stator is shown in Appendix B.3.

Windings terminal voltage and flux linkage equations with rotor quantities referred to the stator and in actual units results as

$$[v]_{sdq}^{|V|} = -[R]_{sdq}^{|\frac{V}{A}|}[i]_{sdq}^{|A|} - [T]_{sw}^{|\frac{1}{s}|}[\Psi]_{sdq}^{|Vs|} - \frac{d}{dt}[\Psi]_{sdq}^{|Vs|}, \quad (2.9)$$

$$[v]_{rdq}^{\prime|V|} = [R]_{rdq}^{\prime|\frac{V}{A}|}[i]_{rdq}^{\prime|A|} + [T]_{rw}^{\prime|\frac{1}{s}|}[\Psi]_{rdq}^{\prime|Vs|} + \frac{d}{dt}[\Psi]_{rdq}^{\prime|Vs|}, \quad (2.10)$$

$$[\Psi]_{sdq}^{|\frac{V}{s}|} = [L]_{ssdq}^{|\frac{Vs}{A}|}[i]_{sdq}^{|A|} + [L]_{srdq}^{\prime|\frac{Vs}{A}|}[i]_{rdq}^{\prime|A|}, \text{ and} \quad (2.11)$$

$$[\Psi]_{rdq}^{\prime|Vs|} = [L]_{rsdq}^{\prime|\frac{Vs}{A}|}[i]_{sdq}^{|A|} + [L]_{rrdq}^{\prime|\frac{Vs}{A}|}[i]_{rdq}^{\prime|A|}. \quad (2.12)$$

A detailed explanation of the voltage, current, flux linkage, resistance, inductance and transformation matrices that are presented above are shown in Appendix B.3.

2.3.6. Windings Terminal Voltage and Flux Linkage Equations in Normalized Quantities

The conversion of any parameter or variable X, from its actual units to normalized units is performed according to the rule $X^{pu} = \frac{X^{actualunits}}{X_b^{actualunits}}$, where X^{pu} is the normalized or per unit value of X, $X^{actualunits}$ is the value of X in actual units, and $X_b^{actualunits}$ is the base value of X in actual units. Normalized or pu representation helps to correlate different machine's electrical and mechanical parameters in a more meaningful way. Depending on the rating of the DFIG, the machine's actual quantities vary in a wide range compared to the pu or normalized values. The advantages of the pu system will be more significant in the case of complicated systems involving transformers with different turn ratios. The two different types of base quantities are selected base and derived base quantities. The values of the selected base quantities are identical to the DFIG name plate ratings and are defined as $V_b^{|V|} = V_{bsrated}^{|V|}$, $S_b^{|VA|} = S_{bsrated}^{|VA|}$, $\omega_{bs}^{|elrad/s|} = \omega_{srated}^{|elrad/s|}$, respectively, and by using the selected base quantities, the derived base quantities results as: $I_b^{|A|} = \frac{S_b^{|VA|}}{V_b^{|V|}}$, $Z_b^{|\frac{V}{A}|} =$

$\frac{V_b^{2|V^2|}}{S_b^{|VA|}}$, $t_{bs}^{|s|} = \frac{1}{\omega_{bs}^{|elrad/s|}}$, $L_b^{|\frac{Vs}{A}|}$ $\frac{V_b^{2|V^2|}}{\omega_{bs}^{|elrad/s|}S_b^{|VA|}}$, $\Psi_b^{|Vs|} = \frac{V_b^{|V|}}{\omega_{bs}^{|elrad/s|}}$, $T_b^{|Nm|} = \frac{p_p S_b^{|VA|}}{\omega_{bs}^{|elrad/s|}}$, $\omega_{br}^{|geom.rad/s|} = \frac{\omega_{bs}^{|elrad/s|}}{p_p}$.

Rated per unit is the same as calculating per unit values considering the generator name plate ratings as base quantities. The quantities in actual units shown in equations (2.9 - 2.12) are converted to rated per unit quantities by using the base quantities defined above. The prime on the rotor quantities in equations (2.9-2.12), indicating them as being referred to the stator, will be ignored from now on. Such, the final winding terminal voltages and flux linkage equations on dqo axes, with all quantities referred to as the stator and defined in rated per unit, are

$$[v]_{sdq}^{|rpu|} = -[R]_{sdq}^{|rpu|}[i]_{sdq}^{|rpu|} - [T]_{sw}^{|rpu|}[\Psi]_{sdq}^{|rpu|} - \frac{d}{dt^{|rpu|}}[\Psi]_{sdq}^{|rpu|}, \tag{2.13}$$

$$[v]_{rdq}^{|rpu|} = [R]_{rdq}^{|rpu|}[i]_{rdq}^{|rpu|} + [T]_{rw}^{|rpu|}[\Psi]_{rdq}^{|rpu|} + \frac{d}{dt^{|rpu|}}[\Psi]_{rdq}^{|rpu|}, \tag{2.14}$$

$$[\Psi]_{sdq}^{|rpu|} = [L]_{ssdq}^{|rpu|}[i]_{sdq}^{|rpu|} + [L]_{srdq}^{|rpu|}[i]_{rdq}^{|rpu|}, \text{ and} \tag{2.15}$$

$$[\Psi]_{rdq}^{|rpu|} = [L]_{rsdq}^{|rpu|}[i]_{sdq}^{|rpu|} + [L]_{rrdq}^{|rpu|}[i]_{rdq}^{|rpu|}. \tag{2.16}$$

Expanding the equations (2.13 – 2.16), it results as

$$v_{sd} = -R_s i_{sd} + \omega_{del}\Psi_{sq} - \frac{d\Psi_{sd}}{dt}, \tag{2.17}$$

$$v_{sq} = -R_s i_{sq} - \omega_{del}\Psi_{sd} - \frac{d\Psi_{sq}}{dt}, \tag{2.18}$$

$$v_{so} = -R_s i_{so} - \frac{d\Psi_{so}}{dt}, \tag{2.19}$$

$$v_{rd} = R_r i_{rd} - (\omega_{del} - \omega_{rel})\Psi_{rq} + \frac{d\Psi_{rd}}{dt}, \tag{2.20}$$

$$v_{rq} = R_r i_{rq} + (\omega_{del} - \omega_{rel})\Psi_{rd} + \frac{d\Psi_{rq}}{dt}, \tag{2.21}$$

$$v_{ro} = R_r i_{ro} + \frac{d\Psi_{ro}}{dt}, \tag{2.22}$$

$$\Psi_{sd} = (L_{sl} + L_m)i_{sd} - L_m i_{rd}, \quad (2.23)$$

$$\Psi_{sq} = (L_{sl} + L_m)i_{sq} - L_m i_{rq}, \quad (2.24)$$

$$\Psi_{so} = L_{sl} i_{so}, \quad (2.25)$$

$$\Psi_{rd} = -L_m i_{sd} + (L_{rl} + L_m)i_{rd}, \quad (2.26)$$

$$\Psi_{rq} = -L_m i_{sq} + (L_{rl} + L_m)i_{rq}, \text{ and} \quad (2.27)$$

$$\Psi_{ro} = L_{rl} i_{ro}. \quad (2.28)$$

The equivalent circuits shown in Figure 2.4 are constructed based on the equations (2.17 – 2.28).

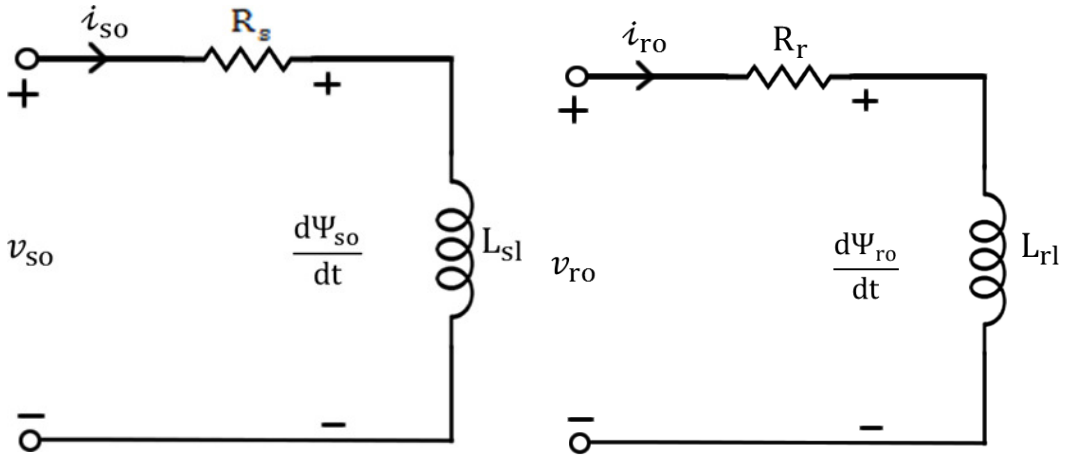

Figure 2.4.a. DFIG machine model on o-axis

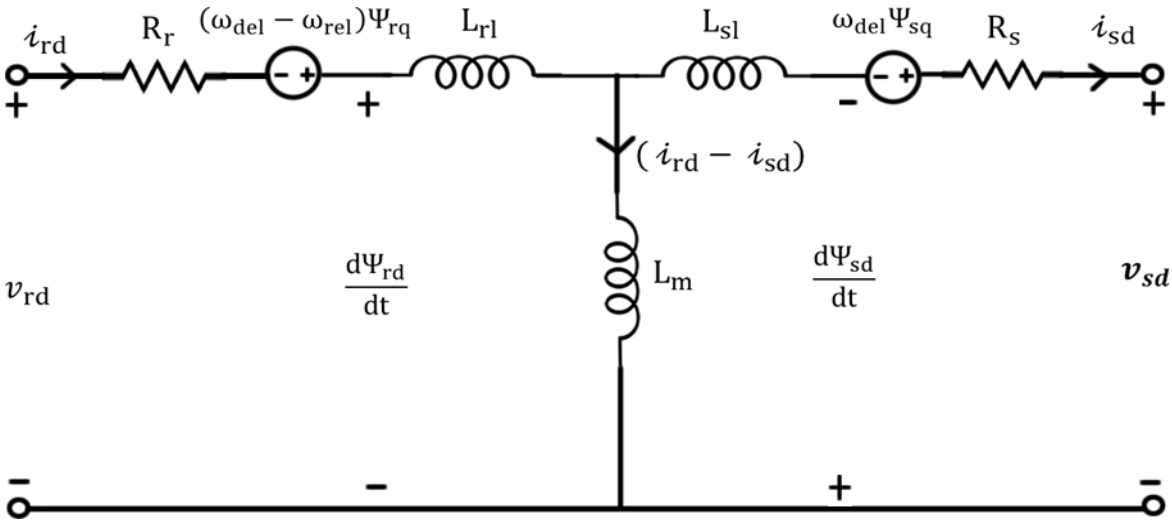

Figure 2.4.b. DFIG machine model on d-axis

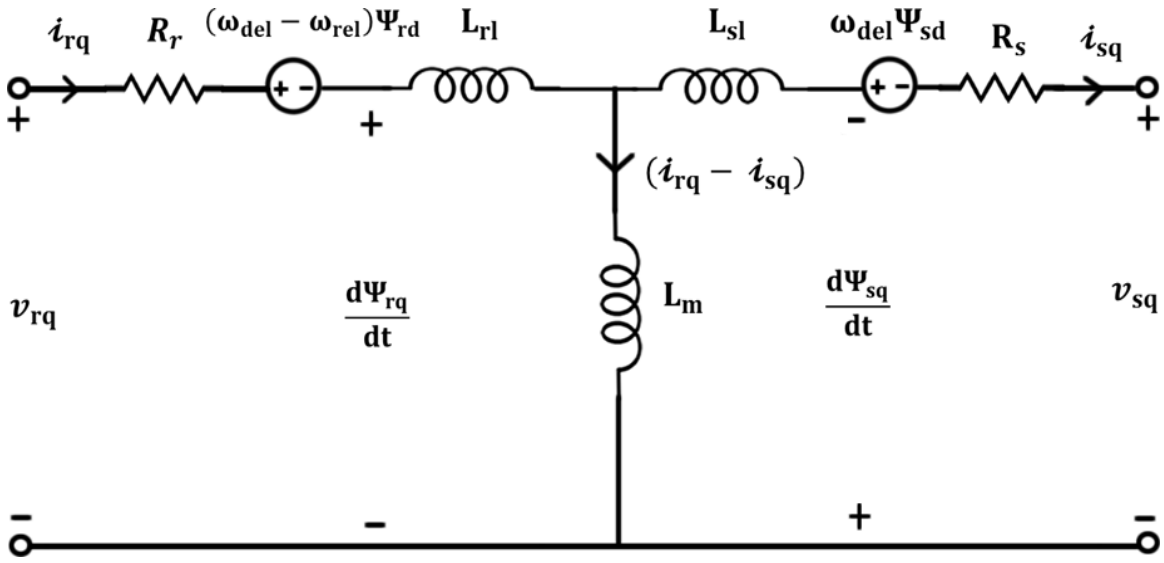

Figure 2.4.c. DFIG machine model on q-axis

Figure 2.4. Equivalent Circuit of DFIG Machine Model in dqo Reference Frame

2.4. Movement Equations

The machine movement equation is obtained by using the power balance equation, that is, the electrical power entering the stator and rotor terminals minus the corresponding electrical losses, plus mechanical power entering the shaft minus the corresponding mechanical losses, equals the increment of the internal magnetic and mechanical energy. As such the following equation applies:

$$(p_{\text{mec}} - \Delta p_{\text{mec}}) + \left\{[v]_{\text{rdq}}^{\text{T}}[i]_{\text{rdq}} - \Delta \text{p}_{\text{el.r}}\right\} + \left\{-[v]_{\text{sdq}}^{\text{T}}[i]_{\text{sdq}} - \Delta \text{p}_{\text{el.s}}\right\} = \frac{\text{dW}_{\text{magn}}}{\text{dt}} + \frac{\text{dW}_{\text{mec.internal}}}{\text{dt}}.$$

In all equations of this section the terminal powers are considered as entering into the machine and the electromagnetic power, P_{elm}, is considered to be positive if it has the same direction as the rotor movement. The detailed derivations of the movement equations defined in this section with all quantities in |rpu| are presented in Appendix B.4.

The final movement equations of the DFIG machine derived in Appendix B.4 are

$$(P_{mec} - \Delta P_{mec})^{|rpu|} + P_{elm}^{|rpu|} = \tau_m{}^{|rpu|}\omega_r^{|rpu|}\frac{d\omega_r^{|rpu|}}{dt^{|rpu|}}, \tag{2.29}$$

$$(T_{mec} - \Delta T_{mec})^{|rpu|} + T_{elm}^{|rpu|} = \tau_m{}^{|rpu|}\frac{d\omega_r^{|rpu|}}{dt^{|rpu|}}, \tag{2.30}$$

with

$$P_{elm}^{|rpu|} = \omega_{rel}{}^{|rpu|}L_m^{|rpu|}\left(i_{sd}^{|rpu|}i_{rq}^{|rpu|} - i_{sq}^{|rpu|}i_{rd}^{|rpu|}\right), \tag{2.31}$$

$$T_{elm}^{|rpu|} = L_m^{|rpu|}\left(i_{sd}^{|rpu|}i_{rq}^{|rpu|} - i_{sq}^{|rpu|}i_{rd}^{|rpu|}\right), \text{ and} \tag{2.32}$$

$$\tau_m{}^{|rpu|} = \frac{J^{|kgm^2|}\left(\omega_{bs}^{|elrad/s|}\right)^3}{p_p^2 S_{bs}^{|VA|}} = \frac{J^{|kgm^2|}\left(\omega_{br}^{|geomr/s|}\right)^2}{S_{bs}^{|VA|}}\omega_{bs}^{|elrad/s|}. \tag{2.33}$$

All the remaining definitions related to P_{elm} and T_{elm} in actual units and in rated per unit are shown in Appendix B.4.

2.5. Three phase Symmetrical Steady State

Three phase symmetrical steady state happens when the DFIG is connected to the grid and has been in operation for a finite amount of time. During the three phase symmetrical steady-state or predisturbance steady state, any changes to the machine variables with respect to time will be zero. To simplify the analysis of the DFIG during the three phase symmetrical steady state, a set of phasors are defined which gives the DFIG machine model in the phasor domain as shown below,

$$\bar{V}_s = v_{sd} + j\, v_{sq}, \tag{2.34}$$

$$\bar{V}_r = v_{rd} + j\, v_{rq}, \tag{2.35}$$

$$\bar{I}_s = i_{sd} + j\, i_{sq}, \tag{2.36}$$

$$\bar{I}_r = i_{rd} + j\, i_{rq}, \tag{2.37}$$

$$\bar{\Psi}_s = \Psi_{sd} + j\,\Psi_{sq}, \tag{2.38}$$

$$\bar{\Psi}_r = \Psi_{rd} + j\,\Psi_{rq}. \tag{2.39}$$

By using the above equations (2.34- 2.39) and with derivatives in equations (2.17– 2.22), equal to zero, the following equations are obtained:

$$\bar{V}_s = -R_s * \bar{I}_s - j\,\omega_{del} * \bar{\Psi}_s, \tag{2.40}$$

$$\bar{V}_r = R_r * \bar{I}_r + j\,(\omega_{del} - \omega_{rel}) * \bar{\Psi}_r, \tag{2.41}$$

$$\bar{\Psi}_s = (L_{sl} + L_m) * \bar{I}_s - L_m * \bar{I}_r, \tag{2.42}$$

$$\bar{\Psi}_r = -L_m * \bar{I}_s + (L_{rl} + L_m) * \bar{I}_r. \tag{2.43}$$

By considering the slip of the DFIG as defined on page 29, substituting equations (2.42 - 2.43) into equations (2.40-2.41), and combining the terms, the final DFIG machine model equations in phasor domain during the three phase symmetrical steady state are

$$\bar{V}_s = -(R_s + j\,X_{sl}) * \bar{I}_s + j\,X_m * (\bar{I}_r - \bar{I}_s), \tag{2.44}$$

$$\bar{V}_r = (R_r + js * X_{rl}) * \bar{I}_r + j\,s * X_m * (\bar{I}_r - \bar{I}_s). \tag{2.45}$$

The equivalent circuit shown in Figure 2.5 is constructed based on the equations (2.44 – 2.45).

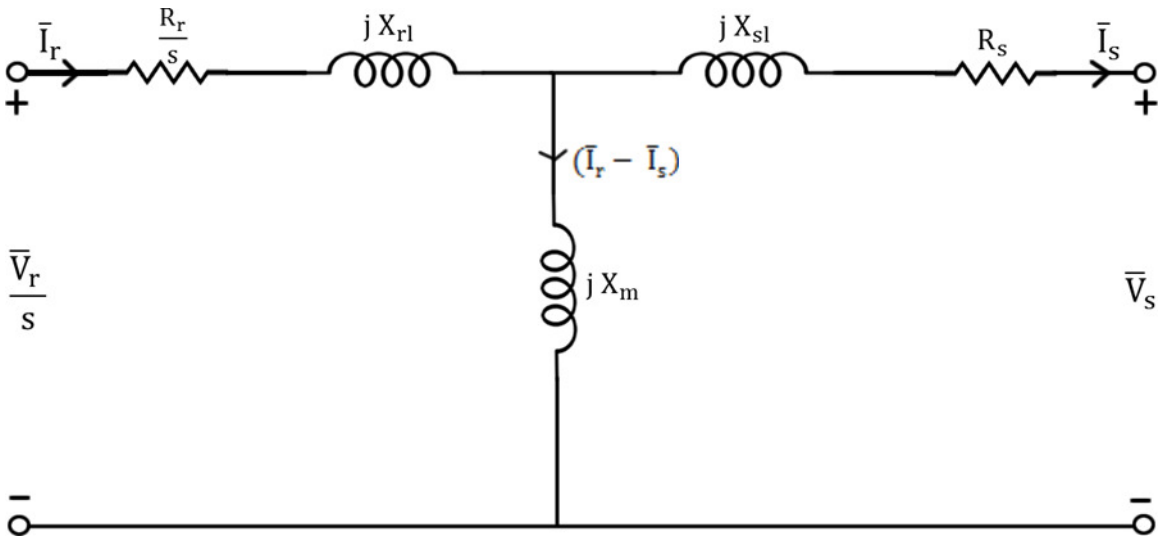

Figure 2.5. DFIG Machine Model in Phasor Domain

CHAPTER 3

DFIG Steady-State Characteristics

This chapter studies the steady-state power characteristics of the DFIG machine modeled in Chapter 2. Based on the machine rating, the model parameters are selected as shown in section 3.1. Interdependence of the DFIG variables i.e., the stator active and reactive powers, rotor active and reactive powers, and the total active and reactive powers delivered to the grid with the rotor voltage and slip are analyzed in sections 3.2 and 3.3. First, the dependence of the rotor voltage, active and reactive powers at the rotor terminals with the stator active and reactive powers is studied. Secondly, the dependence of the stator and rotor terminal powers with the applied rotor voltage and slip is analyzed. The analytical equations that are used for the analysis are based on the DFIG machine equations (2.34 – 2.45) defined in Chapter 2, pages (40-41), particularized for a three phase symmetrical steady state. The variations of the DFIG variables i.e., stator and rotor terminal powers are plotted using MATLAB and MATHEMATICA softwares. The analysis also determines the slip and rotor voltage values for maximum active or reactive powers delivered to the grid.

3.1. DFIG Parameters

The numerical values of the DFIG machine parameters shown in the equations of Chapter 2 were collected from different journals and adjusted to a 3 |MW| machine rating. Their values are as follows [20], [21]:

$$R_s = 0.0061 \text{ /rpu/}, \qquad R_r = 0.005 \text{ /rpu/},$$

$$X_{sl} = 0.0734 \text{ /rpu/}, \qquad X_{rl} = 0.1034 \text{ /rpu/},$$

$$X_m = 3.4734 \text{ /rpu/},$$

$$X_s = X_{sl} + X_m = 0.0734 + 3.4734 = 3.5468 \text{ /rpu/, and}$$

$$X_r = X_{rl} + X_m = 0.1034 + 3.4734 = 3.5768 \text{ /rpu/}.$$

Where /rpu/ represents rated per unit values of the parameters obtained by considering the DFIG rated power and rated stator voltage as the base quantities. The same numerical values of the DFIG parameters will be used for studying both the general power characteristics of the DFIG and the power flow in the Vestas V90 DFIG.

3.2. Interdependence of DFIG Variables

3.2.1. Dependence of the Rotor Windings Terminal Powers with the Slip and the Stator Windings Terminal Powers

3.2.1.1. Derivation of Analytical Relationship

All quantities shown from now onward are defined in |rpu|, and their units will not be mentioned hereafter. For a three-phase symmetrical steady-state operation the active and reactive powers delivered at the stator terminals (P_{delbys}, Q_{delbys}) or consumed at the rotor terminals (P_{absbyr}, Q_{absbyr}) are defined by the equations that follow. The meaning of different voltages and currents in the equations below is shown in Chapter 2, Section 2.3.6, pages (36-38).

$$P_{delbys} = v_{sd} i_{sd} + v_{sq} i_{sq}, \tag{3.1}$$

$$Q_{delbys} = v_{sq} i_{sd} - v_{sd} i_{sq}, \tag{3.2}$$

$$P_{absbyr} = v_{rd} i_{rd} + v_{rq} i_{rq}, \tag{3.3}$$

$$Q_{absbyr} = v_{rq} i_{rd} - v_{rd} i_{rq}, \tag{3.4}$$

$$P_{deltot} = P_{delbys} - P_{absbyr}, \text{ and} \tag{3.5}$$

$$Q_{deltot} = Q_{delbys} - Q_{absbyr}. \tag{3.6}$$

The stator windings of the DFIG are connected to the grid through a power system network. The rotor windings of the DFIG are connected to the power system network through the power electronics converters. The power system network consists of transformers and

transmission lines that export the electric power generated by the DFIG to the grid. An example of the DFIG connection to the grid is shown in Figure 3.1.

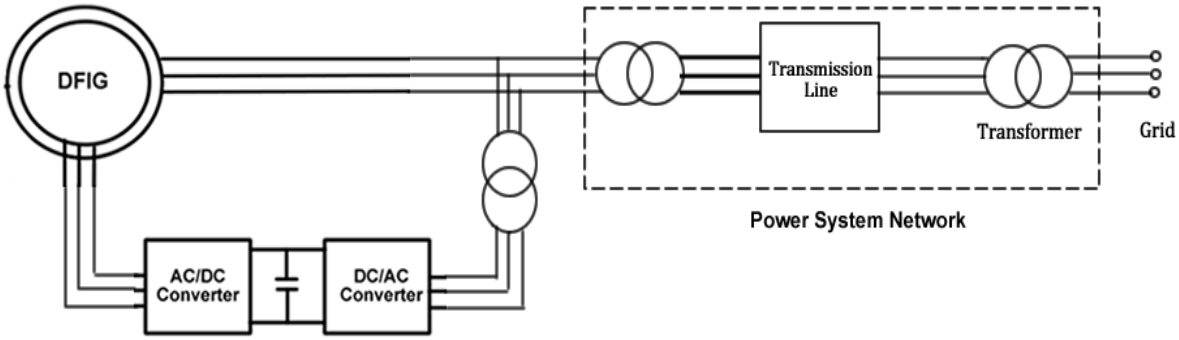

Figure 3.1. Connection of the DFIG to the grid

Considering that with respect to the DFIG rated power the grid capability is much higher, the terminal voltage to the grid is considered as constant in magnitude. The DFIG machine power characteristics are studied considering the magnitude of the DFIG stator voltage to be 1|rpu| and its phase angle to be zero degrees. When referred to the power system level, the per unit value of the stator terminal voltage magnitude will be slightly greater than 1|pu| and the stator voltage phasor will have both the d-axis and q-axis components. All the resulting graphs and numerical values in this chapter are valid for the assumption that the q-axis components of the stator voltage equals zero and the d-axis component equals 1|rpu|. Analytical equations of $\overline{V}_r$, P_{absbyr}, Q_{absyr}, P_{deltot}, Q_{deltot} are derived as a function of slip, P_{delbys} and Q_{delbys}. The stator windings terminal voltage is defined as

$$\overline{V}_s = v_{sd} + j\, v_{sq} = 1 \text{ /rpu/} = 1\angle 0^0 \text{ /rpu/}$$

$$v_{sd} = 1 \text{ /rpu/} \qquad v_{sq} = 0 \text{ /rpu/} \tag{3.7}$$

With $v_{sq} = 0$, in equations (3.1) and (3.2), the stator current on d and q-axes results as $i_{sd} = \frac{P_{delbys}}{v_{sd}}$, and $i_{sq} = \frac{-Q_{delbys}}{v_{sd}}$, and the stator phase current results as

$$\bar{I}_s = \frac{P_{delbys}}{v_{sd}} - j\frac{Q_{delbys}}{v_{sd}}. \quad (3.8)$$

The d and q-axes components of the rotor voltage and current phasors are obtained as below using equations (2.44), (3.7), (3.8), and (2.45).

$$v_{rd} =$$

$$= \frac{-R_r R_s Q_{delbys} + R_r X_s P_{delbys} - sX_m^2 Q_{delbys} + sX_r v_{sd}^2 + sX_r R_s P_{delbys} + sX_s X_r Q_{delbys}}{X_m * v_{sd}}$$

$$v_{rq} = \frac{R_r v_{sd}^2 + R_r R_s P_{delbys} + X_s R_r Q_{delbys} + sX_m^2 P_{delbys} - sX_s X_r P_{delbys} + sX_r R_s Q_{delbys}}{X_m * v_{sd}}$$

$$i_{rd} = \frac{-R_s Q_{delbys} + X_s P_{delbys}}{X_m * v_{sd}}$$

$$i_{rq} = \frac{-v_{sd}^2 - R_s R_{delbys} - X_s Q_{delbys}}{X_m * v_{sd}}$$

Substituting the above equations in (3.3) and (3.4), the active and reactive powers absorbed by the rotor results as

$$P_{absbyr} = (R_r X_s^2 + R_r R_s^2 + sX_m^2 R_s)\frac{P_{delbys}^2}{X_m^2 v_{sd}^2} + (R_r X_s^2 + R_r R_s^2 + sX_m^2 R_s)\frac{Q_{delbys}^2}{X_m^2 v_{sd}^2} +$$

$$\left(R_r v_{sd}^2 + 2R_r R_s P_{delbys} + 2X_s R_r Q_{delbys} + sX_m^2 P_{delbys}\right)\frac{1}{X_m^2}, \text{ and} \quad (3.9)$$

$$Q_{absyr} = (-sX_m^2 X_s + sX_s^2 X_r + sX_r R_s^2)\frac{P_{delbys}^2}{X_m^2 v_{sd}^2} + (sX_r R_s^2 - sX_s X_m^2 + sX_s^2 X_r)\frac{Q_{delbys}^2}{X_m^2 v_{sd}^2} +$$

$$\left(sX_r v_{sd}^2 + sR_s X_r P_{delbys} + sX_r X_s Q_{delbys} - sX_m^2 Q_{delbys} + sR_s X_r P_{delbys} + \right.$$

$$\left. sX_r X_s Q_{delbys}\right)\frac{1}{X_m^2}. \quad (3.10)$$

Total active and reactive powers delivered to the grid (P_{deltot}, Q_{deltot}) are obtained substituting equations (3.9) and (3.10) into equations (3.5) and (3.6).

3.2.1.2. Analysis Using Graphs and the Analytical Expressions

Since the analytical equations for the rotor voltage ($\overline{V}_r$), rotor terminal powers (P_{absbyr}, Q_{absbyr}), and for the total terminal powers delivered to the grid (P_{deltot}, Q_{deltot}) derived above are function of three variables (P_{delbys}, Q_{delbys} and slip), the graphing and the corresponding analysis is done counting the dependence of these quantities on the three variables. For that purpose two cases are considered.

Case 1

The quantities V_r, P_{absbyr}, Q_{absbyr}, P_{deltot} and Q_{deltot}, are graphed with P_{delbys} and Q_{delbys} varied from -1.5 /rpu/ to 1.5 /rpu/, and value of slip chosen from the set {- 0.2, - 0.1, 0, + 0.1, + 0.2}. Graphing of all specified quantities as a function of variables within the range mentioned above is done by using the MATLAB software. Of all of the graphs, only two of them show the dependence of P_{deltot} and Q_{deltot} on P_{delbys}, Q_{delbys} and slip are shown in Figure 3.2. and Figure 3.3.

The analysis of the graphs obtained is divided into four different cases i.e., ($P_{delbys} > 0, Q_{delbys} > 0$), ($P_{delbys} > 0, Q_{delbys} < 0$), ($P_{delbys} < 0, Q_{delbys} > 0$) and ($P_{delbys} < 0, Q_{delbys} < 0$). The range of values attained by the rotor voltage ($\overline{V}_r$), active and reactive powers absorbed by the rotor (P_{absbyr}, Q_{absbyr}), total active and reactive powers delivered to the grid (P_{deltot}, Q_{deltot}) for five different values of slip i.e., (- 0.2,- 0.1, 0, + 0.1, + 0.2) and the four cases of P_{delbys} and Q_{delbys} mentioned above are tabulated and shown in the Appendix D. Below are few conclusions that are drawn looking to the graphs shown in Figures 3.2 and 3.3, and to the table in Appendix D

- The total active power delivered from the stator to the grid (P_{deltot}) is independent of the variation in reactive power delivered by the stator (Q_{delbys}).

- Similarly, the total reactive power delivered to the grid (Q_{deltot}) is independent of the variation in active power delivered by the stator (P_{delbys}).
- P_{deltot} has the same sign as P_{delbys}, i.e., $P_{deltot} > 0$ if $P_{delbys} > 0$, and $P_{deltot} < 0$ if $P_{delbys} < 0$. The sign of P_{deltot} depends only on P_{delbys} and it is independent of the slip variation.
- The range of total active and reactive powers delivered to the grid is widened when the slip value is negative.
- The active power is delivered by the rotor ($P_{absbyr} < 0$) only if the numerical value of the slip is negative and vice-versa.

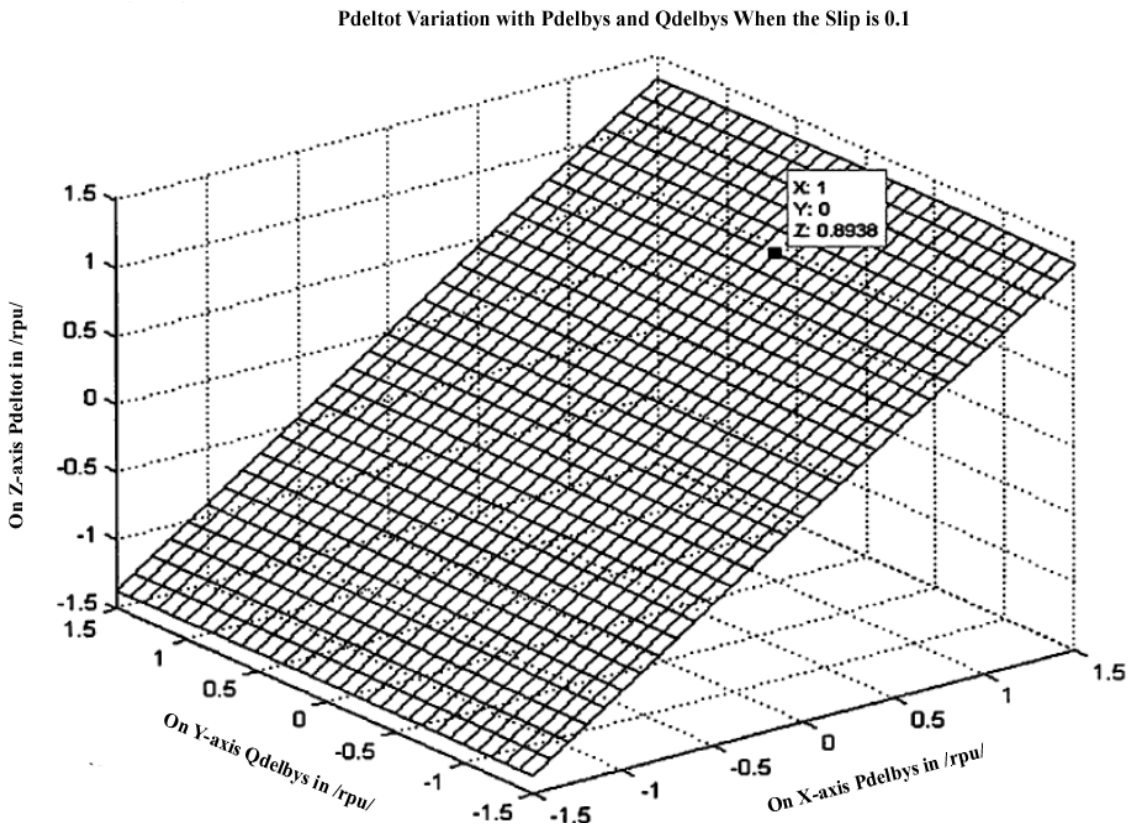

Figure 3.2. Dependence of the Total Active Power Delivered to the Grid with P_{delbys}, Q_{delbys} and Slip

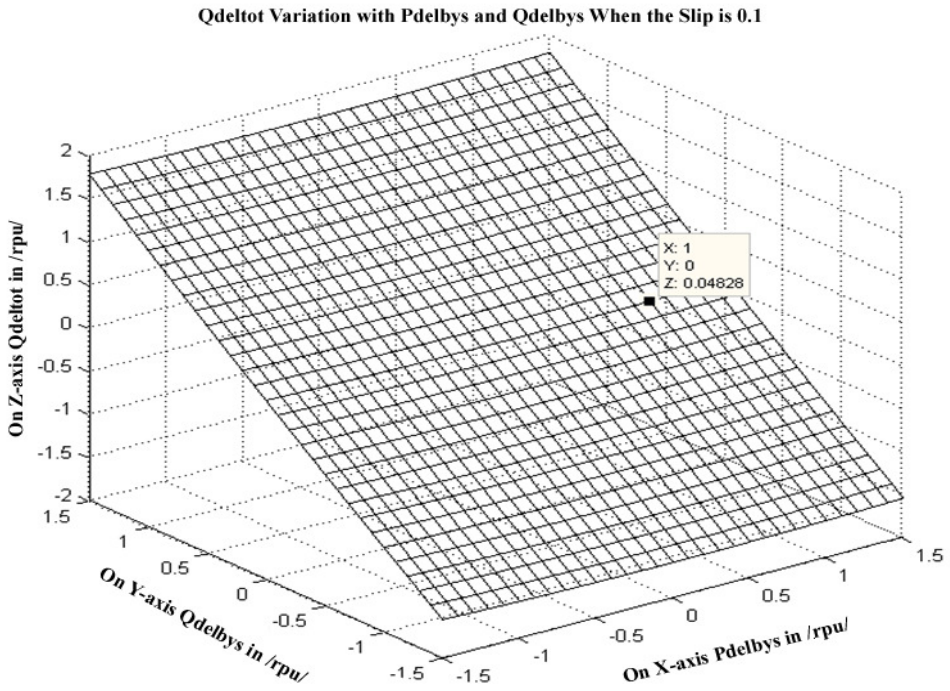

Figure 3.3. Dependence of theTotal Reactive Power Delivered to the Grid with P_{delbys}, Q_{delbys} and Slip

Case 2

The quantities V_r, P_{absbyr}, Q_{absbyr}, P_{deltot} and Q_{deltot} are graphed with the values of slip varied in the range of {- 0.2 to 0.2}, and by giving a specific set of values for P_{delbys} and Q_{delbys}, from the set {[$P_{delbys} = 1$ /rpu/, $Q_{delbys} = -0.5$ /rpu/], or [$P_{delbys} = 1$ /rpu/, Q_{delbys}= 0/rpu/], or [P_{delbys}=1 /rpu/, Q_{delbys}= 0.5 /rpu/], or [P_{delbys} =0.5 /rpu/, $Q_{delbys} = -0.5$ /rpu/], or [$P_{delbys} = 0.5$ /rpu/, $Q_{delbys} = 0$ /rpu/], or [$P_{delbys} = 0.5$ /rpu/, $Q_{delbys} = 0.5$ /rpu/]}. From the given set, only positive values of P_{delbys} were considered, that is the DFIG is assumed to operate as a generator. All the graphs used for the analysis are plotted using MATLAB software, but for reference only two are presented in Figure 3.4 and Figure 3.5.

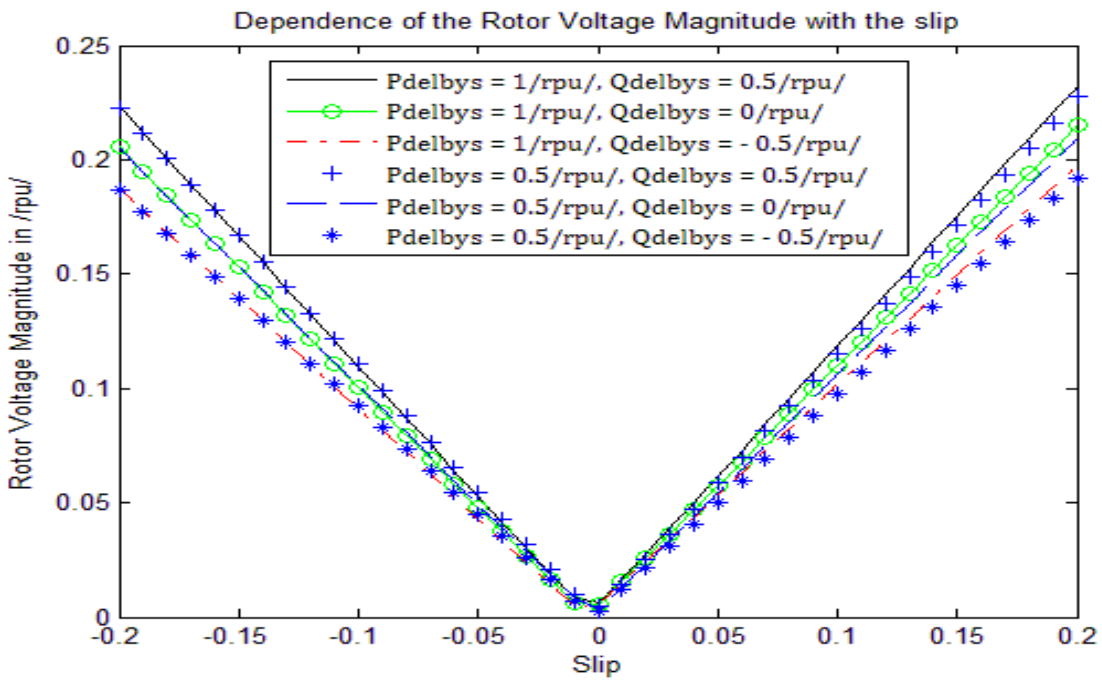

Figure 3.4. Dependence of the Rotor Voltage Magnitude with the slip

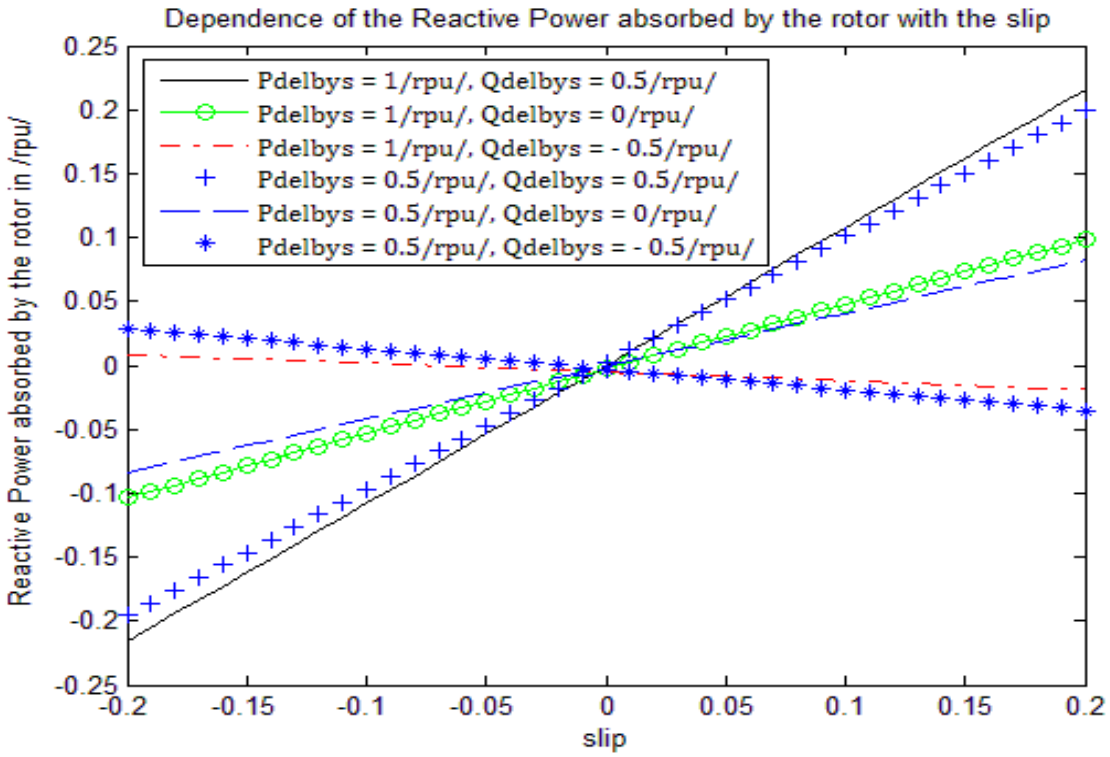

Figure 3.5. Dependence of the Reactive Power absorbed by the rotor with the Slip

Below are the conclusions that can be drawn from the graphs:

- The rotor voltage magnitude (V_r) practically has the same value for slip s = + a or s = - a. Hence V_r changes only when the absolute value of slip changes and the relationship between them is linear, i.e., as the absolute value of slip increases, the rotor voltage magnitude also increases and its mathematical relation can be expressed as $V_r = 1.65 * \text{abs (slip)}$.
- As the slip is varied from – 0.2 to 0, or from 0 to + 0.2, the rotor voltage magnitude V_r takes the values between 0 to + 0.23, i.e., $0 < V_r < + 0.23$ as shown in Figure 3.4.
- Active power absorbed by the rotor varies linearly with the variation in the slip and is influenced more by P_{delbys}. From the graphs it results that P_{absbyr} follows the relation $P_{absbyr} = P_{delbys}$*s. In order for the rotor to deliver active power, i.e., $P_{absbyr} < 0$, the value of the slip should be negative, since only positive values were considered for P_{delbys}.
- Reactive power absorbed by the rotor varies linearly with the variation in the slip and is influenced more by Q_{delbys}. From the graphs in Figure 3.5, it results that Q_{absbyr} follows the relation $Q_{absbyr} = (0.5 + 1.2*Q_{delbys})$*s. It is observed that to have $Q_{absbyr} < 0$, it is preferred to have the slip as negative.
- Total active power delivered to the grid varies linearly with the variation in the slip, and is influenced only by P_{delbys}. From the graphs it results that P_{deltot} = (1-s)* P_{delbys}. It is observed that to have P_{deltot} highest, slip s should be negative maximum.
- Total reactive power delivered to the grid varies linearly with the variation in the slip and is influenced only by Q_{delbys}. From the graphs, it results that $Q_{deltot} =$

$-0.5 * s + 0.25 * Q_{delbys}$. It is observed that to have Q_{deltot} positive, s should be negative.

3.2.2. Dependence of the DFIG Terminal Powers with the Slip and the Rotor Voltage

3.2.2.1. Derivation of the Analytical Expressions

Complex powers delivered by the stator and absorbed at the rotor terminals of the DFIG are defined as

$$\underline{S}_{delbys} = \overline{V}_s \bar{I}_s^* = P_{delbys} + j\, Q_{delbys}, \text{ and} \tag{3.11}$$

$$\underline{S}_{absbyr} = \overline{V}_r \bar{I}_r^* = P_{absbyr} + j\, Q_{absbyr}. \tag{3.12}$$

The relation between the stator and rotor current phasors shown in the above equations are derived using equations (2.44 & 2.45) in Chapter 2, Section 2.5, page 41, and result as:

$$\bar{I}_s = \frac{j\, X_m\, \overline{V}_r - [R_r + j\, s(X_{rl} + X_m)]\, \overline{V}_s}{[R_s R_r - sX_{sl}X_{rl} - sX_m(X_{sl} + X_{rl})] + j\, [sR_sX_{rl} + R_rX_{sl} + X_m(sR_s + R_r)]}, \text{ and} \tag{3.13}$$

$$\bar{I}_r = \frac{[R_s + j\, (X_{sl} + X_m)]\, \overline{V}_r - j\, sX_m \overline{V}_s}{[R_s R_r - sR_sR_r - sX_m(X_{sl} + X_{rl})] + j\, [sR_sX_{rl} + R_rX_{sl} + X_m(sR_s + R_r)]}. \tag{3.14}$$

Rationalizing the denominator of the current phasors and separating the real and imaginary parts, currents are defined as $\bar{I}_s = \frac{a + j\, b}{d}$ and $\bar{I}_r = \frac{e + j\, f}{d}$. With these current phasors, the stator voltage phasor as in equation (3.7), and the rotor voltage phasor as $\overline{V}_r = v_{rd} + j\, v_{rq}$, the complex powers can be expressed as

$$\underline{S}_{delbys} = \bar{I}_s^* = \left(\frac{a + j\, b}{d}\right)^* = \frac{a - j\, b}{d}, \text{ and}$$

$$\underline{S}_{absbyr} = (v_{rd} + j\, v_{rq}) \left(\frac{e + j\, f}{d}\right)^*.$$

Then the terminal active and reactive powers of the DFIG machine are as follows:

$$P_{delbys} = \frac{a}{d}, \tag{3.15}$$

$$Q_{delbys} = -\frac{b}{d}, \tag{3.16}$$

$$P_{absbyr} = \frac{v_{rd}e + v_{rq}f}{d}, \tag{3.17}$$

$$Q_{absbyr} = \frac{v_{rq}*e - v_{rd}*f}{d}, \tag{3.18}$$

$$P_{deltot} = \frac{a}{d} - \frac{v_{rd}e + v_{rq}f}{d}, \text{ and} \tag{3.19}$$

$$Q_{deltot} = -\frac{b}{d} - \frac{v_{rq}*e - v_{rd}*f}{d}. \tag{3.20}$$

Where

$$a = -R_s R_r^2 + sR_r X_r X_{sl} + sR_r X_m X_{rl} - R_s R_r X_m v_{rq} + sX_{sl} X_r X_m v_{rq} + sX_m^2 X_{rl} v_{rq} + R_r X_s X_m v_{rd} + sR_s X_r X_m v_{rd} - sR_r X_r X_s - s^2 R_s X_r^2,$$

$$b = R_r^2 X_s + sR_s R_r X_r + R_r X_s X_m v_{rq} + sR_s X_r X_m v_{rq} + R_s R_r X_m v_{rd} - sX_{sl} X_r X_m v_{rd} - sX_m^2 X_{rl} v_{rd} - sR_s R_r X_r + s^2 X_{sl} X_r^2 + s^2 X_m X_{rl} X_r,$$

$$e = R_r R_s^2 v_{rd} - sR_s X_{sl} X_r v_{rd} - sR_s X_m X_{rl} v_{rd} - R_s R_r X_s v_{rq} + sX_{sl} X_r X_s v_{rq} + sX_{rl} X_s X_m v_{rq} + R_s R_r X_s v_{rq} + sR_s^2 X_r v_{rq} + R_r X_s^2 v_{rd} + sR_s X_s X_r v_{rd} - s^2 R_s X_r X_m - sR_r X_s X_m,$$

$$f = R_r X_s^2 v_{rq} - sR_s^2 X_r v_{rq} + sR_s X_r X_s v_{rq} + R_s^2 R_r v_{rq} - sR_s X_{sl} X_r v_{rq} - sR_s X_{rl} X_m v_{rq} - sX_m X_{rl} X_s v_{rd} - sX_{sl} X_r X_s v_{rd} - sR_s R_r X_m + s^2 X_{sl} X_r X_m + s^2 X_m^2 X_{rl}, \text{and}$$

$$d = (R_s R_r - sX_{sl} X_r - sX_m X_{rl})^2 + (R_r X_s + sR_s X_r)^2.$$

3.2.2.2 Analysis using Graphs and Analytical Expressions

In the last analytical equations derived above, the stator and rotor terminal active and reactive powers are defined in terms of the rotor voltage components (v_{rd}, v_{rq}) and the slip.

The graphing of terminal powers of the DFIG is done by using the MATHEMATICA software. Study of the stator and rotor terminal powers dependence with slip, v_{rd} and v_{rq} is done in two different cases.

Case 1

Graphs of P_{delbys}, Q_{delbys}, P_{absbyr}, $Q_{absbyr,}$ P_{deltot}, Q_{deltot} are plotted for $v_{rd} = 0$ /rpu/, with the slip varied from – 0.2 to 0, and from 0 to + 0.2, and v_{rq} varied between - 0.16 /rpu/ to 0.28/rpu/, in steps of 0.04. For reference, only the graphs of P_{delbys} and Q_{absbyr} are shown in Figures 3.6 and 3.7.

Observing the graphs and by using the analytical equations (3.15 – 3.20), the following conclusions are drawn:

- For the slip in the range of - 0.03 < s < 0, and 0 < s < + 0.03, the active power delivered by the stator (P_{delbys}) increases as the slip magnitude increases. For slip values above 0.03 and below - 0.03, i.e., (s > +0.03 or s< -0.03), P_{delbys} decreases as the slip value increases as shown in Figure 3.6.
- For v_{rq} < 0 and slip s > 0, the reactive power delivered by the stator (Q_{delbys}) decreases as the slip increases. For v_{rq} > 0 and slip s > 0 the reactive power delivered by the stator (Q_{delbys}) increases as the slip increases.
- For slip s > 0, the active power absorbed by the rotor (P_{absbyr}) decreases as the slip increases, and increases as the slip decreases.
- As shown in Figure 3.7, the numerical value of the reactive power absorbed by the rotor (Q_{absbyr}) is positive when slip is positive and vice-versa.
- Maximum total active and reactive powers are delivered to the grid when the active and reactive powers absorbed by the rotor are kept to minimum.

- The total maximum active power is delivered to the grid when the slip of the DFIG is s = 0.2712 and the q-axis component of the rotor voltage is $v_{rq} = -0.6223/\text{rpu}/$. This is obtained by simultaneously solving the derivatives of the equations (3.17) and (3.19), and imposing them to be zero.
- The maximum total reactive power is delivered to the grid when the slip of the DFIG and the q-axis component of the rotor voltage (v_{rq}) are s = 0.0270 $v_{rq} = -0.5019/\text{rpu}/$ or s = − 0.00004 and $v_{rq} = -0.9794\ /\text{rpu}/$, or s = − 0.0301 and $v_{rq} = -0.4757\ /\text{rpu}/$. These values are obtained by simultaneously solving the derivatives of the equations (3.18) and (3.20), and imposing them to be zero.

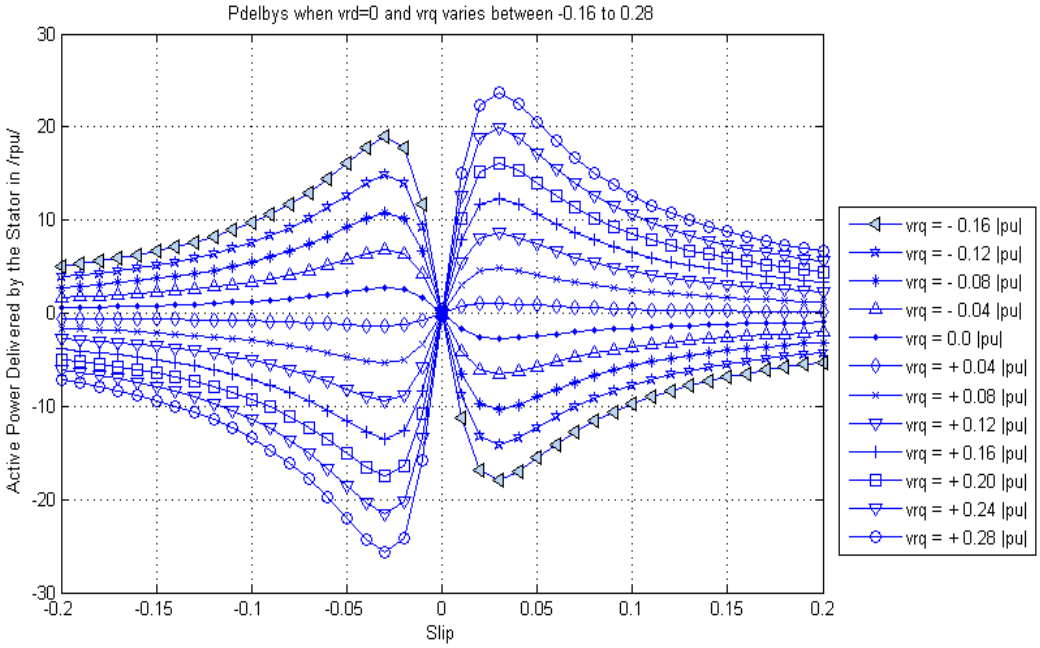

Figure 3.6. Variation of P_{delbys} with Slip and v_{rq}

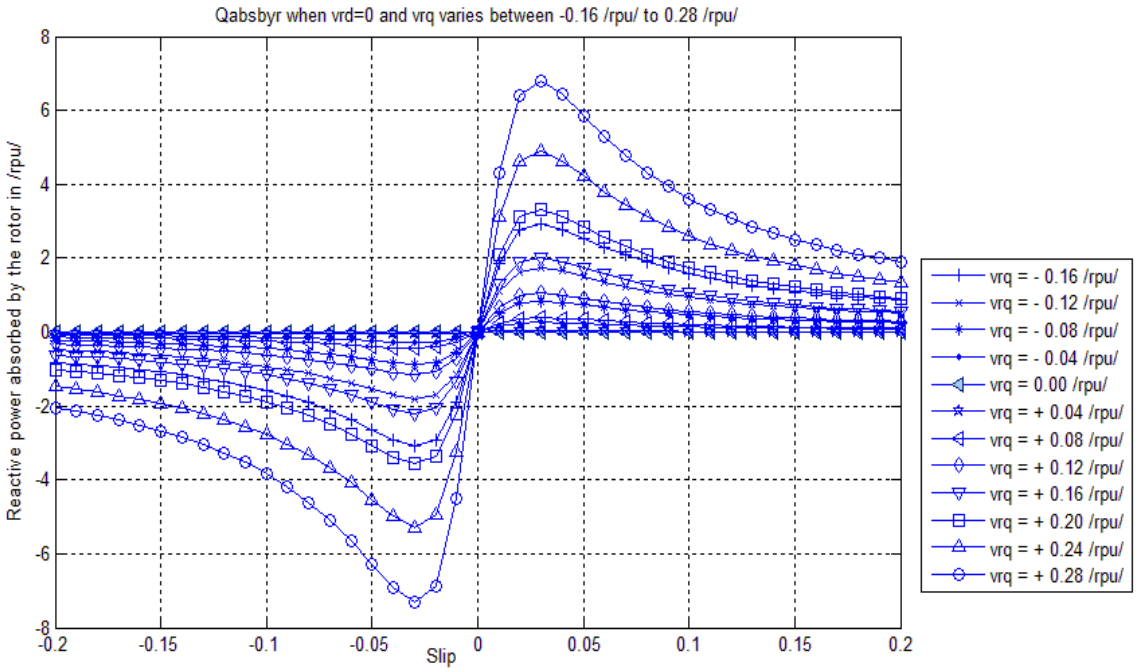

Figure 3.7. Variation of Q_{absbyr} with Slip and v_{rq}

Case 2

Graphs of P_{delbys}, Q_{delbys}, P_{absbyr}, $Q_{absbyr,}$ P_{deltot}, Q_{deltot} are plotted for $v_{rq} = 0$, slip varied from – 0.2 to 0, and from 0 to + 0.2, and v_{rd} varied from - 0.1 /rpu/ to + 0.1 /rpu/ in steps of 0.02. For reference, only the graphs showing the dependence of P_{delbys} and Q_{absbyr} with the slip and v_{rq} are shown in Figures 3.8 and 3.9.

From the analysis of the graphs and the numerical data recorded it results that:

- Active power delivered by the stator is positive only if d-axis component of the rotor voltage is less than + 0.02. And also for v_{rd} < + 0.02 and slip s > 0, P_{delbys} increases as the slip increases as seen in Figure 3.8.
- For slip values in the range of - 0.03 < s < 0 and 0 < s < + 0.03, the reactive power delivered by the stator (Q_{delbys}) increases as the slip magnitude increases. For slip values above 0.03 and below - 0.03, i.e., (s > + 0.03 or s < - 0.03), Q_{delbys} decreases as the slip magnitude increases.

- For slip s > 0, the active power absorbed by the rotor (P_{absbyr}) decreases as the slip increases, and increases as the slip decreases.
- As seen in Figure 3.9, the numerical value of the reactive power absorbed by the rotor (Q_{absbyr}) is positive when the slip is positive and vice-versa.
- The maximum active power is delivered to the grid when the slip and the d-axis rotor voltage component are $s = -0.0012$ and $v_{rd} = 0.4890$ /rpu/. This is obtained by simultaneously solving the derivatives of equations (3.17) and (3.19), and forcing them to zero.
- The maximum reactive power is delivered to the grid when the slip and the d-axis rotor voltage component (v_{rd}) are $s = 0.0270$ and $v_{rd} = 0.5019$ /rpu/, or $s = -0.0301$ and $v_{rd} = 0.47567$ /rpu/. These values are obtained by simultaneously solving the derivatives of equations (3.18) and (3.20), and forcing them to zero.

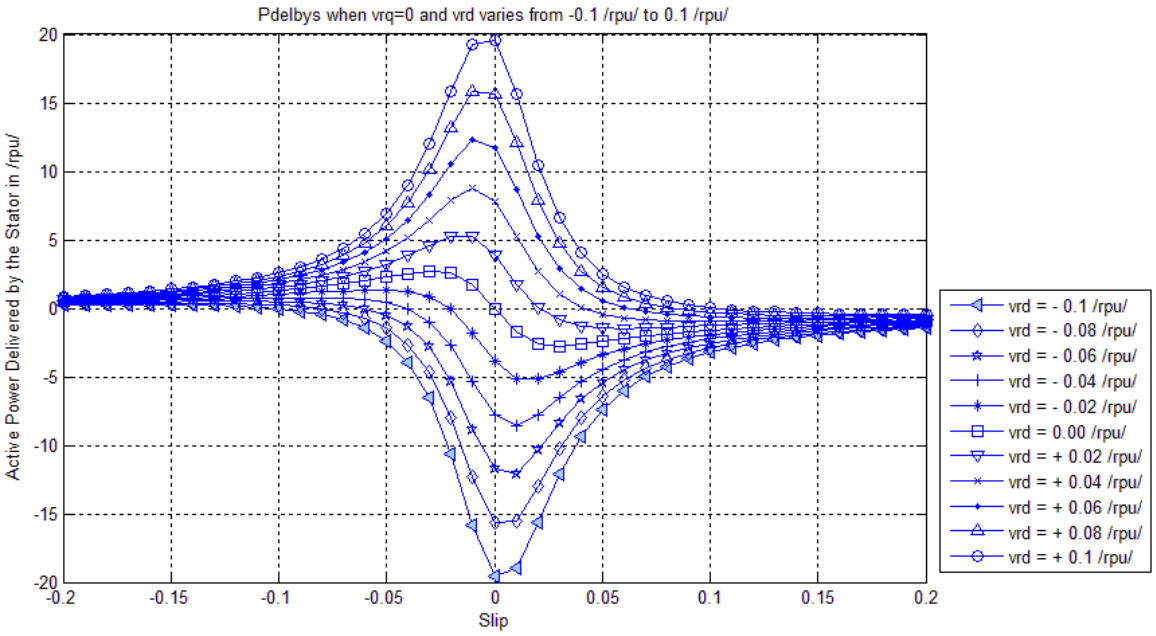

Figure 3.8. Variation of P_{delbys} with Slip and v_{rd}

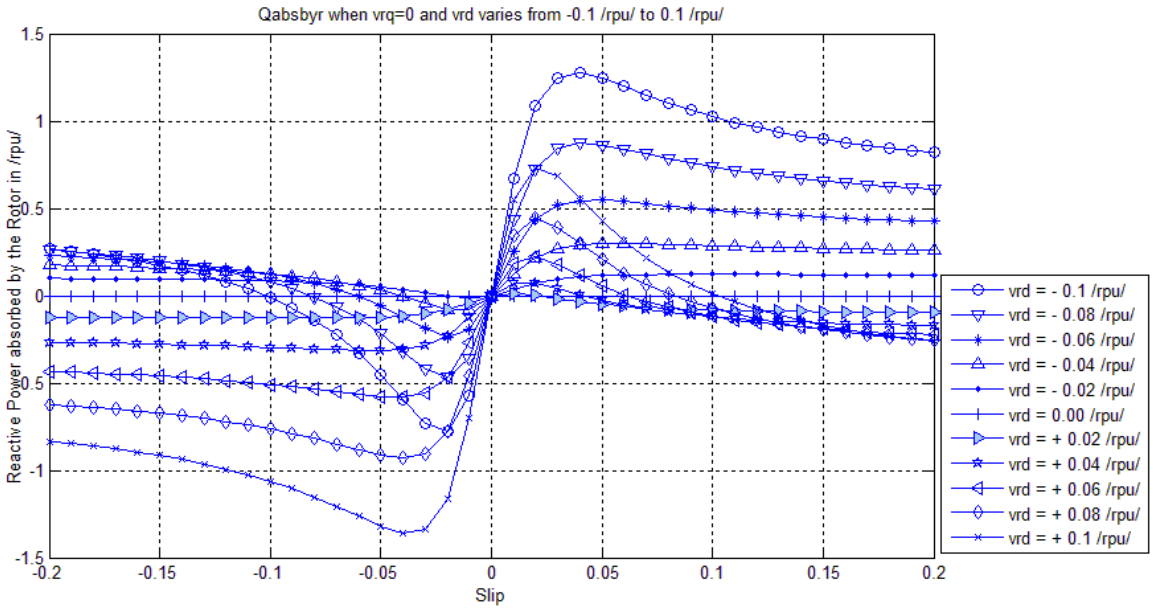

Figure 3.9. Variation of Q_{absbyr} with Slip and v_{rd}

3.2.2.3 Conclusions

It is observed that the d and q axes components of the rotor voltage have significant individual effects on active and reactive power of the rotor, the same as the results shown on [22], [23]. The rotor reactive power can either be absorbed or delivered, depending on the combination of v_{rd} and v_{rq}. If the slip is positive, for the DFIG to supply reactive power to the grid, the rotor voltage d-axis component should be greater compared to the rotor voltage q-axis component. If the slip is negative, for the DFIG to supply reactive power to the grid the rotor voltage q-axis component should be greater than the rotor voltage d-axis component. This result is helpful for decoupled control of active and reactive powers of the DFIG machine during faults, as shown in Chapter 5. The applied rotor voltage can shift the DFIG in generating mode from over-synchronous to under-synchronous speed range that helps improving the stability of the DFIG.

It can be concluded that the stator and rotor terminal powers depend on the combination of the slip, v_{rd} and v_{rq}. In the DFIG machine the active power should always be delivered to

the grid irrespective of slip being positive or negative, which can be achieved by applying specific values of the rotor voltage d and q-axes components at the rotor terminals of the DFIG. The values of the rotor voltage components that need to be applied across the rotor terminals of the DFIG are calculated by using equations (3.15 - 3.20).

3.3. Case Study of the Vestas V90 DFIG Wind Turbine

3.3.1. Snyder Wind Farm in Texas

Snyder wind farm is an onshore wind farm developed by WKN AG, and is being operated by Enel Green Power since Dec 2010. The yearly estimated production of this wind farm is 155 |GWh|.

Snyder wind farm consists of 21 Vestas V90 DFIG 3|MW| wind turbines accounting for a total capacity of 63 |MW| [24]. These wind turbines use a Doubly Fed Induction Generator (DFIG) and variable speed generation concept illustrated in Figure 1.7, page 15, Chapter1. Few Vestas V90 turbines were tested and the recorded data was documented in 2004. This general specifications data released by the R&D department is used for the case study. The transient characteristics of this Vestas V90 DFIG are analyzed in Chapter 5 of this thesis.

3.3.2 General Specifications of Vestas V90 DFIG

Vestas V90 wind turbine houses the DFIG which has the machine model shown in Chapter 2, and hence the interdependence of the DFIG machine variables will be same as those shown in Section 3.2 of this Chapter. The general specifications of Vestas V90 DFIG wind turbines used in the Snyder wind farm are given in [25]. The data on pages 25, 26 and 28 of the general specifications document that are used in this section are shown below,

Rated Frequency: 60 |Hz|

Rated Power: 3.0 |MW|

Type: Asynchronous with wound rotor, slip rings

Voltage: 1000 VAC

No of poles of DFIG: 4

Rated Speed: 1758 |rpm|

Speed of the wind turbine rotor: 16.1284 |rpm|

Diameter of the Rotor: 90 |m|

Gear Box Ratio: 1:109

Rated power factor, default at 1000 V: 1.0

Stator synchronous speed, $n_s = \frac{60*f_s}{p_p} = \frac{60*60}{2} = 1800$ |rpm|, given rated speed $n_r =$ 1758|rpm|.

So, the rated slip of the DFIG machine is $s = \frac{n_s - n_r}{n_s} = 1800 = \frac{1800-1758}{1800} = 0.023\overline{3}$.

Base voltage and base power of the DFIG are chosen from the rated data of the machine i.e., $V_b = 1000$ |V| and $S_b = 3$ |MVA|.

3.3.3. Possible Versions of Power Flow Through the DFIG Stator and Rotor

Since in the rated data of the Vestas V90 DFIG it is not specified, if the 3 |MW| corresponds to the active power delivered by the stator or the total active power delivered to the grid, two possible versions of how the active and reactive powers flow through the DFIG stator and rotor are described below.

Version 1

With the Vestas V90 DFIG rated data, imposing the conditions that $s = 0.023\overline{3}$, $P_{delbys} = 1$ /rpu/ and $Q_{delbys} = 0$ /rpu/ in the analytical expressions (3.15 - 3.16), the d and q-axes components of the rotor voltage across the rotor winding terminals of the DFIG results as $v_{rd} = 0.0293$ /rpu/ and $v_{rq} = 0.00273$/rpu/. With these rotor voltage components, the

absorbed active and reactive powers at the rotor and total active and reactive powers delivered to the grid, calculated by using equations (3.17- 3.20), are

$P_{absbyr} = 0.0291$ /rpu/, $Q_{absbyr} = 0.0113$ /rpu/, $P_{deltot} = 0.9709$ /rpu/, and

$Q_{deltot} = -0.0113$ /rpu/.

Figure 3.10 shows Version 1 of the active and reactive power flow through the stator and rotor terminals of the DFIG.

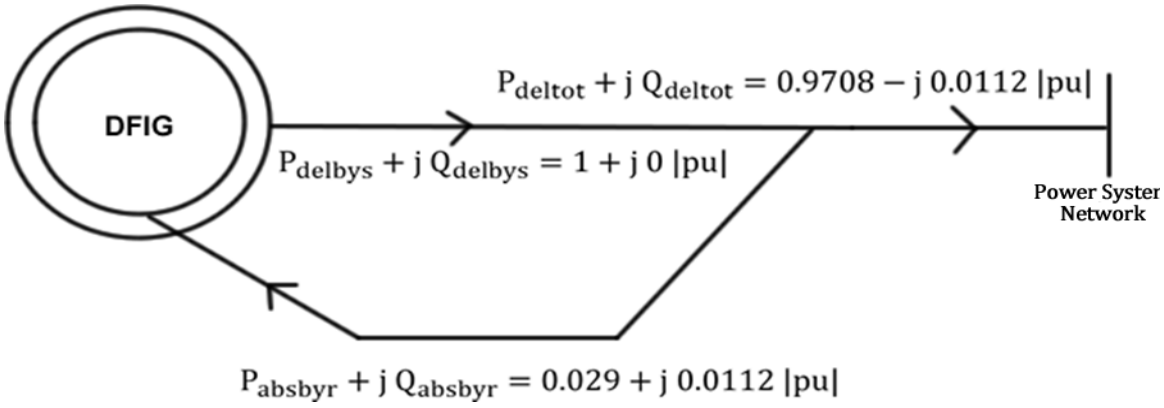

Figure 3.10. Version 1 of Active and Reactive Power Flow through the DFIG

Version 2

By imposing the conditions that s = $0.023\overline{3}$, $P_{deltot} = 1$/rpu/ and $Q_{delbys} = 0$ /rpu/ in the analytical equations (3.15 – 3.16), the d and q axes components of the rotor voltage across the rotor winding terminals of the DFIG results as $v_{rd} = 0.0294$ /rpu/ and $v_{rq} = 0.00285$ /rpu/. With these rotor voltage components, the absorbed active and reactive powers at the rotor and the active and reactive power delivered by the stator calculated using equations (3.15 - 3.20) are

$P_{absbyr} = 0.0301$ /rpu/, $Q_{absbyr} = 0.0115$ /rpu/,

$P_{delbys} = 1.0301$ /rpu/, and $Q_{delbys} = 0$ /rpu/.

Figure 3.11 shows Version 2 of the active and reactive power flow through the stator and rotor terminals of the DFIG.

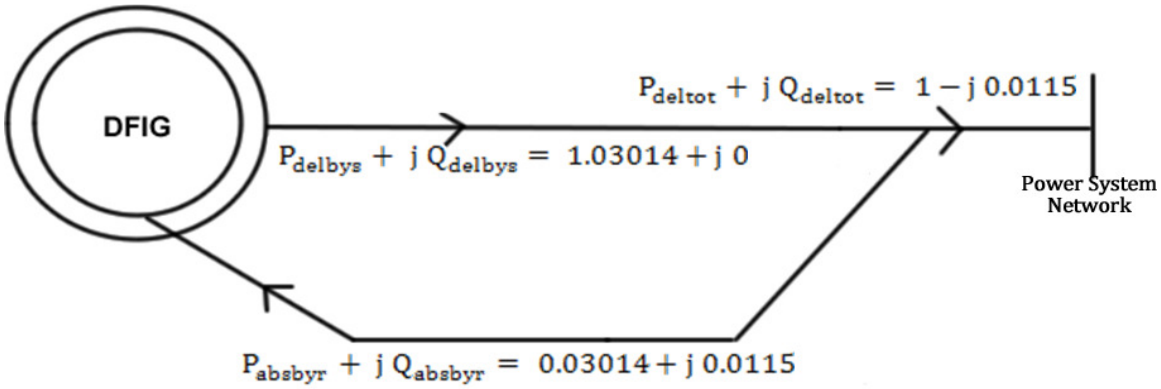

Figure 3.11. Version 2 of the Active and Reactive Power Flow through the DFIG

3.3.4. Power Flow Diagram of Vestas V90 Wind Turbine

The power flow diagram of the Vestas V90 wind turbine is necessary as the numerical results, such as mechanical power and the power coefficient (Cp), are used for transient analysis of the DFIG in Chapter 5, and are also required as inputs for the simulations done in Chapter 6. From the National Oceanic and Atmospheric Administration (NOAA) website, the average wind speed at Synder, Texas wind farm site is considered to be 15m/s [25]. Version 2 of the active and reactive power flow through the DFIG stator and rotor shown in Figure 3.11 is considered, where the total active power delivered to the grid through the power system network is 1 /rpu/ i.e., $P_{deltotgrid} = 1$ /rpu/, or 3|MW|. A value of 2.995 |MW| taken from the reference [25] is the active power delivered to the grid through the power system network before the step up transformer as shown in Figure 3.12. Hence, the efficiency of the transformer is obtained as

$$\eta_{tr} = \frac{P_{grid}^{|KW|}}{P_{deltotgrid}^{|KW|}} = \frac{2995}{3000} = 0.998\bar{3}$$

Losses of the DFIG estimated are 1.5 %, which is divided as 0.5% mechanical and 1% electrical losses. The losses in the power electronic converter are estimated to be 0.65%.

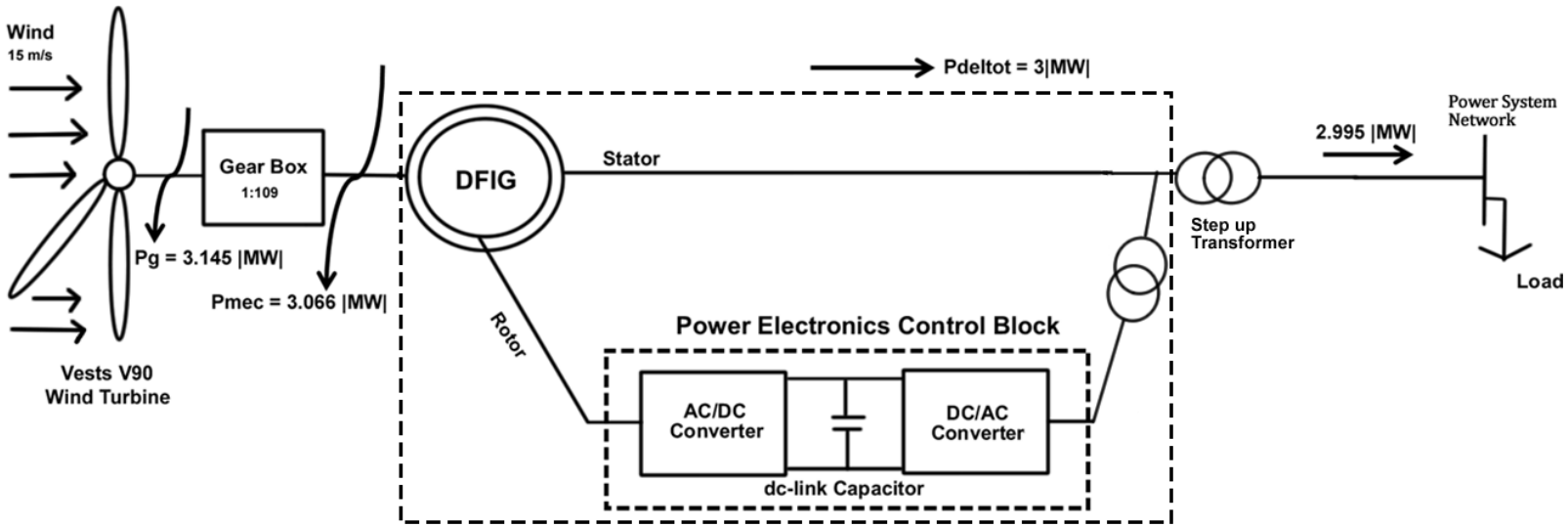

Figure 3.12. Active Power Flow Diagram of a Vestas V90 Wind Turbine

These values are taken from an article about the efficiency of wind turbines [27]. Hence the input mechanical power supplied to the DFIG results as

$$P_{mec} = \frac{P_{deltotgrid}^{|MW|}}{\eta_{DFIGsystem}} = \frac{3.0000}{(1-(0.015+0.0065))} = 3.0659\ |MW|.$$

Since, the gear box losses are around 2.5%, the power available from the wind is

$$P_g = \frac{P_{mec}^{|MW|}}{\eta_{gearbox}} = \frac{3.0659}{(1-0.025)} = 3.1445\ |MW|.$$

Power Coefficient C_P

This section verifies that it is possible to produce $P_g = 3.145\ |MW|$ as shown in Figure 3.12, with Vestas V90 wind turbine installed in Snyder, Texas, at an average wind speed of 15m/s with an achievable value of power coefficient (C_P). Power coefficient C_P gives measure of the total amount of power that can be extracted from the wind to the total power available in wind. Theoretically no wind turbine can capture more than 59.3% of the kinetic energy present in the wind, and its called as Betz's law. Betz's limit is an idealization, and a C_P value of 35 percent is the realistic design goal for a workable wind turbine [28]. This value is further reduced due to the intermittency factor associated with the wind. The relation between the wind speed and the power output of the wind turbine is

$$P_g = \frac{1}{2}\,\rho\,\pi\,r^2 C_P V^3.$$

Where

P_g = Output power (watts) = 3.1630 |MW|,

r = Radius of the wind turbine rotor (m) taken from [24] = 45 |m|,

V = Velocity of wind (m/s) = 15 |m/s|,

ρ = Density of air (kg/m^3) = 1.225 | kg/m^3|, and

C_P = Coefficient of performance or Betz limit

$$\text{Therefore, } C_P = \frac{P_g}{\frac{1}{2}\rho\,\pi\,r^2V^3} \cong 0.24$$

Alternative method for calculation of C_P

The power Coefficient C_P can be determined by using the general specifications of the Vestas V90 wind turbine or from the λ - C_P curves. Tip speed ratio λ is a non-dimensional factor that characterizes the relation between wind speed and the rate of rotation of the rotor.

$$\lambda = \frac{\text{speed of the rotor tip}}{\text{wind speed}} = \frac{\omega * r}{V},$$

V = velocity of the wind speed in |m/s|,

r = radius of the wind turbine rotor |m|, and

$\omega = 2\,\pi\,f$ = angular velocity of the wind turbine rotor in |radians/sec|.

If the rotor runs too slow most of the wind escapes between the openings of the blades and results in low power extraction. On the other hand if it runs too fast the rotating blades acts as a solid disc blocking the wind, again reducing the power extraction. As it is required to match the rotor angular velocity to the wind speed, the wind turbines must be designed to run at an optimum tip speed ratio to extract as much power as possible from the wind stream. Wind tip ratios depend on the particular wind turbine design used, the rotor airfoil profile, and also the number blades of the rotor.

Rated speed of the wind turbine is 16.1284 |rpm| and radius of the rotor blades is 45 |m|. Wind speed at Amarillo, Texas is 15m/s. Hence, the tip speed ratio of the wind turbine is

$$\lambda = \frac{\omega\,r}{V} = \frac{2\,\pi\frac{16.1284}{60} * 45}{15} = 5.06688.$$

From the λ - C_P curves in [29], the approximate value of C_P is 0.24 corresponding to the λ value calculated above. This value of C_P is identical to the one calculated using a different

method. This is done for the verification of the values taken from Vestas V90 wind turbine and assumptions made.

CHAPTER 4

DFIG Control Using Back to Back Converter

The power electronic AC-DC-AC converter system shown in Figure 1.7, page 15, Chapter 1 is the most common configuration used to interface the variable speed DFIG wind turbines to the grid. This power electronic converter system is also called as the back-to-back Voltage Source Converter (VSC) configuration. Few of the advantages of the Back-to-Back Converters (BBC) are 1) it is a well established technology and many manufacturers produce components especially designed for the BBC's 2) decoupling of the two VSC's through a capacitor allows for individual control of both the rotor-side and grid-side converters, as explained in Section 4.4 and 4.5 of this chapter.

4.1 Configuration of the Back-to-Back Converter

The back-to-back converter configuration shown in Figure 4.1 is a bidirectional power electronic IGBT converter consisting of two voltage source converters connected back-back. It consists of a three-phase controlled rectifier and a three-phase controlled inverter, coupled through a capacitor, called the dc link. Since, the back-to-back converter configuration is implemented with the variable-speed DFIG, the rectifier is also called as the Grid-Side Converter (GSC), and the inverter is also called as the Rotor-Side Converter (RSC).

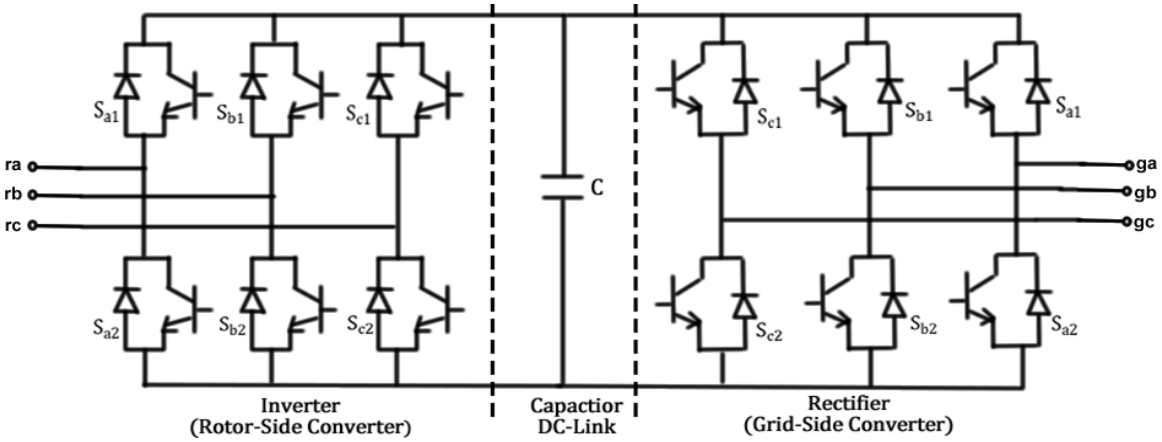

Figure 4.1. Configuration of the Back-to-Back Converter

4.1.1. Model of the Back-to-Back Converter in Phasor Domain

An average model is used to derive the equations of the BBC configuration in phasor domain. Based on the average model, a switch can be replaced by its equivalent circuit [30]. By using the average model of the switch, the equivalent circuit of the BBC is shown in Figure 4.2. The matricial form of the time-domain equations for the BBC can be expressed as follows:

$$[v]_{\mathrm{gph}} = [\mathrm{R}]_{\mathrm{grec}}[i]_{\mathrm{oph}} + [\mathrm{L}]_{\mathrm{grec}}\left[\frac{\mathrm{d}i}{\mathrm{dt}}\right]_{\mathrm{oph}} + [v]_{\mathrm{oph}}, \text{ and} \tag{4.1}$$

$$[v]_{\mathrm{rph}} = -[\mathrm{R}]_{\mathrm{rinv}}[i]_{\mathrm{iph}} - [\mathrm{L}]_{\mathrm{rinv}}\left[\frac{\mathrm{d}i}{\mathrm{dt}}\right]_{\mathrm{iph}} + [v]_{\mathrm{iph}}. \tag{4.2}$$

And the time-domain equations for current through the capacitor are

$$\mathrm{C}\frac{\mathrm{d}v_{\mathrm{dc}}}{\mathrm{dt}} = (\mathrm{S}_1 i_{\mathrm{oa}} + \mathrm{S}_2 i_{\mathrm{ob}} + \mathrm{S}_3 i_{\mathrm{oc}}) - (\mathrm{S}_4 i_{\mathrm{ia}} + \mathrm{S}_5 i_{\mathrm{ib}} + \mathrm{S}_6 i_{\mathrm{ic}}), \text{ and} \tag{4.3}$$

$$i_{\mathrm{dc}} = i_{\mathrm{oa}} - i_{\mathrm{ia}}, \tag{4.4}$$

where, $[v]_{\mathrm{gph}} = \begin{bmatrix} v_{\mathrm{ga}} \\ v_{\mathrm{gb}} \\ v_{\mathrm{gc}} \end{bmatrix}$, $[v]_{\mathrm{rph}} = \begin{bmatrix} v_{\mathrm{ra}} \\ v_{\mathrm{rb}} \\ v_{\mathrm{rc}} \end{bmatrix}$, $[v]_{\mathrm{oph}} = \begin{bmatrix} v_{\mathrm{oa}} \\ v_{\mathrm{ob}} \\ v_{\mathrm{oc}} \end{bmatrix}$, $[v]_{\mathrm{iph}} = \begin{bmatrix} v_{\mathrm{ia}} \\ v_{\mathrm{ib}} \\ v_{\mathrm{ic}} \end{bmatrix}$,

$[i]_{\mathrm{oph}} = \begin{bmatrix} i_{\mathrm{oa}} \\ i_{\mathrm{ob}} \\ i_{\mathrm{oc}} \end{bmatrix}$, $[i]_{\mathrm{iph}} = \begin{bmatrix} i_{\mathrm{ia}} \\ i_{\mathrm{ib}} \\ i_{\mathrm{ic}} \end{bmatrix}$, $[\mathrm{R}]_{\mathrm{grec}} = \mathrm{R}_{\mathrm{grec}}[1]_{3\mathrm{x}3}$, $[\mathrm{L}]_{\mathrm{grec}} = \mathrm{L}_{\mathrm{grec}}[1]_{3\mathrm{x}3}$,

$[\mathrm{R}]_{\mathrm{rinv}} = \mathrm{R}_{\mathrm{rinv}}[1]_{3\mathrm{x}3}$, $[\mathrm{L}]_{\mathrm{rinv}} = \mathrm{L}_{\mathrm{rinv}}[1]_{3\mathrm{x}3}$ and $\mathrm{S}_1, \mathrm{S}_2, \mathrm{S}_3, \mathrm{S}_4, \mathrm{S}_5, \mathrm{S}_6$ symbolically describe the converters switching states.

A more detailed explanation of the matrices is shown in Appendix C, pages (127-131).

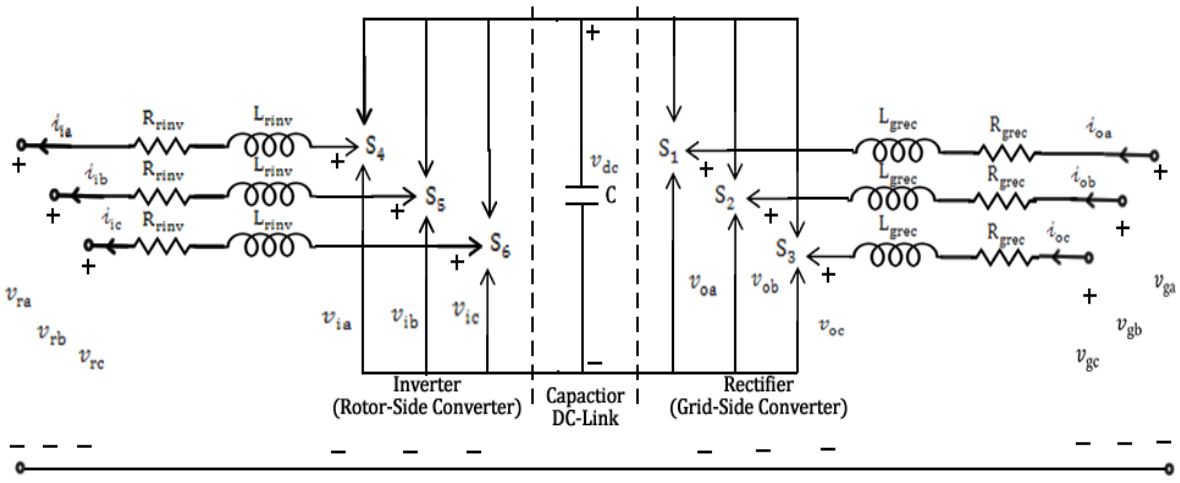

Figure 4.2. Equivalent Circuit of the Back-to-Back Converter [30]

4.1.2. Model of the Back-to-Back Converter in dqo Reference Frame

Both the grid-side rectifier and rotor-side inverter phasor domain equations are converted to dqo reference frame using the transformation matrices shown below,

$$[\mathrm{T}]_{\mathrm{rinv}} = \sqrt{\frac{2}{3}} * \begin{bmatrix} \cos(\theta_{\mathrm{dinv}}) & \cos(\theta_{\mathrm{dinv}} - 120^0) & \cos(\theta_{\mathrm{dinv}} - 240^0) \\ -\sin(\theta_{\mathrm{dinv}}) & -\sin(\theta_{\mathrm{dinv}} - 120^0) & -\sin(\theta_{\mathrm{dinv}} - 240^0) \\ \frac{1}{\sqrt{2}} & \frac{1}{\sqrt{2}} & \frac{1}{\sqrt{2}} \end{bmatrix}, \text{ and}$$

$$[\mathrm{T}]_{\mathrm{grec}} = \sqrt{\frac{2}{3}} * \begin{bmatrix} \cos(\theta_{\mathrm{drec}}) & \cos(\theta_{\mathrm{drec}} - 120^0) & \cos(\theta_{\mathrm{drec}} - 240^0) \\ -\sin(\theta_{\mathrm{drec}}) & -\sin(\theta_{\mathrm{drec}} - 120^0) & -\sin(\theta_{\mathrm{drec}} - 240^0) \\ \frac{1}{\sqrt{2}} & \frac{1}{\sqrt{2}} & \frac{1}{\sqrt{2}} \end{bmatrix}.$$

This dqo transformation has the same advantages explained in Chapter 2, Section 2.3.4. The chosen dqo reference frame for the rotor-side inverter rotates with the angular frequency of the rotor and the dqo reference frame of the grid-side rectifier rotates with the angular frequency of the stator. θ_{dinv} is the angle between the rotor-side inverter d-axis and the stator phase "a" axis. θ_{drec} is the angle between the grid-side rectifier and the stator phase "a" axis. Therefore equations of the BBC equivalent circuit in dqo reference frame are obtained as below,

$$[v]_{\mathrm{gdq}} = [\mathrm{R}]_{\mathrm{grec}}[i]_{\mathrm{odq}} + [\mathrm{L}]_{\mathrm{gdq}}\left[\frac{\mathrm{d}i}{\mathrm{d}t}\right]_{\mathrm{odq}} + [v]_{\mathrm{odq}}, \tag{4.5}$$

$$[v]_{\mathrm{rdq}} = -[\mathrm{R}]_{\mathrm{rinv}}[i]_{\mathrm{idq}} - [\mathrm{L}]_{\mathrm{rinv}}\left[\frac{\mathrm{d}i}{\mathrm{dt}}\right]_{\mathrm{idq}} + [v]_{\mathrm{idq}}, \text{ and} \tag{4.6}$$

$$\frac{\mathrm{d}v_{\mathrm{dc}}}{\mathrm{dt}} = \frac{3}{4}\frac{\mathrm{A_{mo}}}{\mathrm{C}} i_{\mathrm{od}} \cos(\alpha_{\mathrm{mo}} - \alpha_{\mathrm{drec}}) + \frac{3}{4}\frac{\mathrm{A_{mo}}}{\mathrm{C}} i_{\mathrm{oq}} \sin(\alpha_{\mathrm{mo}} - \alpha_{\mathrm{drec}}) - \frac{3}{4}\frac{\mathrm{A_{mi}}}{\mathrm{C}} i_{\mathrm{id}} \cos(\alpha_{\mathrm{mi}} - \alpha_{\mathrm{dinv}}) + \frac{3}{4}\frac{\mathrm{A_{mi}}}{\mathrm{C}} i_{\mathrm{iq}} \sin(\alpha_{\mathrm{mi}} - \alpha_{\mathrm{dinv}}). \tag{4.7}$$

A more detailed explanation for the derivation of equations of the rectifier and inverter in dqo reference frame is shown in APPENDIX C, in pages (127-131) using [30].

4.2. Classification and Description of the DFIG Control Strategies

There are a number of control strategies that can be implemented with the variable-speed DFIG wind turbines. The selection of a particular type of control strategy depends on the operating conditions of the wind turbine, efficiency, cost and other factors. This section categorizes the control strategies that can be used with the variable speed wind turbines, and explains in detail the control strategies that are considered to be implemented with the Vestas V90 DFIG wind turbine. Also, the wind turbine library block used for simulations in chapter 6 in the Matlab/Simulink software implements the control strategies described in this chapter.

4.2.1. Classification of the Control Strategies

Control strategies implemented with the variable-speed DFIG wind turbines can be classified into one of the three control levels shown in Figure 4.3 [31].

Control Level I

This control level is termed as rotor and grid side control as it regulates the active and reactive powers exchanged between the DFIG and the grid

- The rotor-side converter is controlled in such a way that it provides independent control of the stator active and reactive powers.

- The grid-side converter provides a decoupled control of active and reactive power flowing between the converter and the grid.
- The grid-side converter is controlled to maintain the DC bus voltage constant and to provide a path for rotor power to and from the AC system at unity power factor.
- The crowbar circuit protects the rotor side converter when a voltage dip occurs.

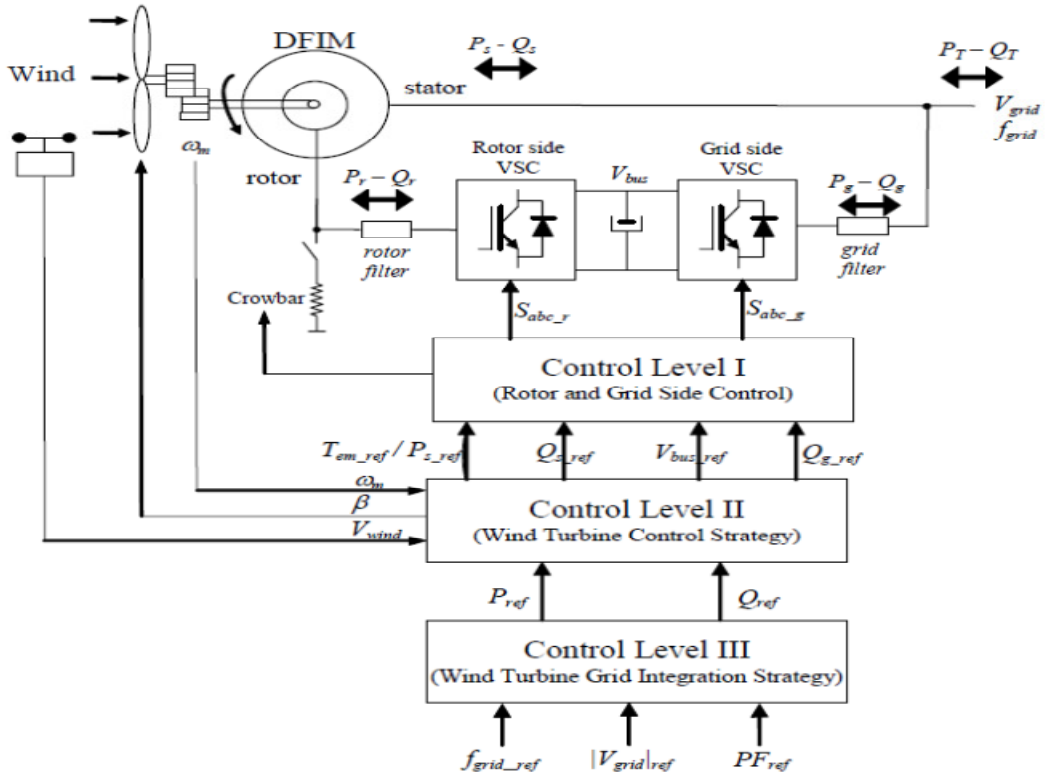

Figure 4.3. DFIG Control Levels [31]

Control Level II

This control level is termed as wind turbine control strategy as it controls the turbine power characteristics to stay on the turbine tracking characteristic which is explained in Section 4.3. Any control strategy implemented at this level accomplishes the following

- Controls the turbine to operate on the Maximum Power Point tracking (MPPT) characteristic curve.

- Generates pitch angle (β) references such that the wind turbine operates in the speed limits.
- Responds to active and reactive power references from the higher control level.

Control Level III

Control level III is dedicated to the wind turbine grid integration. Several different control strategies as in [32] and [33] can be implemented, but all of them will accomplish the following

- Control the Voltage (V_{grid}) and frequency (f_{grid}) at which the DFIG delivers active and reactive powers.
- Respond to the active and reactive power references from the grid operator or from the wind farm centralized control.

4.3. Control strategy for Maximum Wind Power Extraction

This control strategy is one of the wind turbine control strategies and comes under a level II category as shown in Figure 4.3. As explained in Chapter 3, Section 3.3.4, page 63, there is a limit on the maximum power that can be extracted from the wind, based on the beltz limit or maximum coefficient of power (C_{pmax}). Since the velocity of the wind speed or the kinetic energy present in the wind is not always constant, as the wind speed varies, the maximum power that can be extracted from the wind also varies. The main purpose of this control strategy is to extract maximum power from the wind's kinetic energy at various wind speeds and hence to generate maximum output power.

With the variation in the wind speed, the rotational speed of the generator rotor (angular frequency of the rotor, ω_{rel}) also varies, producing a change in the power output of the generator. A typical wind turbine characteristic that shows the dependence of the generator speed with the generator power at different wind speeds is shown in Figure

4.4(a). The mathematical relation between the generator speed and the optimum power extracted from the wind can be described as

$$P_{opt} = K_{opt}\omega_{rel}^{3} \text{ and } T_{opt} = K_{opt}\omega_{rel}^{2}.$$

A maximum power extraction-speed curve is plotted so as to intersect the C_{pmax} at different wind speeds, and such that the (P_{opt}) curve represents the maximum active power that can be captured from the wind at different wind speeds. The control objective of this strategy is to keep the wind turbine on this curve as the wind speed varies [34]. V on the Figure 4.4 represents the velocity of the wind speed in m/s.

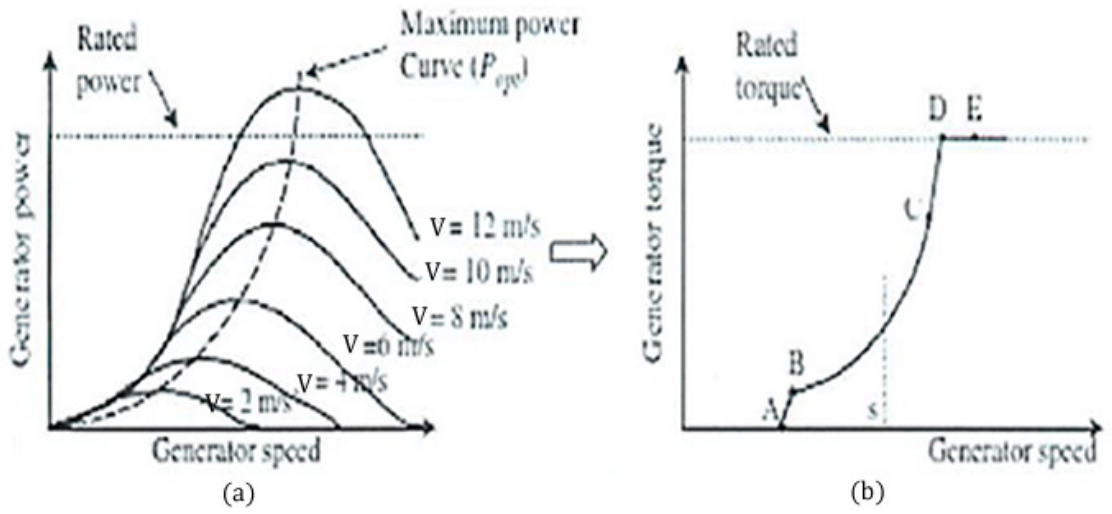

Figure 4.4. DFIG Wind Turbine Characteristics for Maximum Power Extraction [34]

The generator torque-speed characteristic shown in Figure 4.4(b) is applied to the controller model to obtain maximum power extraction at different wind speeds. The torque-speed characteristic curve seen in Figure 4.4(b) is described by five critical points (A, B, C, D, and E). The optimum power extraction is possible only for a certain range of wind speeds due to the limitation of the power converter ratings. From zero generator speed to the point A, the generator electromagnetic torque also equals zero. For very low

wind speeds, the model operates at almost constant rotational speed (A-B), i.e., the tracking characteristic is a straight line as shown in Figure 4.4(b). The electrical power generated in this region is very less and the wind turbine electrical generator does not generate any useful active power. The section (B-C) is where the wind turbine electrical generator generates useful power. As the wind speed and the corresponding generator rotor speed increases, the electromagnetic torque generated also increases until the point D. Point D corresponds to the rated electromagnetic torque generated at the rated generator speed, i.e., at point D the electromagnetic torque is 1/rpu/. The section (B-D) is the locus of the maximum power extracted at different wind speeds, i.e., P_{opt} in Figure 4.4(a). For very high wind speeds, that exceed the turbine torque rating, the control objective follows the (D-E) section of the curve, where the electromagnetic torque is constant even if the generator speed increases. When the system reaches point E, pitch regulation takes over the torque control to limit aerodynamic input power as explained in detail in the pitch angle control strategy in Section 4.5 of this Chapter.

4.4. Current-Mode Controller (PVdq) Strategy

Current-mode controller strategy is considered as the electrical control of the DFIG. As the name suggests, this control strategy is applied to the rotor-side converter, and it is one of the Level I control strategies shown in Figure 4.3. DFIG steady state characteristics studied in Chapter 3 prove that d and q axes components of the rotor voltage have individual effects on the active and reactive power of the DFIG. Hence, the d and q axes components of the DFIG rotor current are used individually to regulate the electromagnetic torque of the DFIG and the power factor at a given terminal voltage, or in other terms the reactive power delivered to the grid, respectively, and this control strategy is termed as PVdq control [35].

4.4.1. Electromagnetic Torque Control Strategy

The purpose of this electromagnetic torque control strategy is to modify the electromagnetic torque of the DFIG according to wind speed variations and drive the system to the required operating reference. The schematic of the electromagnetic torque control strategy is as illustrated in Figure 4.5.

The active power ($P_{deltotmes}$) and the rotor speed (ω_{rel}) measurements, given as inputs to the torque control block shown in Figure 4.6, generate a reference torque signal using the maximum wind power extraction control. The torque signal (T_{refsp}) is modified to generate a reference value for the rotor current in the d-axis (i_{rdref}) by using the stator flux estimator block.

The d-axis rotor voltage component ($v_{rd}^{'}$), required to operate at the reference torque set point, is obtained through a PI controller. The PI controller is assisted by the feed forward terms that calculate the resulting d-axis component of the rotor voltage v_{rd}, that needs to be applied at the rotor terminals of the DFIG.

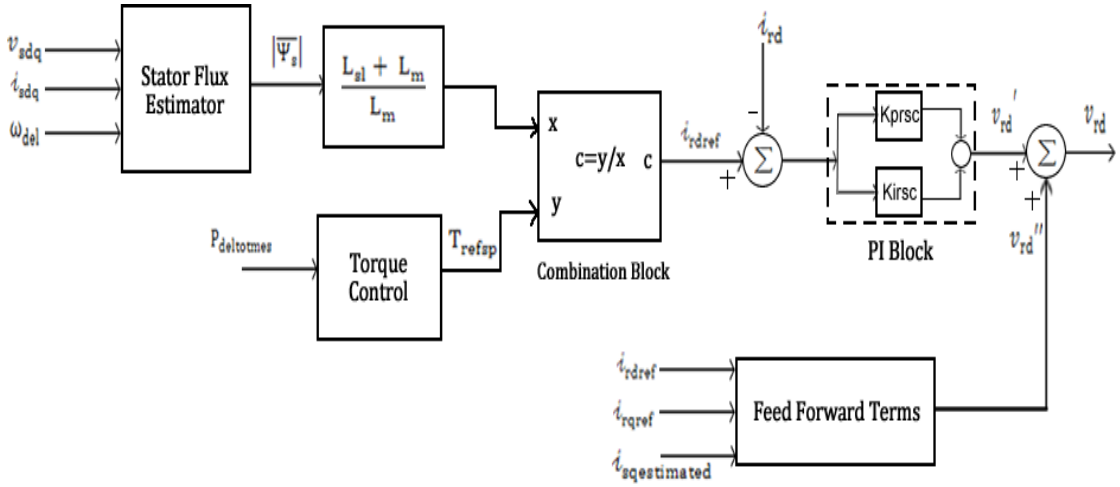

Figure 4.5. DFIG Torque Control Strategy

Torque Control Block

As seen in Figure 4.6, by using the measured active power and the turbine power tracking characteristic curve, the torque control block generates a reference value for the rotor speed(ω_{relref}). The difference in the actual rotor speed (ω_{rel}) and the rotor speed reference value is processed through the PI controller to generate the reference torque set point (T_{refsp}) .

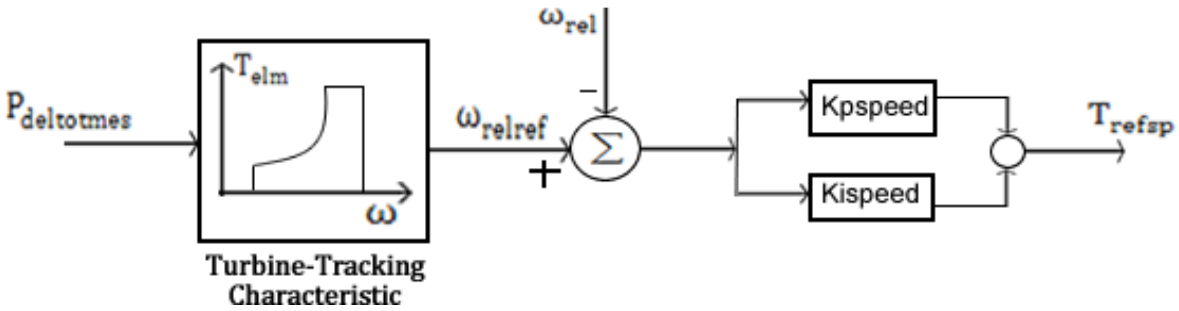

Figure 4.6. Torque Control Block

The reference value of the d-axis rotor current is then calculated by using the reference torque as below,

$$i_{rdref} = \left[\frac{L_{ss}}{L_m * |\overline{\Psi}_s|}\right] T_{refsp}.$$

The difference in the d-axis rotor current (i_{rd}) from the reference value (i_{rdref}) forms the error signal that is processed by the PI compensator to reduce it to zero and produce the d-axis rotor voltage(v'_{rd}) . The PI compensator consists of the proportional and integral gain blocks connected as shown in Figure 4.5.

4.4.2. Reactive power or Voltage Control Strategy

Reactive power or voltage control strategy is a Level I control strategy as explained in Section 4.2. Reactive power control can be obtained by using either the network-side or the rotor-side power converters, depending on the type of the electrical generator used in the wind turbine. For DFIG wind turbine, application of any of the voltage control strategies to

the rotor-side converter is preferred as the rotor-side converter reactive power will be effectively amplified by a factor of 1/s when referred to the stator.

The reactive power or voltage control strategy, illustrated in Figure 4.7, is designed to provide terminal voltage or power factor control by using the rotor-side converter. In the reactive power control strategy, as long as the reactive component of the rotor current (i_{rq}) is within its maximum limits, the reactive power delivered to the grid is regulated at its reference value $Q_{gridref}$. As seen in Figure 4.7, both the stator voltage actual value ($|\bar{V}_s|$) and the stator voltage reference signal ($|\bar{V}_{sref}|$) generated by the var regulator, are used by voltage regulator to generate the q-axis rotor current reference component. The error between the actual i_{rq} and reference (i_{rqref}) is processed through a PI controller to give the q-axis component of the rotor voltage (v_{rq}'). The PI controller is assisted by the feed forward terms, to calculate the resulting q-axis component of the rotor voltage that needs to be applied at the rotor terminals of the DFIG, for the reactive power delivered to the grid to remain at the reference value.

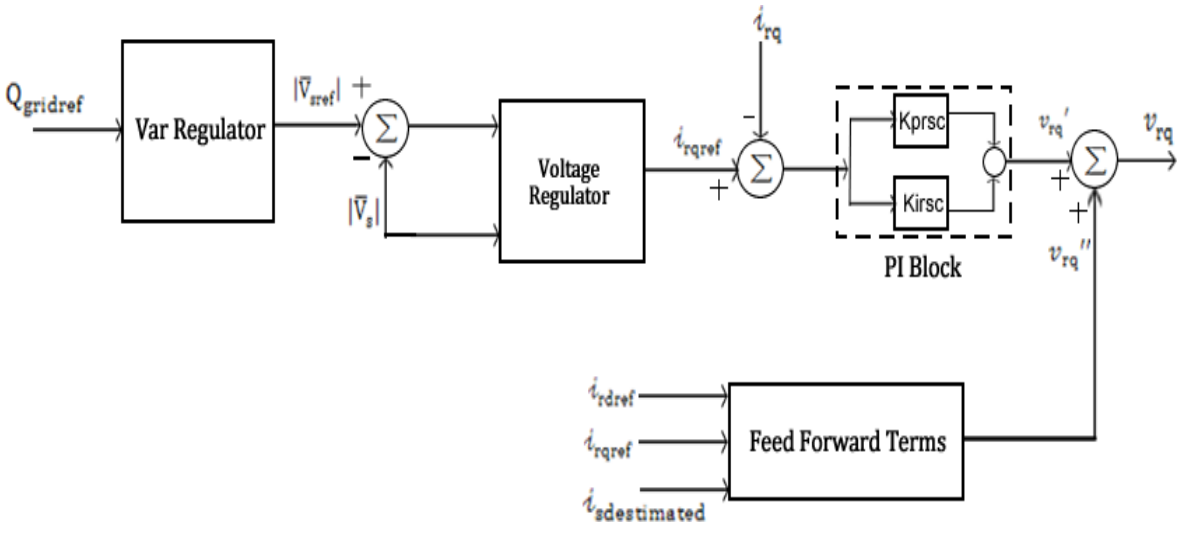

Figure 4.7. Reactive Power Control Strategy

The difference in the reference and measured reactive powers delivered by the stator to the grid as seen in Figure 4.8 is processed through an integrator control block to generate the stator voltage reference signal ($|\overline{V}_{sref}|$). This reference stator voltage signal is used as an input by the voltage regulator block as shown in Figure 4.9.

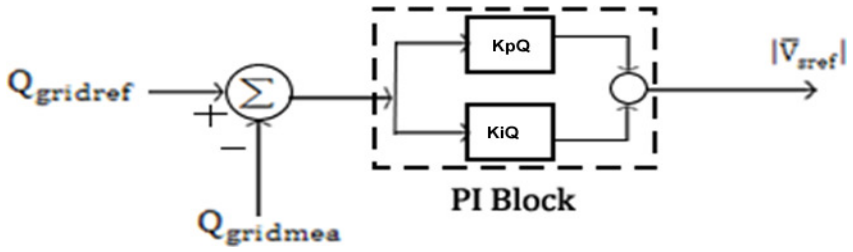

Figure 4.8. Var Regulator Block

Voltage Regulator Block

The control logic for voltage regulator block is as shown in Figure 4.9

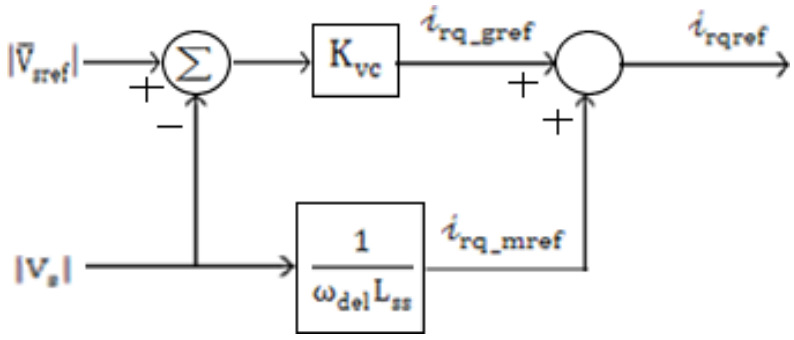

Figure 4.9. Voltage Regulator Block

As the reactive power delivered by the stator to the grid increases or decreases, the terminal voltage increases or decreases correspondingly. The voltage control strategy illustrated in Figure 4.7 fulfills the following requirements: (i) the reactive power consumed by the DFIG is compensated by i_{rq_m}, and (ii) if the terminal voltage is too low or too high compared with the reference value then i_{rq_g} is adjusted appropriately using the gain value (Kvc).

PI Block

The input error signal to this PI block, i.e., the difference between the reference and actual q-axis component of rotor current, is modified by the proportional and integral gain blocks connected as shown in Figure 4.7 to give the q-axis component of the rotor voltage $(v_{\mathrm{rq}}{}')$.

Feed Forward Terms

As shown in Figure 4.5 and Figure 4.7, to minimize the cross-coupling between torque and voltage control loops, feed-forward terms are added to the PI compensator in both the electromagnetic torque and reactive power control strategies. The feed forward terms assist the PI compensator block to calculate the resulting d-axis and q-axis component of the rotor voltage that needs to be applied at the rotor terminals of the DFIG. The inputs to the feed forward block in Figure 4.5 are i_{rdref}, i_{rqref}, and $i_{\mathrm{sqestimated}}$. The inputs to the feed forward block in Figure 4.7 are i_{rdref}, i_{rqref}, and $i_{\mathrm{sdestimated}}$. The equations that determine these feed forward terms are given below,

$$v''_{\mathrm{rd}} = \mathrm{R_r} i_{\mathrm{rdref}} - (\omega_{\mathrm{del}} - \omega_{\mathrm{rel}}) * (-\mathrm{L_m} i_{\mathrm{sqestimated}} + \mathrm{L_{rr}} i_{\mathrm{rqref}}), \text{ and} \tag{4.8}$$

$$v''_{\mathrm{rq}} = \mathrm{R_r} i_{\mathrm{rqref}} + (\omega_{\mathrm{del}} - \omega_{\mathrm{rel}}) * (-\mathrm{L_m} i_{\mathrm{sdestimated}} + \mathrm{L_{rr}} i_{\mathrm{rdref}}). \tag{4.9}$$

Where

$$i_{\mathrm{sdestimated}} = \left[v_{\mathrm{sd}} + \frac{\omega_{\mathrm{del}}{}^2 \mathrm{L_{ss}} \mathrm{L_m}}{\mathrm{R_s}} i_{\mathrm{rdref}} + \omega_{\mathrm{del}}\, \mathrm{L_m} i_{\mathrm{rq}}\right] \left[\frac{\mathrm{R_s}}{\omega_{\mathrm{del}}{}^2 \mathrm{L_{ss}}{}^2 - \mathrm{R_s}{}^2}\right], \tag{4.10}$$

$$i_{\mathrm{sqestimated}} = -\left[\frac{\omega_{\mathrm{del}}\, \mathrm{L_{ss}}}{\mathrm{R_s}}\right] * i_{\mathrm{sdestimated}} - \left[\frac{\omega_{\mathrm{del}}\, \mathrm{L_m}}{\mathrm{R_s}}\right] * i_{\mathrm{rdref}}. \tag{4.11}$$

4.5. DC-Link Voltage Control Strategy

Dc-link voltage control is a strategy that is implemented in control level I. This control strategy is applied to the grid-side converter for the DFIG wind turbines. The main purpose of this control strategy is to maintain the dc-link capacitor voltage constant at the specified reference value $\mathrm{V_{dcref}}$. The implementation of the dc-link voltage control strategy is

illustrated in Figure 4.10 [36]. As seen in the Figure 4.10, the control strategy consists of a Vdc regulator block, grid current measurement block and a current regulator block.

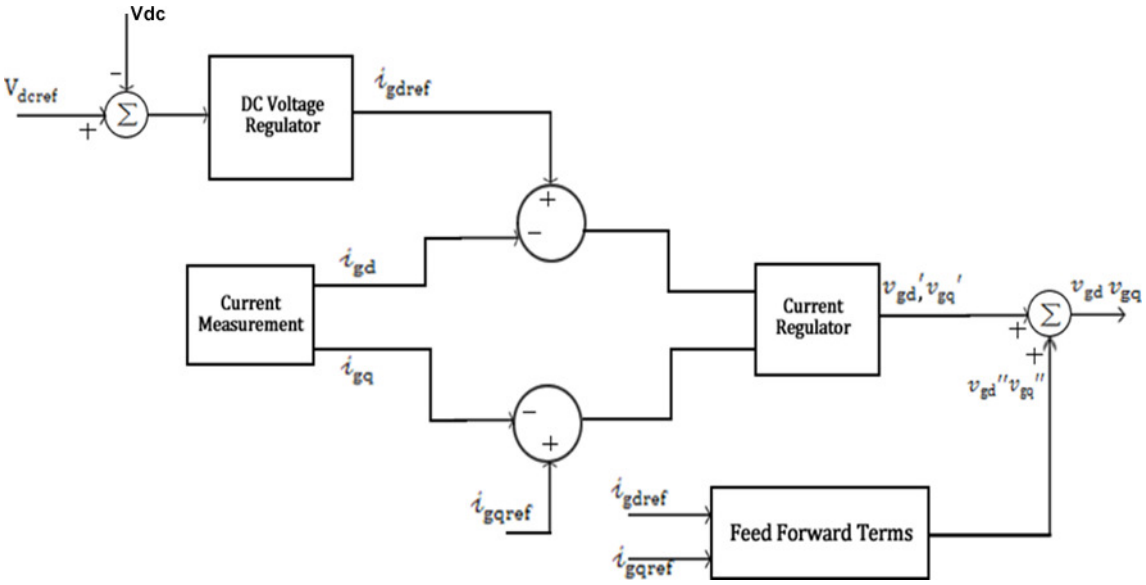

Figure 4.10. Dc-Link Voltage Control Strategy

Vdc Regulator Block

The inputs to the Vdc regulator block as shown in Figure 4.11 are the reference and measured values of voltage across the dc-link capacitor. The difference in the reference and measured dc-link capacitor voltages is processed through a PI control block to generate the reference value for d-axis component of the grid current. This grid current reference signal is used as input by the current regulator block as shown in Figure 4.12.

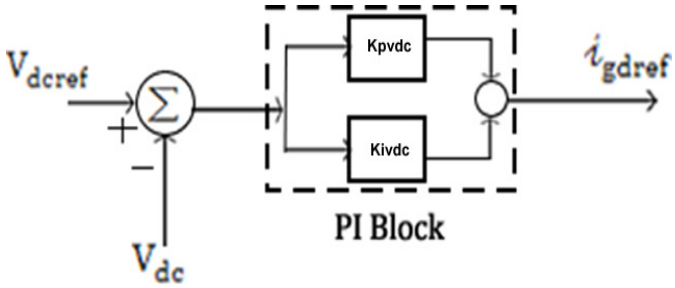

Figure 4.11. Vdc Regulator Block

Current Regulator Block

As shown in Figure 4.12, $i_{\mathrm{gdref}}, i_{\mathrm{gqref}}, i_{\mathrm{gd}}, i_{\mathrm{gq}}$ are the inputs to the current regulator block. i_{gdref} is obtained from the Vdc regulator block described above and a certain value is specified for i_{gqref}. The currents i_{gd} and i_{gq} are outputs of the current measurement block across the network converter terminals. The logic implemented in the current regulator block is similar to the voltage control strategy. The error between d-axis component of grid current reference (i_{gdref}) and measured values (i_{gd}) is processed through a PI control block to generate d-axis component of the grid voltage (v_{gd}'). The error between q-axis component of grid current reference (i_{gqref}) and measured values (i_{gq}) is processed through a PI control block to generate q-axis component of the grid voltage (v_{gq}'). Feed forward terms are provided at the PI controller to calculate the required v_{gd} and v_{gq}.

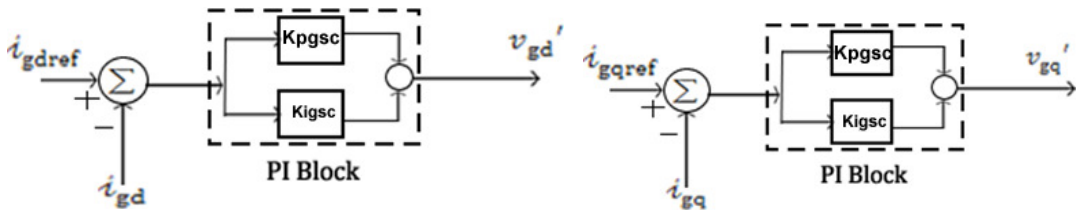

Figure 4.12. Current Regulator Block

Feed Forward Terms

As seen in Figure 4.10, i_{gdref}, i_{gqref} are inputs to the feed forward terms block. These feed forward terms at the PI controller block prevents the cross-coupling between the d and q axes current control loops. The grid d-axis and q-axis voltage are obtained using the relations defined below

$$v_{\mathrm{gd}}'' = v_{\mathrm{sd}} - \mathrm{R_g} i_{\mathrm{gdref}} + \omega_{\mathrm{del}} \mathrm{L_{gl}} i_{\mathrm{gqref}}, \text{ and} \quad (4.12)$$

$$v_{\mathrm{gq}}'' = v_{\mathrm{sq}} - \mathrm{R_g} i_{\mathrm{gqref}} - \omega_{\mathrm{del}} \mathrm{L_{gl}} i_{\mathrm{gdref}}. \quad (4.13)$$

4.6. Pitch Angle Control Strategy

Pitch angle control is a level II control strategy that controls the input mechanical power of the wind turbine generator at high wind speeds. The pitch angle (β) or blade pitch refers to the angle of attack of the blades of the wind turbine rotor. Such, by adjusting the pitch angle, the rotational speed of the wind turbine rotor can be controlled and hence the generator rotor speed. The pitch angle control system keeps the generator rotor speed within the operating limits as the wind speed increases.

In the pitch angle control strategy illustrated in Figure 4.13, the pitch angle of the wind turbine is kept constant at zero degrees until the generator speed (ω_{rel}) reaches the point D of the tracking characteristic shown in Figure 4.4(b). The point D on the tracking characteristic corresponds to generator rated speed and the corresponding rated generator torque. If any wind speed causes the generator speed to go above the rated generator speed, the pitch angle control calculates the pitch angle (β) that should be applied to the wind turbine rotor blades so as to maintain the generator speed at the rated value. In this control strategy, the pitch angle calculated is proportional to the deviation of the generator speed from the point D. A compensation term with PI controller is added to the pitch angle control as shown in Figure 4.13 for more accurate calculation [36].

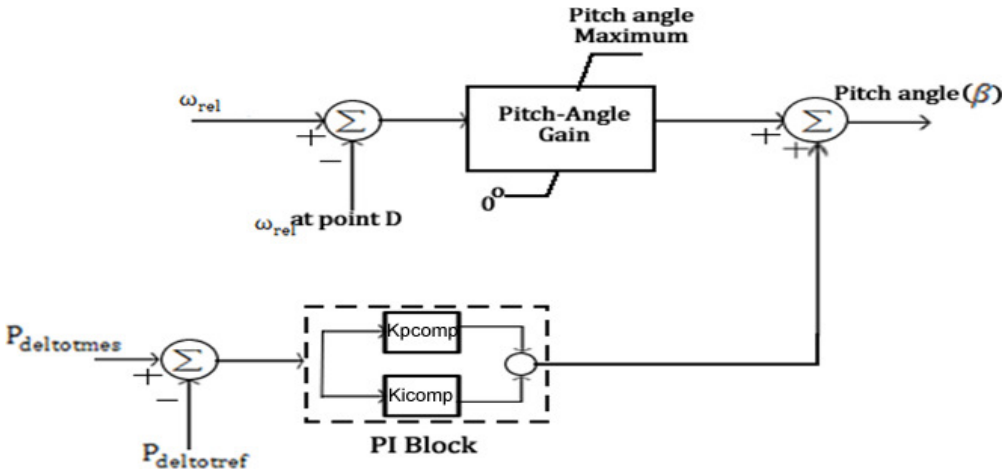

Figure 4.13. Pitch Angle Control Strategy

CHAPTER 5

DFIG Transient Characteristics

This chapter studies the effect on the stator and rotor currents of a DFIG, and the effect on the currents through the power electronic converters when a three phase fault occurs on the stator terminals of the DFIG. As explained in page 19, Chapter 1, if the DFIG is not equipped with Fault Ride Through (FRT) capability, it should be completely isolated from the grid during the occurrence of a fault. Three phase fault is considered as it will have the maximum fault current flowing through the DFIG (worst case scenario). First section of this chapter proves that during the pre-fault steady state, the derivatives of the DFIG flux linkages and the derivatives of the currents flowing through the back-to-back power electronic converters are equal to zero. Second section shows the simulated results of a three phase fault on the stator terminals of the DFIG.

5.1. Transient Model of the DFIG

During the pre-disturbance steady state the rate of change of the flux linkage and the rate of change of the angular frequency of the rotor should be equal to zero. To verify this, the relation between the rate of change of flux linkages and the flux linkages of the machine on dqo axes are derived. The relation between the rate of change of the angular frequency of the rotor and of the angular frequency itself is also determined. These relations are derived by using the DFIG machine model equations derived in Chapter 2.

With equations (2.15) and (2.16) in page 37**,** the algebraic form of the current-flux linkage equations results as

$$[i]_{sdq} = [A] * [\Psi]_{sdq} + [B] * [\Psi]_{rdq}, \tag{5.1}$$

$$[i]_{rdq} = [B] * [\Psi]_{sdq} + [C] * [\Psi]_{rdq}. \tag{5.2}$$

Expanding the above matrices it results

$$\begin{bmatrix} i_{sd} \\ i_{sq} \\ i_{so} \\ \cdots \\ i_{rd} \\ i_{rq} \\ i_{ro} \end{bmatrix} = \left[\left(\begin{array}{ccc|ccc} b & 0 & 0 & c & 0 & 0 \\ 0 & b & 0 & 0 & c & 0 \\ 0 & 0 & d & 0 & 0 & 0 \\ \cdots & \cdots & \cdots & \cdots & \cdots & \cdots \\ c & 0 & 0 & a & 0 & 0 \\ 0 & c & 0 & 0 & a & 0 \\ 0 & 0 & 0 & 0 & 0 & e \end{array}\right)\right] * \begin{bmatrix} \Psi_{sd} \\ \Psi_{sq} \\ \Psi_{so} \\ \cdots \\ \Psi_{rd} \\ \Psi_{rq} \\ \Psi_{ro} \end{bmatrix}, \tag{5.3}$$

where,

$a = \frac{L_s}{L_s * L_r - L_m^2}$, $b = \frac{L_r}{L_s * L_r - L_m^2}$, $c = \frac{L_m}{L_s * L_r - L_m^2}$, $d = \frac{1}{L_{sl}}$, $e = \frac{1}{L_{rl}}$, $L_s = L_{sl} + L_m$ and

$L_r = L_{rl} + L_m$.

The transient model of the DFIG, with differential equations for the flux linkages and angular frequency of the rotor, is obtained by using the above equations, equations (2.17-2.28), from pages (37-38) and 2.29 from page 40, Chapter 2 as

$$\frac{d}{dt}[X] = [E] * [Si] + [V], \tag{5.4}$$

where,

$$[X] = [Si] = \begin{bmatrix} \Psi_{sd} \\ \Psi_{sq} \\ \Psi_{so} \\ \cdots \\ \Psi_{rd} \\ \Psi_{rq} \\ \Psi_{ro} \\ \cdots \\ \omega_{rel} \end{bmatrix}, \quad [V] = \begin{bmatrix} -v_{sd} \\ -v_{sq} \\ -v_{so} \\ \cdots \\ v_{rd} \\ v_{rq} \\ v_{ro} \\ \cdots \\ \frac{T_{mec}}{\tau_m} \end{bmatrix}, \text{ and} \tag{5.5}$$

$$[E] = \left[\begin{array}{cccc|cc|c} -b*R_s & \omega_{del} & & & -c*R_s & & 0 \\ -\omega_{del} & -b*R_s & & & & -c*R_s & \\ & & -d*R_s & & & & \cdots\cdots\cdots \\ \cdots\cdots\cdots\cdots\cdots\cdots\cdots\cdots\cdots & & & & \cdots\cdots\cdots\cdots\cdots\cdots\cdots\cdots\cdots\cdots\cdots & & \\ -c*R_r & & & & -a*R_r & (\omega_{del}-\omega_{rel}) & \\ & -c*R_r & & & -(\omega_{del}-\omega_{rel}) & -a*R_r & \\ & & & & & & e*R_r \\ \cdots\cdots\cdots\cdots\cdots\cdots\cdots\cdots\cdots & & & & \cdots\cdots\cdots\cdots\cdots\cdots\cdots\cdots\cdots\cdots\cdots & & \cdots\cdots\cdots \\ \frac{c*\Psi_{rq}}{\tau_m} & \frac{-c*\Psi_{rd}}{\tau_m} & & & & & \frac{-K_{mec}}{\tau_m} \end{array}\right].$$

(5.6)

5.2. Predisturbance Steady -State of the DFIG

During the pre-disturbance steady state all the machine variables of the DFIG such as flux linkages, currents, voltages and powers do not change with time. Hence during the pre-disturbance steady state, the matrix $\frac{d}{dt}$ [X] described in the transient model given by equation (5.4) should be equal to zero. The steady state operating conditions of the DFIG machine are considered based on the Vestas V90 wind turbine operating data. This section proves that the matrix $\frac{d}{dt}$ [X] is zero by using the general specifications of the Vestas V90 DFIG [24] and the calculations shown in Chapter 3, pages 58-65.

Calculation of the Elements of Matrix [Si]

As the DFIG is operating at steady state, equations (2.40 - 2.45) shown in Chapter 2, page 41 are valid. The values of the flux linkages shown in the matrix [Si], in equation (4.5), are calculated by using equations (2.23-2.28) shown in Chapter 2, pages (37-38). The parameters shown in equations (2.23-2.28) are defined in Chapter 3, Section 3.1, page 42. The values of the current d and q-axis components shown in equations (2.23-2.28) are calculated by using the following data: $P_{deltot} = 1/rpu/$, $Q_{deltot} = 0\ /rpu/$, slip $s = 0.023\overline{3}$, $v_{rd} = 0.0294377\ /rpu/$ and $v_{rq} = 0.00285368\ /rpu/$, which are obtained from Version 2 of the power flow through the DFIG, shown in Chapter 3, Section 3.3.3, page (59-61).

Since ω_{del}, the angular frequency with which the dq axis rotates is equal to the synchronous angular frequency, its value is taken as 1/rpu/. ω_{rel}, angular frequency of the rotor in /rpu/, is calculated as

$$\omega_{rel} = \omega_{del} - s * \omega_{del} \text{ with } \omega_{del} = 1 \text{ /rpu/}, \tag{5.7}$$

$$[Si] = \begin{bmatrix} \Psi_{sd} \\ \Psi_{sq} \\ \Psi_{so} \\ \cdots\cdots \\ \Psi_{rd} \\ \Psi_{rq} \\ \Psi_{ro} \\ \cdots\cdots \\ \omega_{rel} \end{bmatrix} = \begin{bmatrix} -8.8818 * 10^{-6} \\ 1.0062 \\ 0 \\ \cdots\cdots \\ 0.1844 \\ -1.0362 \\ 0 \\ \cdots\cdots \\ 0.9767 \end{bmatrix}. \tag{5.8}$$

Calculation of Elements of the Matrix [E]

The first six rows of the matrix [E], shown in equation (5.6), are calculated by using the parameters of the DFIG defined on Chapter 3, page 42 and equation (5.7) shown above. To calculate the elements on the seventh row of the matrix in rated per unit /rpu/, the mechanical power available on the rotor shaft of the DFIG calculated from the Section 3.3.4, Chapter 3 on page 63, and equations shown on Appendix B4, pages 124-126 are used, and it results as follows:

$$P_{mec}^{|pu|} = \frac{P_{mec}^{|MW|}}{S_b} = \frac{3.06591722 \text{ |MW|}}{3 \text{ |MW|}} = 1.02197/\text{rpu/},$$

$$T_{mec} = \frac{P_{mec}}{\omega_{rel}} = \frac{1.02197}{0.9767} = 1.0464/\text{rpu/}, \text{ and}$$

$$K_{mec} = T_{mec} + c\left(\Psi_{sd}\Psi_{rq} - \Psi_{rd}\Psi_{sq}\right) = 9.8109 * 10^{-3}.$$

Inertial time constant (τ_m)

$$\tau_m = \frac{J * \omega_{delb}^3}{p_p^2 * S_b},$$

where J is the inertia of the wind turbine from = $\frac{1}{2}mr^2$ [37],

where m = 8500 |kg|, r = 550 |mm| from [24], and hence

$$J = 1{,}285.625\ |kg - m^2|.$$

Substituting J from above equation, with S_b=3|MW|, $p_p = 2$ and $\omega_{delb} = 2\pi * 60$, the inertial time constant (τ_m) results as

$$\tau_m = 5.74019 * 10^3\ |rpu|.$$

By using all the calculations shown above, the matrix [E] is obtained as follows:

$$\left[\begin{array}{ccc|ccc|c} -0.03491 & 1 & 0 & -0.0339 & 0 & 0 & 0 \\ -1 & -0.03491 & 0 & 0 & -0.0339 & 0 & 0 \\ 0 & 0 & -0.0826 & 0 & 0 & 0 & 0 \\ \hline -0.0279 & 0 & 0 & -0.0285 & 0.0233 & 0 & 0 \\ 0 & -0.0279 & 0 & 0.0233 & -0.0285 & 0 & 0 \\ 0 & 0 & 0 & 0 & 0 & -0.0484 & 0 \\ \hline -0.0010 & -0.0002 & 0 & 0 & 0 & 0 & -1.8024 * 10^{-3} \end{array}\right]. \quad (5.9)$$

Calculation of Matrix [V]

To calculate the elements of the matrix [V], the d and q axes components of the stator and rotor voltages shown in equation (3.7), Chapter 3, Section 3.2.1.1, page 43 and Chapter 3, Section 3.3.3, page 59 respectively, and also the values of T_{mec} and τ_m calculated above are used. Hence, the matrix [V] is obtained as follows:

$$[V] = \begin{bmatrix} -v_{sd} \\ -v_{sq} \\ -v_{so} \\ \cdots \\ v_{rd} \\ v_{rq} \\ v_{ro} \\ \cdots \\ \frac{-K_{mec}}{\tau_m} \end{bmatrix} = [V] = \begin{bmatrix} -1.0000 \\ 0 \\ 0 \\ \cdots \\ 2.9438 * 10^{-2} \\ 2.8538 * 10^{-3} \\ 0 \\ \cdots \\ 1.8229 * 10^{-4} \end{bmatrix}. \quad (5.10)$$

Calculation of the Matrix $\frac{d}{dt}$ [Si]

The calculation of the matrix $\frac{d}{dt}$ [X] is done in MATLAB software by using the analytical equation shown in equation (5.4) and results as

$$\frac{d}{dt}[Si] = \begin{bmatrix} \frac{d\Psi_{sd}}{dt} \\ \frac{d\Psi_{sq}}{dt} \\ \frac{d\Psi_{so}}{dt} \\ \cdots\cdots \\ \frac{d\Psi_{rd}}{dt} \\ \frac{d\Psi_{rq}}{dt} \\ \frac{d\Psi_{ro}}{dt} \\ \cdots\cdots \\ \frac{d\omega_{rel}}{dt} \end{bmatrix} = \begin{bmatrix} 1.1102 * 10^{-15} \\ 8.8124 * 10^{-16} \\ 0 \\ \cdots\cdots\cdots\cdots\cdots\cdots \\ -1.3878 * 10^{-17} \\ -1.7347 * 10^{-17} \\ 0 \\ 3.9880 * 10^{-8} \end{bmatrix}.$$

Hence it is proved that, during the pre-disturbance steady-state the rate of change of flux linkages and rate of change of angular frequency of the rotor are practically zero.

5.3. Simulation of Three Phase Fault on Stator Terminals of the DFIG

The DFIG is considered to be operating in steady state from t = 0^- |sec|. To analyze the transient behavior of the DFIG, a solid three-phase fault is applied across the stator terminals of the DFIG for 0.5 |sec| at time t = 1 |sec|. At t = 1.5 |sec|, the fault is cleared and the voltages return to their pre-disturbance or steady state values. At the instant of the fault, i.e. t = 1|sec|, it is assumed that the rotor windings of the DFIG are short circuited and at the same moment the power electronic equipment on the rotor side of the DFIG is also disconnected as a result of which the DFIG goes to an asynchronous machine operating mode. A resistance in parallel to the dc-link capacitor needs to be provided for the capacitance to discharge.

The steady state values calculated in Chapter 3 are used as initial values for solving the differential equations in (5.4).

Figures 5.1 to 5.12 show the behavior of the DFIG currents, electromagnetic torque and angular frequency of the rotor during the occurrence of a three phase fault on the stator terminals of the DFIG.

Figures from 5.1 to 5.6 show the variations of d and q axes currents of the DFIG stator and rotor windings during the occurrence of a three phase fault. As shown in the figures, the oscillations in the graphs correspond to the variation of the flux linkage of the machine during the transient period.

Figure 5.1 shows the variation of stator d-axis current with time. At the moment of the fault, the d-axis rotor current goes to a very high value, i.e. approximately 6 times higher than the steady state value.

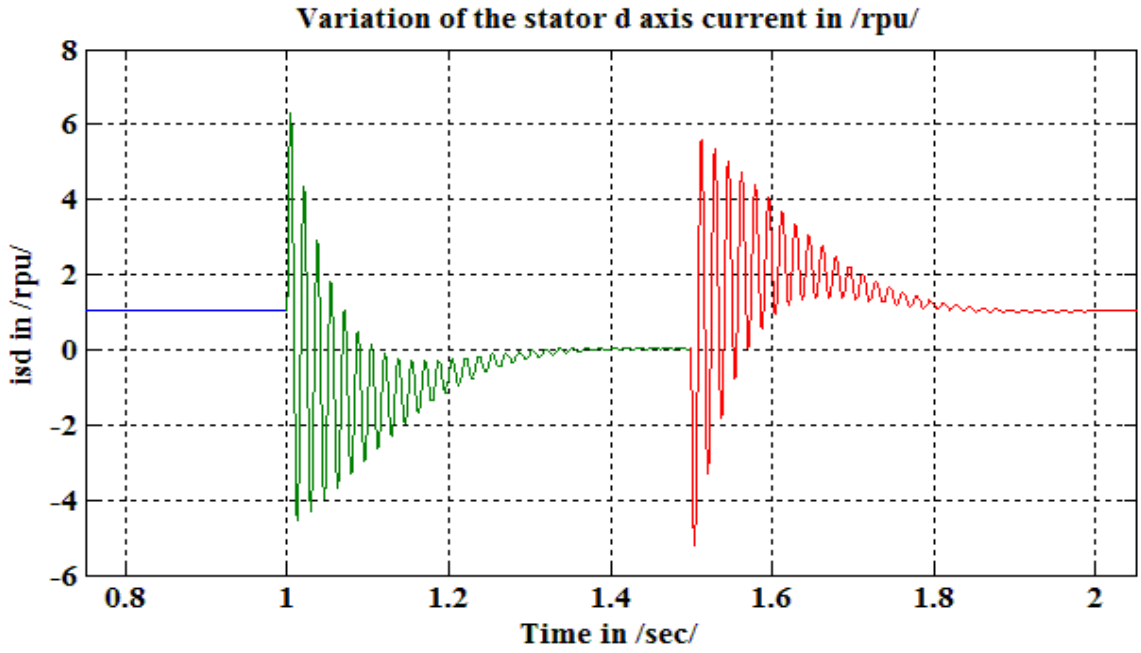

Figure 5.1. Variation of d-axis Stator Current with time

Figure 5.2 shows the variation of stator q-axis current with time. At the moment of the fault, the q-axis rotor current goes to a very high value in the negative direction.

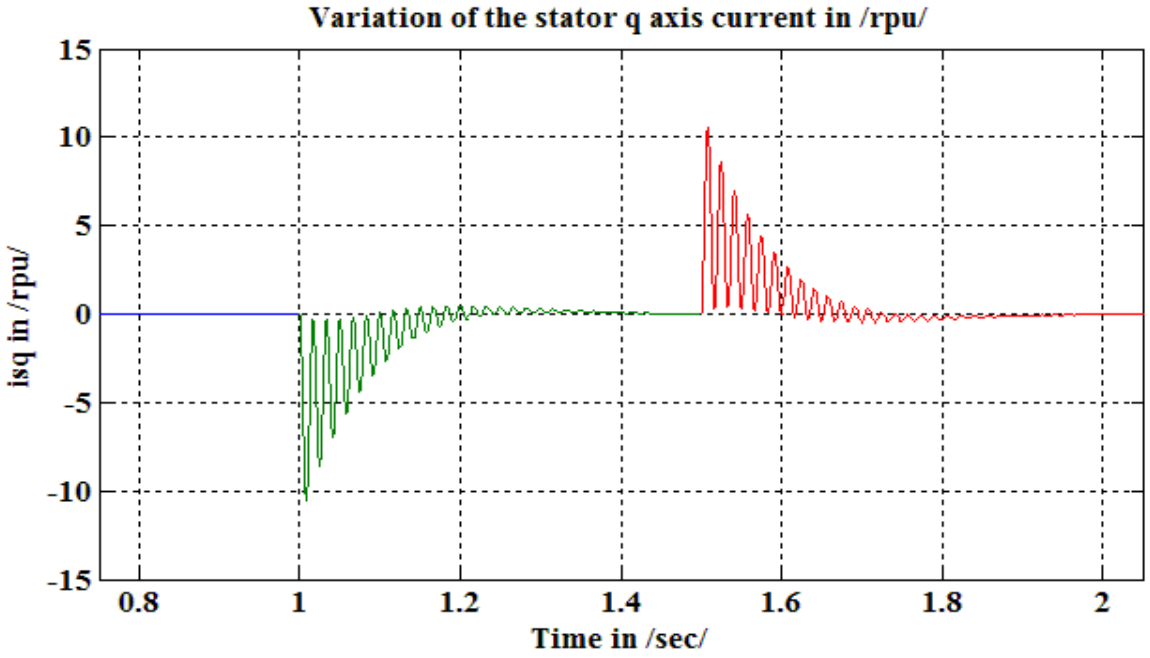

Figure 5.2. Variation of q-axis Stator Current with time

Figure 5.3 shows the variation of rotor d-axis current with time. At the moment of the fault, the d-axis rotor current goes to a very high value, i.e., approximately 6 times higher than the steady state value.

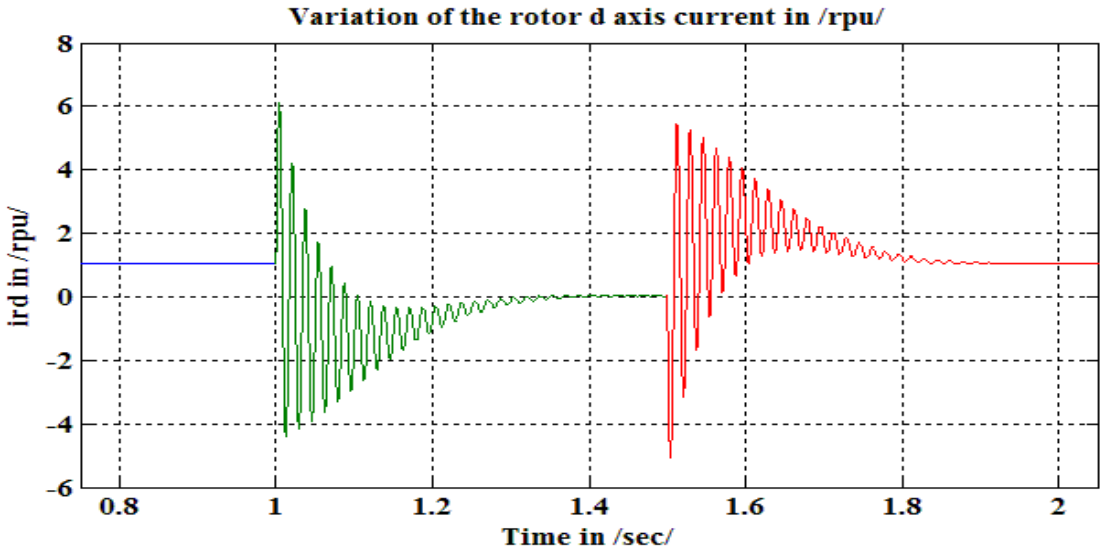

Figure 5.3. Variation of d-axis Rotor Current with time

Figure 5.4 shows the variation of rotor q-axis current with time. At the moment of the fault, the q-axis rotor current goes to a very high value in the negative direction.

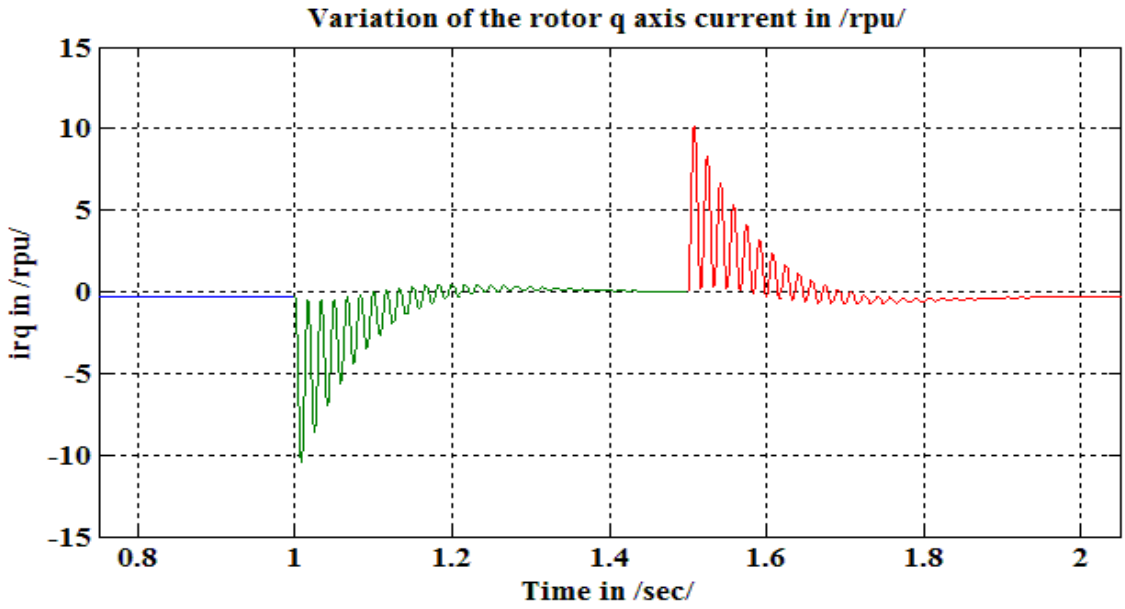

Figure 5.4. Variation of q-axis Rotor Current with time

Figure 5.5 shows the variation of the rotor angular frequency with time. As seen in Figure 5.5, during the transient period, the rotor angular frequency goes on increasing and eventually the machine may lose its synchronism if the fault is not cleared at the earliest.

The frequency of the voltage applied across the rotor windings to achieve the frequency of 60 |Hz| at the stator terminals of the DFIG depends on the rotor angular frequency as shown in Chapter 2, Section 2.1.1, page 26. Hence, the control strategies applied to the rotor side converter should continuously sense any change in speed of the rotor angular frequency (ω_{rel}) to determine the frequency of the voltage applied across the rotor windings. From Figure 5.5, it can be said that the value of the frequency of voltages applied across the rotor windings after the clearance of the fault will be different from the one corresponding to the pre fault steady state operation as the rotor angular frequency (ω_{rel}) after the clearance of the fault settles at a different value than its prefault steady state value.

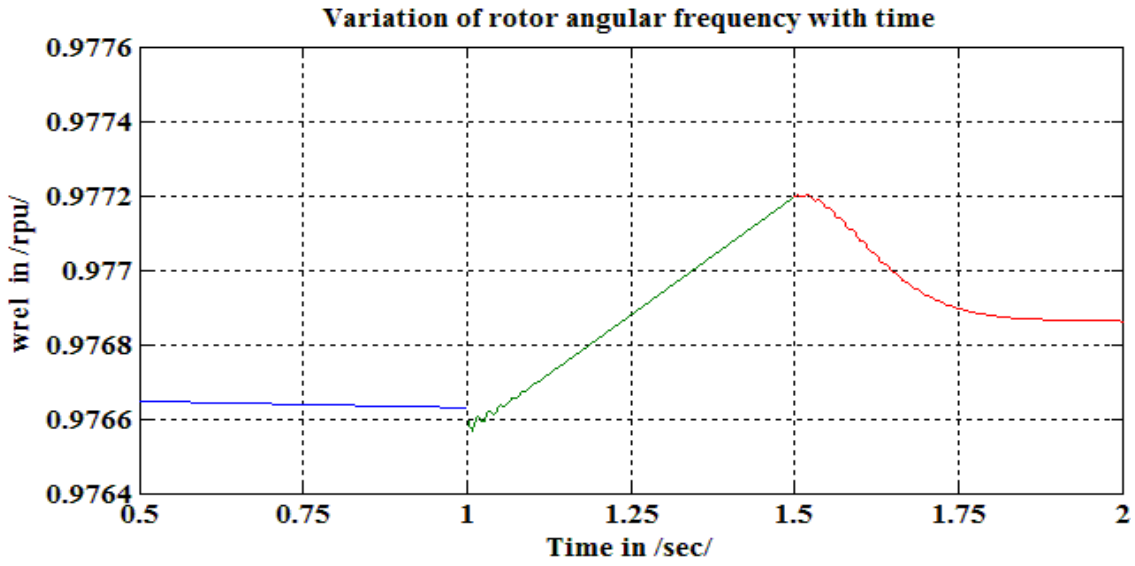

Figure 5.5. Variation of Rotor Angular Frequency with time

5.3.1. Graphing of Three Phase Stator and Rotor currents and Electromagnetic Torque of the DFIG

The machine d and q-axis components of the stator and rotor currents are calculated using the matricial equation shown in (5.3). Since during a fault the machine flux linkages are time varying quantities, the currents obtained are also time dependent. By using the inverse of the transformation matrices $[T]_s$ and $[T]_r$shown on pages (34-35), Chapter 2 the stator and rotor phase currents are calculated as

$$[i]_{sph} = [T]_s^{-1} * [i]_{sdq},$$

$$[i]_{rph} = [T]_r^{-1} * [i]_{rdq}.$$

Figures from 5.6 to 5.12 show the simulated time behavior of the DFIG stator and rotor currents in phases a, b, c and the electromagnetic torque of the machine.

As shown in the figures (5.6 – 5.8), the stator phase currents (i_{sa}, i_{sb}, i_{sc}) graphs, the current amplitudes during the transient period are about 5 to 8 times higher than the corresponding steady state value.

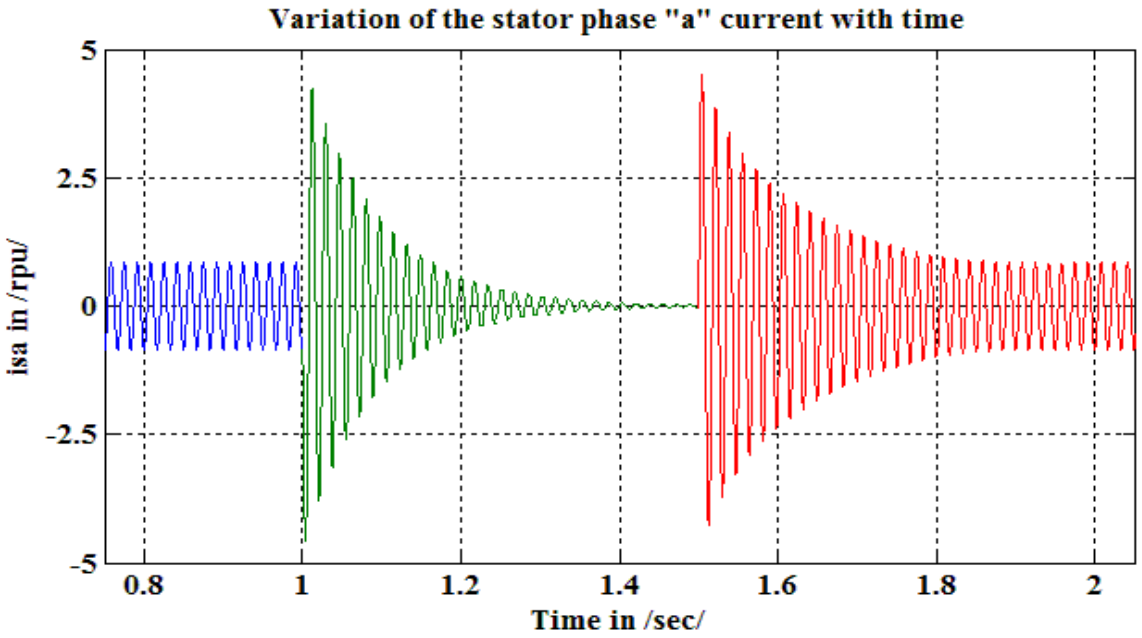

Figure 5.6. Variation of the Stator phase "a" Current with time

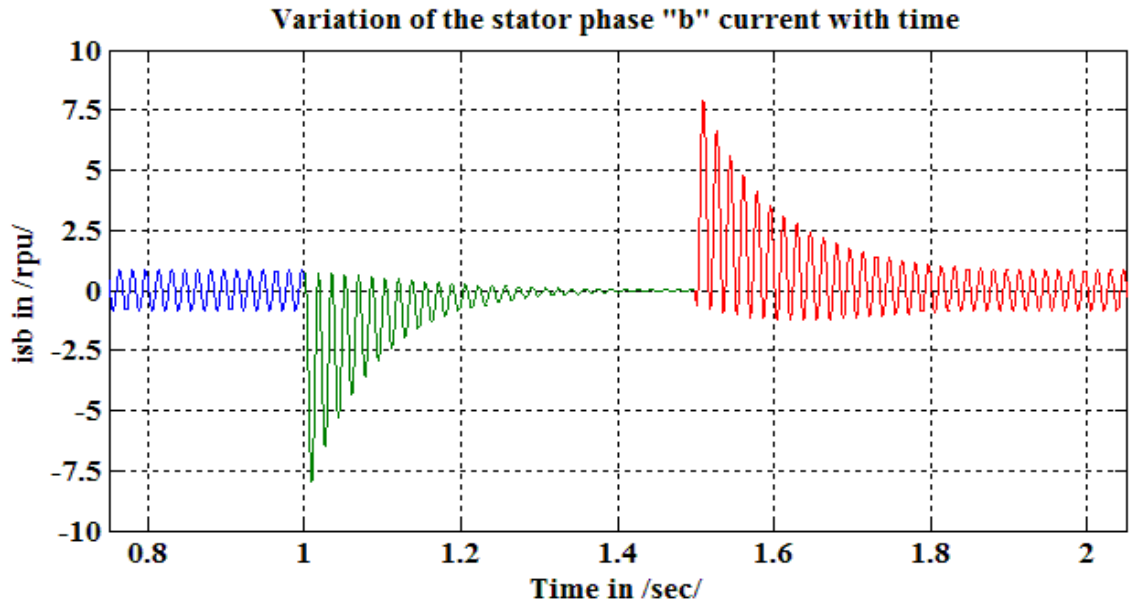

Figure 5.7. Variation of the Stator phase "b" Current with time

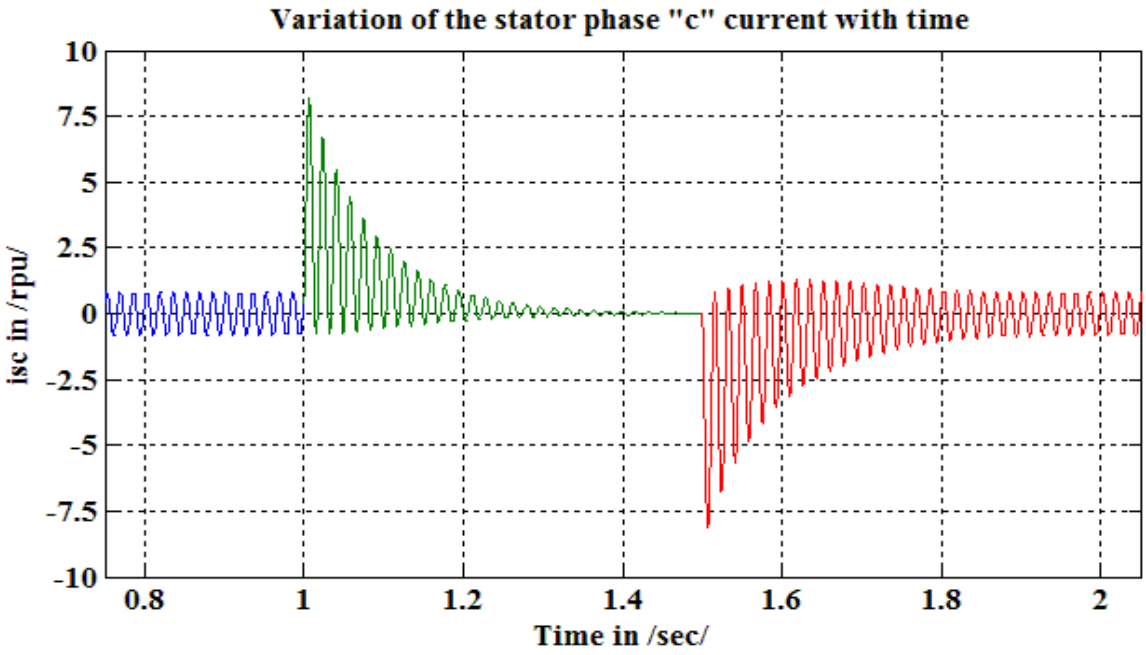

Figure 5.8. Variation of the Stator phase "c" Current with time

As shown in the figures (5.9 – 5.11), the rotor three phase currents (i_{ra}, i_{rb}, i_{rc}) graphs, the current amplitudes during the transient period are about 8 times higher than corresponding steady state value. Such high rotor currents damage the power electronic converters which are too expensive to replace.

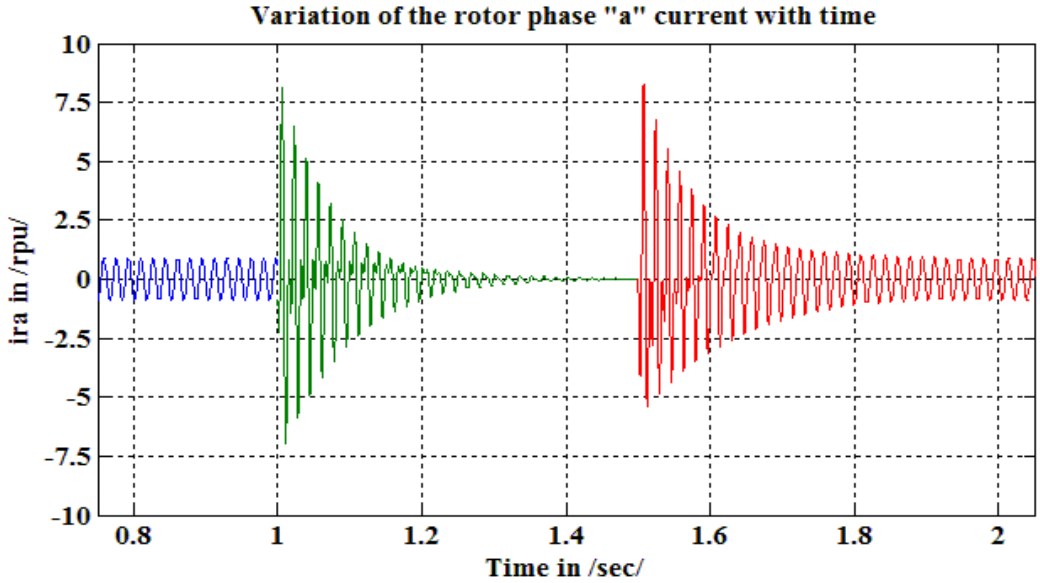

Figure 5.9. Variation of the Rotor phase "a" Current with time

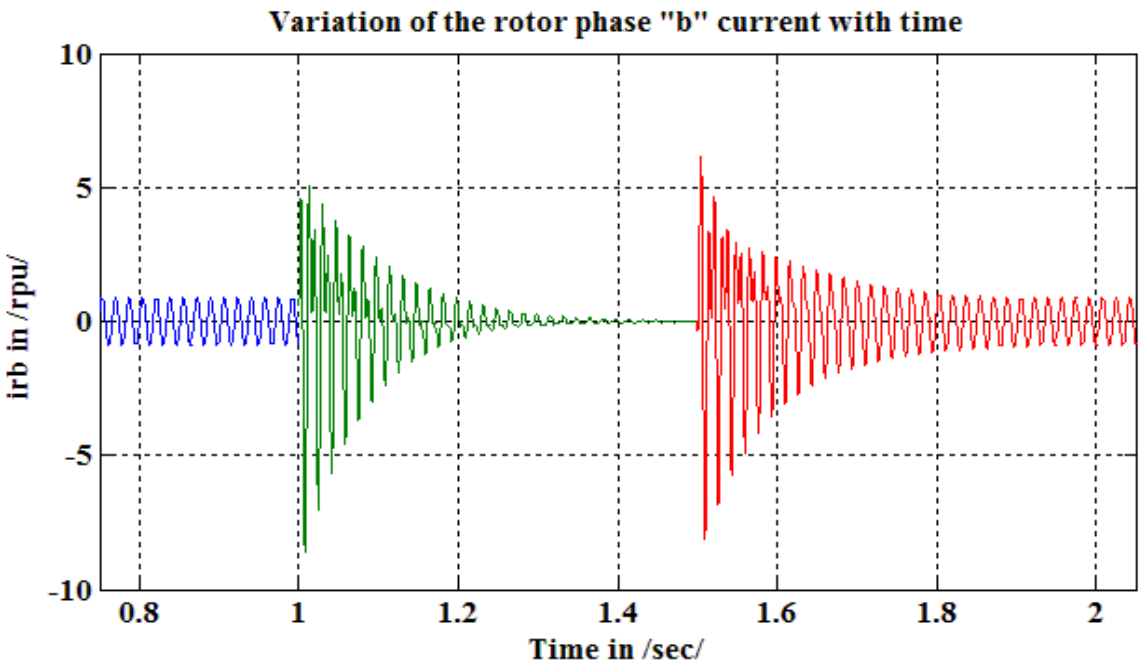

Figure 5.10. Variation of the Rotor phase "b" Current with time

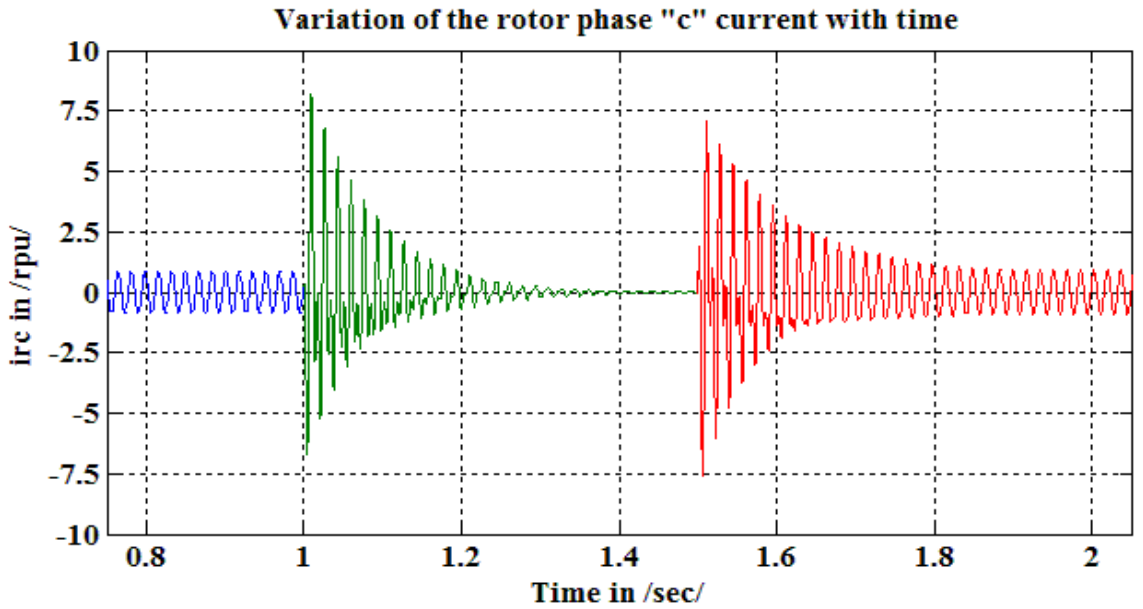

Figure 5.11. Variation of the Rotor phase "c" Current with time

The electromagnetic torque is calculated using the equation (2.32) shown in Chapter 2, page 40, and is plotted as shown in Figure 5.12. As shown in Figure 5.12, the oscillations in the electromagnetic torque are due to the transient currents in both the stator and rotor.

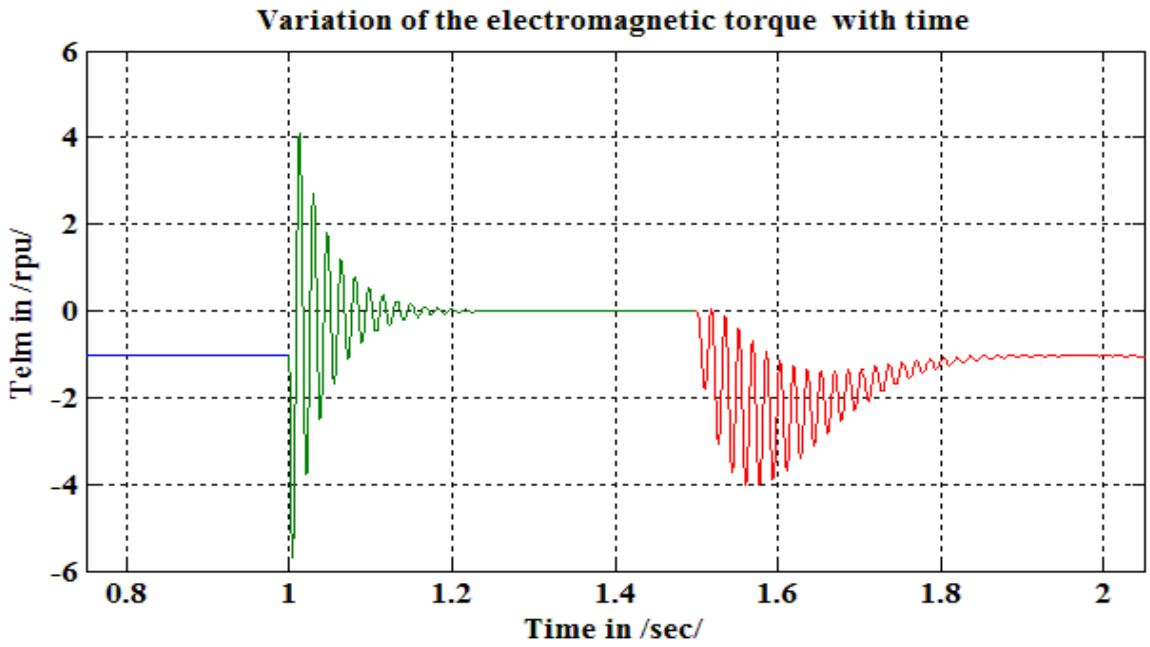

Figure 5.12. Variation of the Electromagnetic Torque with time

CHAPTER 6

DFIG Wind Turbines Steady-State and Transient Analysis Using Matlab/Simulink

The diagram shown in Figure 3.1, Chapter 3, page 44, where the DFIG wind turbine delivers power to the electric grid through the power system network is implemented by using the Simpowersystems toolbox of Matlab/Simulink software [38]. The one line diagram of the model implemented in Matlab/Simulink is shown in Figure 6.1, and the corresponding model simulated in Matlab is shown in Figure 6.2.

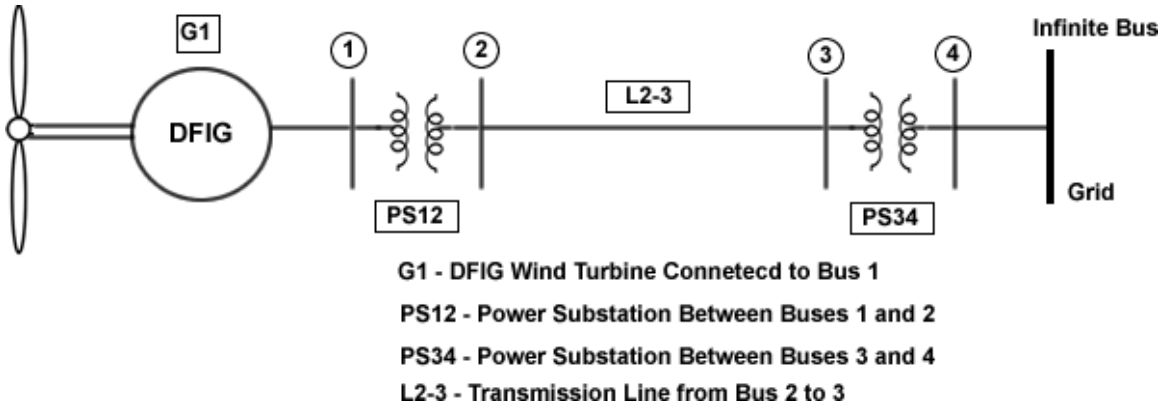

Figure 6.1. One Line Diagram of the Model Implemented in Matlab

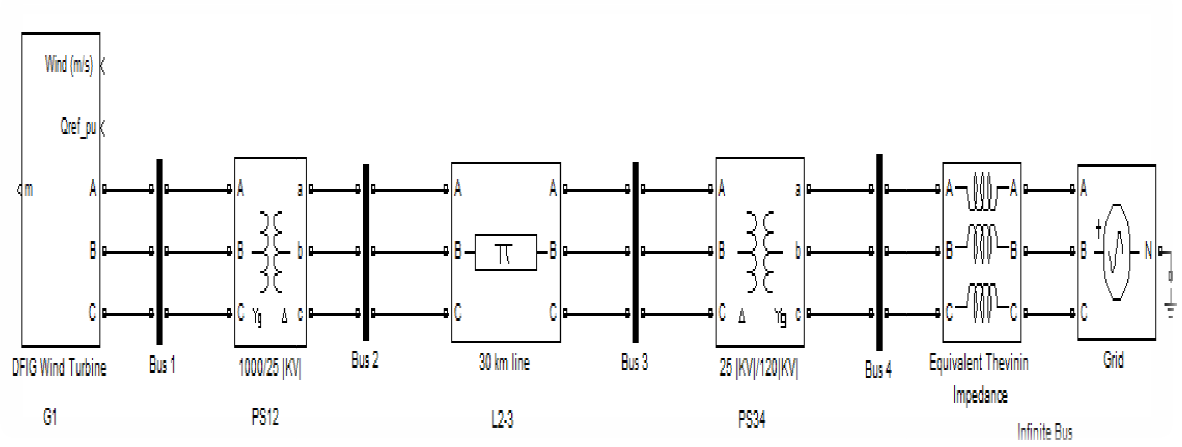

Figure 6.2. Block diagram of the Model Simulated in Matlab/Simulink

6.1. Block Diagram Description

The DFIG wind turbine block (generating unit G1) shown in Figure 6.2, consists of three 3 |MW| DFIG wind turbines connected in parallel and delivers 9|MW| power to a 120|KV| grid through a 30|km|, 25|KV| feeder. Each DIFG wind turbine block is similar to the diagram shown on Figure 3.1, page 44, Chapter 3. The only difference is that the control strategies that are used to control the gating pulses of the power electronic converter by using the Pulse Width Modulation (PWM) technique as explained in Chapter 4 are also included, as shown in Figure 6.3.

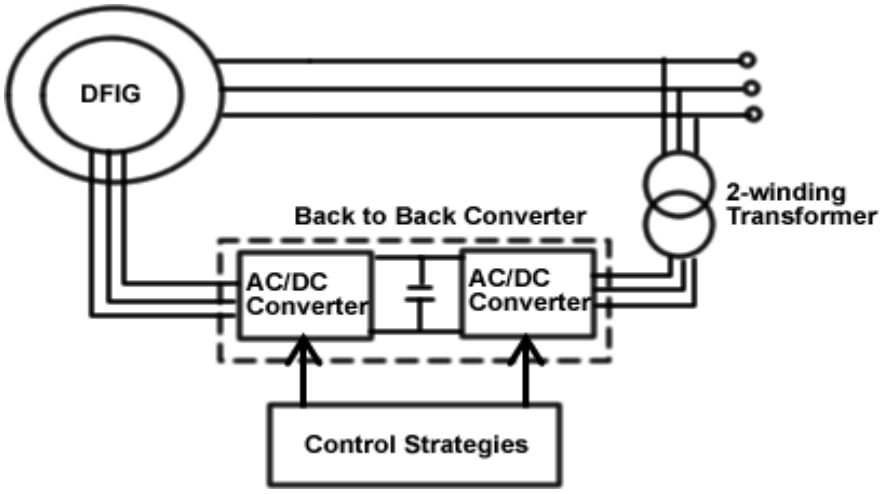

Figure 6.3. Components in the DFIG Wind Turbine Block

The Doubly Fed Induction Generator (DFIG) shown in Figure 6.3 is modeled as described in Chapter 2, with parameters and steady state characteristics as analyzed in Chapter 3, and the transient model and characteristics as shown in Chapter 5. The AC-DC-AC converter (or BBC) model and the control strategies that are applied to the converters are as explained in Chapter 4. The 2-winding transformer shown in the above Figure 6.3, steps down the voltage from 1000 |V| to 400|V|, so that it is used by the back to back converter on the rotor of the DFIG.

In Figure 6.2, the step up transformer (PS12) steps up the voltage at the stator terminals of the DFIG from 1000|V| to 25|KV|, such that the DFIG wind turbine can be connected to the distribution system. The distribution system is connected to the 120 |KV| grid through a 30 |km| transmission line (L2-3) and a step-up transformer (PS34) that steps up the voltage at 25|KV| to 120|KV|. The parameter values given as input to each block in Matlab/Simulink are listed in the Appendix E.

6.2. Equivalent Circuits of the Power System Components in the One-Line Diagram

The equivalent circuits of the power system components shown in Figures 6.1 and 6.2 are obtained as below by using the block parameters shown in Appendix E.

System Base Values

For the one-line diagram shown in Figure 6.1, the base values at the power system level are selected as

$$S_b = 9\ |\text{MVA}| \qquad V_b = 1\ |\text{KV}|.$$

Hence, the derived system base values are

$$Z_b = \frac{V_b^2}{S_b}\ |\Omega| = \frac{(1^2)}{9} = 0.111\overline{1}\ |\Omega| \qquad I_b = \frac{S_b}{\sqrt{3}V_b} = \frac{9*10\text{^}6}{\sqrt{3}*(1*10^3)} = 5{,}196.1524\ |\text{A}|.$$

Equivalent Circuit of Unit G1

All the three units of DFIG that are connected in parallel are represented as a single equivalent circuit with the corresponding parameters in |pu|. The equivalent parameters in |pu| are calculated based on number of units connected in parallel and system base values using the formula

$$Z_s^{|\text{pu}|} = Z_s^{/\text{rpu}/} * \left(\frac{S_b^{|\text{system level in |MVA}||}}{\text{no. of generaing units in parallel} * S^{|\text{machine rating in |MVA}|}} \right).$$

$$= Z_s^{/\text{rpu}/} * \left(\frac{9}{3*3}\right)$$

$$= Z_s^{/\text{rpu}/}$$

By using the above equation, the equivalent parameters in pu at power system level are the same as the /rpu/ values of the parameters of the DFIG defined in Chapter 3, page 42. Therefore,

$$R_s^{|pu|} = 0.006067 * \left(\frac{9}{3*3}\right) = 0.006067\ |pu|,\ R_r^{|pu|} = 0.005 * \left(\frac{9}{3*3}\right) = 0.005\ |pu|,$$

$$X_{sl}^{|pu|} = 0.0734 * \left(\frac{9}{3*3}\right) = 0.0734\ |pu|,\ X_{rl}^{|pu|} = 0.1034 * \left(\frac{9}{3*3}\right) = 0.1034\ |pu|, \text{and}$$

$$X_m^{|pu|} = 3.4734 * \left(\frac{9}{3*3}\right) = 3.4734\ |pu|.$$

The equivalent circuit of the DFIG is as shown in Figure 2.4, Chapter 2, pages (38-39), with the equivalent parameter values as shown above.

Equivalent Circuit of the Power Substation PS12

Power substation PS12 is represented by a gamma equivalent circuit shown in Figure 6.4 and the parameters of the equivalent circuit are obtained from Appendix E as below.

Parameters of the star (Yg) connected primary winding (LV) defined with $S_b = 9.48\ |MVA|$ and $V_b = 1|KV|$ are $R_1 = 0.025/30|pu|$ and $X_1 = 0.025\ |pu|$. Parameters of the delta (Δ) connected secondary winding (HV) defined on $S_b = 9.48\ |MVA|$ and $V_b = 25\ |KV|$ are $R_2 = 0.0008|pu|$, $X_2 = 0.025\ |pu|$. The connection of delta is such that the phase voltage on the delta winding leads the phase voltage on the star winding by 30^0. By using the change of base, and referring all parameters to the HV side it results

$$Z_1^{|punew|} = Z_1 * \left(\frac{S_b^{|new|}}{S_b^{|old|}}\right) * \left(\frac{V_b^{|old|}}{V_b^{|new|}}\right)^2,$$

$$R_1'^{|punew|} = 0.0008 * \left(\frac{9}{9.48}\right) * \left(\frac{1}{1}\right)^2 = 7.5949\ \text{x}\ 10^{-4}|pu|,$$

$$X_1'^{|punew|} = 0.025 * \left(\frac{9}{9.48}\right) * \left(\frac{1}{1}\right)^2 = 0.0237\ |pu|,$$

$$R_2^{|punew|} = 0.0008 * \left(\frac{9}{9.48}\right) = 7.5949\ \text{x}\ 10^{-4}|pu|,\quad X_2^{|punew|} = 0.025 * \left(\frac{9}{9.48}\right) = 0.0237\ |pu|.$$

The equivalent series resistance and reactance are

$$R_{12series}^{|pu|} = R_2^{|punew|} + R_1'^{|punew|} = 7.5949 \text{ x } 10^{-4} + 7.5949 \text{ x } 10^{-4} = 0.0015|pu|,$$

$$X_{12series}^{|pu|} = X_2^{|punew|} + X_1'^{|punew|} = 0.0237 + 0.0237 = 0.0474|pu|.$$

Therefore, the series impedance and admittance of the PS12 is

$$\underline{Z}_{tr12series}^{|pu|} = 0.0015 + j\,0.0474|pu| = 0.0474 \llbracket 88.18^0 \,|pu|,$$

$$\underline{Y}_{tr12series}^{|pu|} = 0.6670 - j\,21.0759|pu| = 21.0865 \llbracket -88.18^0 \,|pu|.$$

The magnetizing resistance $R_m^{|pu|} = 500\,|pu|$ and reactance $X_m^{|pu|} =$ infinity is defined on the base $S_b = 9.48\,|MVA|$ and $V_b = 25\,|KV|$. So using the change of base formula mentioned above, it results

$$R_m^{|punew|} = 500 * \left(\frac{9}{9.48}\right) = 474.6835\,|pu|.$$

Therefore, the shunt branch admittance and impedance are

$$\underline{Y}_{tr34sh}{}^{|pu|} = 0.0021|pu| = 0.0021 \llbracket 0^0 \,|pu|,$$

$$\underline{Z}_{tr34sh}{}^{|pu|} = R_m^{|punew|} + j\,X_m^{|punew|} = 474.6835 + j\,0\,|pu| = 474.6835 \llbracket 0^0 \,|pu|.$$

The equivalent circuit of Power Station (PS12) with the parameters calculated above is shown in Figure 6.4.

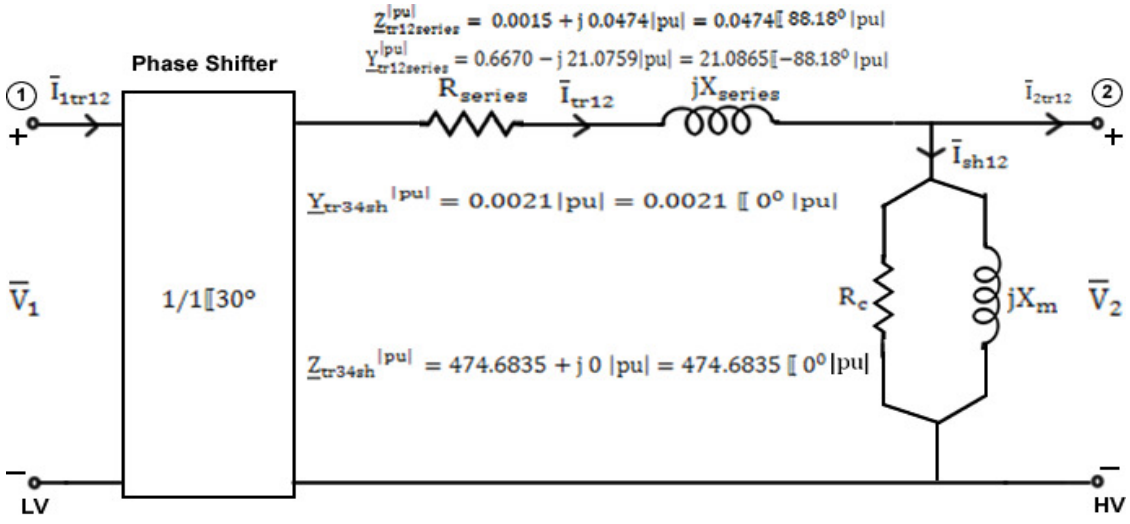

Figure 6.4. Equivalent Circuit of the Power Substation PS12

Equivalent Circuit of the Transmission Line L2-3

The parameters of the pi-equivalent circuit of the transmission line L2-3 shown in Figure 6.5 are calculated as below.

The parameters of the transmission line in actual units as shown in Appendix E are

$$R_{line} = 6.436\ |\Omega|,\ X_{line} = 59.9416\ |\Omega|,\ B_{line} = 1.2814 * 10\text{^} - 4\ |\text{Siemens}|$$

The corresponding base quantities at power system level are defined as

$$S_b = 9\ |\text{MVA}|,\ V_b = 25\ |\text{KV}|,\quad Z_b = \frac{V_b^2}{S_b}\ |\Omega| = \frac{(25^2)}{9} = 69.444\overline{4}\ |\Omega|,\ \text{and}$$

$$Y_b = \frac{1}{Z_b} = \frac{1}{69.4444} = 0.0144\ |\text{Siemens}|.$$

The |pu| values of the parameters at the power system level result as

$$R_{line}^{|pu|} = \frac{R_{line}^{|\Omega|}}{Z_b} = \frac{6.436}{69.444\overline{4}} = 0.0927\ |\text{pu}|,$$

$$X_{line}^{|pu|} = \frac{X_{line}^{|\Omega|}}{Z_b} = \frac{59.9416}{69.444\overline{4}} = 0.8632\ |\text{pu}|,$$

$$B_{line}^{|pu|} = \frac{B_{line}^{|\text{Siemens}|}}{Y_b} = \frac{1.2814 * 10\text{^} - 4}{0.0144} = 0.0089\ |\text{pu}|.$$

Hence, the series and shunt impedances and admittances of the transmission line are

$$\underline{Z}_{23} = 0.0927 + j0.8632\ |\text{pu}| = 0.8681\llbracket 83.87^0\ |\text{pu}|,$$

$$\underline{Y}_{23} = \frac{1}{\underline{Z}_{23}} = 0.1230 - j\ 1.1454 = 1.1519\ \llbracket\ -83.87^0,$$

$$\underline{Y}_{sh2line} = \underline{Y}_{sh3line} = j\frac{B_{line}}{2} = j\ \frac{0.0089}{2} = j0.0045\ |\text{pu}| = 0.0045\llbracket 90^0|\text{pu}|,$$

$$\underline{Z}_{sh2line} = \underline{Z}_{sh3line} = \frac{1}{\underline{Y}_{sh2line}} = -j\ 224.7554\ |\text{pu}| = 224.7555\llbracket -90^0|\text{pu}|.$$

The equivalent circuit of Transmission Line (L2-3) with the parameters calculated above is shown in Figure 6.5.

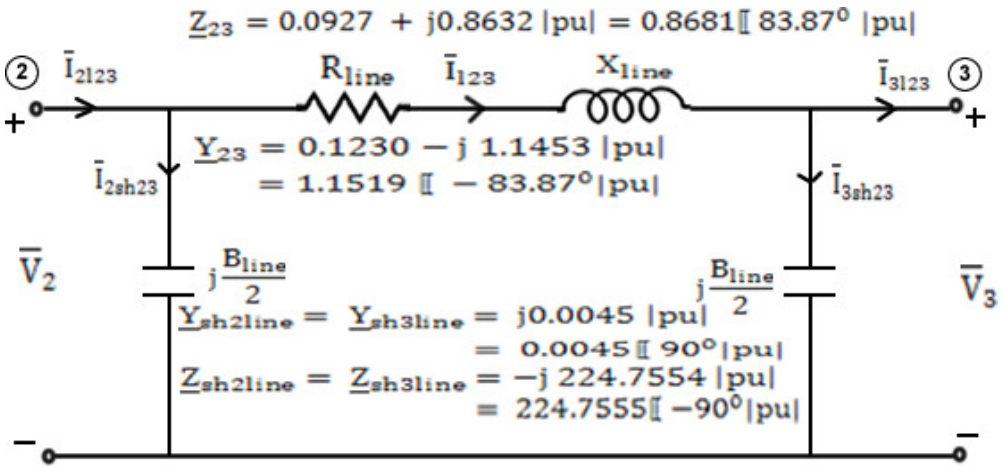

Figure 6.5. Equivalent Circuit of the Transmission Line

Equivalent circuit of the Power Substation (PS34)

The parameters of the equivalent gamma circuit of the power station PS34 shown in Figure 6.6 are obtained from Appendix E as below

Parameters of the star (Yg) connected primary winding (LV) defined on $S_b = 47\ |MVA|$ and $V_b = 25\ |KV|$ are $R_1 = 0.0027\ |pu|$ and $X_1 = 0.08\ |pu|$. Parameters of the delta (Δ) connected secondary winding (HV) defined on $S_b = 47\ |MVA|$ and $V_b = 120\ |KV|$ are $R_2 = 0.0027\ |pu|$ and $X_2 = 0.08\ |pu|$. The connection of delta is such that the phase voltage on the delta winding lags the phase voltage on the star winding by 30^0. By using the change of base and referring all parameters to the HV side it results

$$Z_1^{|punew|} = Z_1 * \left(\frac{S_b^{|new|}}{S_b^{|old|}}\right) * \left(\frac{V_b^{|old|}}{V_b^{|new|}}\right)^2,$$

$$R_1'^{|punew|} = 0.0027 * \left(\frac{9}{47}\right) * \left(\frac{120}{120}\right)^2 = 5.1702\ x\ 10^{-4}\ |pu|,$$

$$X_1'^{|punew|} = 0.08 * \left(\frac{9}{47}\right) * \left(\frac{120}{120}\right)^2 = 0.0153\ |pu|,$$

$$R_2^{|punew|} = 0.0027 * \left(\frac{9}{47}\right) = 5.1702x\ 10^{-4}|pu|, \qquad X_2^{|punew|} = 0.08 * \left(\frac{9}{47}\right) = 0.0153\ |pu|.$$

The equivalent series resistance and reactance are

$$R_{series}^{|pu|} = R_2^{|punew|} + R_1'^{|punew|} = 5.1702 \times 10^{-4} + 5.1702 \times 10^{-4} = 0.00103\ |pu|,$$

$$X_{series}^{|pu|} = X_2^{|punew|} + X_1'^{|punew|} = 0.0153 + 0.0153 = 0.03064|pu|.$$

Therefore, the series impedance and admittance of the PS34 is

$$\underline{Z}_{tr34series} = R_{series} + j\,X_{series} = 0.00103 + j\,0.03064\ |pu| = 0.0307\ [\![\ 88.07^0|pu|,$$

$$\underline{Y}_{tr34series} = 1.0959 - j\,32.6002\ |pu| = 32.6187\ [\![-88.07^0\ |pu|.$$

The magnetizing resistance $R_c^{|pu|} = 500\ |pu|$ and $X_m^{|pu|} = 500\ |pu|$is defined on the base $S_b = 47\ |MVA|$ and $V_b = 120\ |KV|$.

$$So,\ R_m^{|punew|} = X_m^{|punew|} = 500 * \left(\frac{9}{47}\right) = 95.7447\ |pu|.$$

And the shunt branch admittance and impedance results as

$$\underline{Y}_{tr34sh} = 0.0052 - j\,0.0052|pu| = 0.0074\ [\![-45^0|pu|,$$

$$\underline{Z}_{tr34sh} = 95.7447 + j\,95.7447\ |pu| = 135.4034\ [\![\ 45^0\ |pu|.$$

The equivalent circuit of Power Station (PS34) with the parameters calculated above is shown in Figure 6.6.

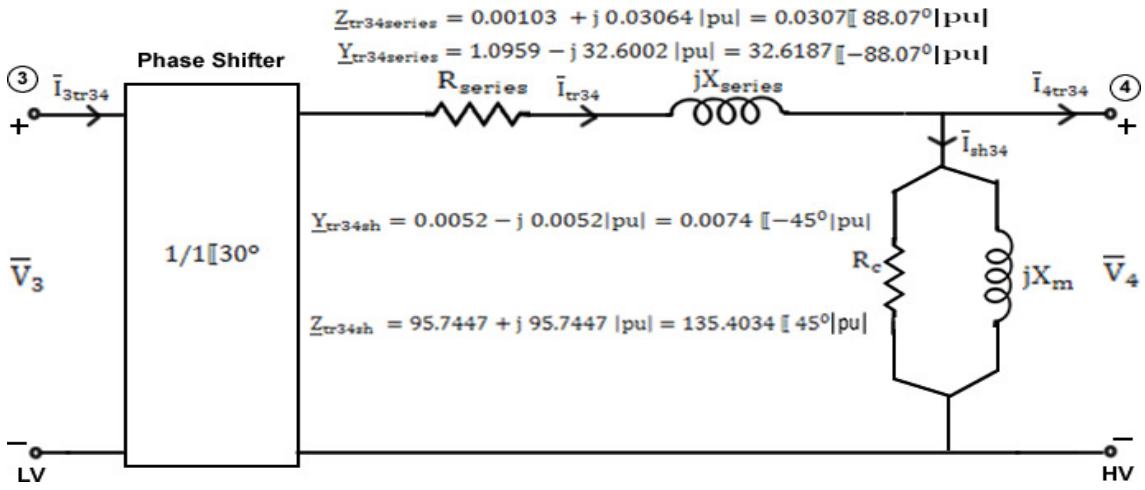

Figure 6.6. Equivalent Circuit of the Power Station PS34

Grid equivalent or source equivalent

Equivalent thevenin impedance was defined as $Z_{th} = 0.1 + j\,1\ |pu|$ defined on the base values $S_b = 2500\ |MVA|$ and $V_b = 120\ |KV|$. Using change of base formal mentioned above it results,

$$R_{th}^{|punew|} = 0.1 * \left(\frac{9}{2500}\right) = 0.0004\ |pu| \quad X_{th}^{|punew|} = 1 * \left(\frac{9}{2500}\right) = 0.0036\ |pu|,$$

$$Z_{th}^{|pu|} = 0.0004 + j0.0036 = 0.0036 \llbracket 84.29^0\ |pu|,$$

$$Y_{th}^{|pu|} = = 27.5028 - j\,275.0275\ |pu| = 276.3992 \llbracket -84.29^0\ |pu|,$$

$$\overline{V}_{th}^{|pu|} = 120\ |pu| = 120 \llbracket 0^0 |pu|.$$

The equivalent circuit of the source with the parameters calculated above is shown in Figure 6.7.

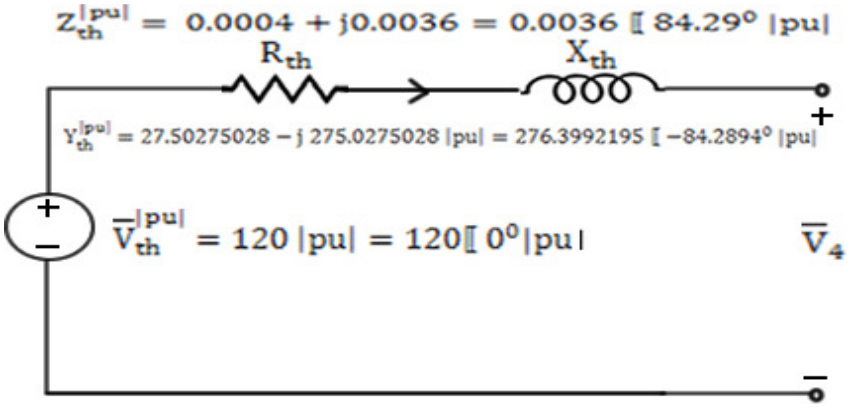

Figure 6.7. Equivalent Circuit of the Infinite Bus

6.3. Simulation of a Three Phase Fault at the Stator Terminals of the DFIG Wind Turbine Using MATLAB/SIMULINK

To study the transient behavior of the DFIG wind turbine and also to compare the results obtained from the analytical model, a three phase fault is imposed at the stator terminals of the DFIG (Bus 1 on Figure 6.2). The fault is applied for about 150|ms| at the time 3.15 seconds, i.e 3.15 seconds after the system has reached steady state. This is the minimum time required for protective elements to operate before disconnecting the wind turbine

from the grid. After 150|ms| from the instance the fault occurred, the voltage at the stator terminal reaches back to its steady state value. According to the proposed grid code requirements in USA as shown in Figure 1.9, page 22, Chapter 1, the DFIG wind turbine should stay connected to the grid for at least 150 |ms|, to achieve the requirement of Zero Voltage Ride through capability explained on page 17, section 1.8.1, Chapter 1. This section analyzes the effect on DFIG variables and current through the power electronic converter if a fault occurs for 150|ms|, and the DFIG is not equipped with Zero Voltage Ride Through Capability.

Figure 6.8 shows the voltage across the stator terminals of the DFIG during fault. The three phase solid ground fault applied at the stator terminals results in a voltage dip of 100% from 3.15|sec| to 3.3 |sec| as observed in Figure 6.8.

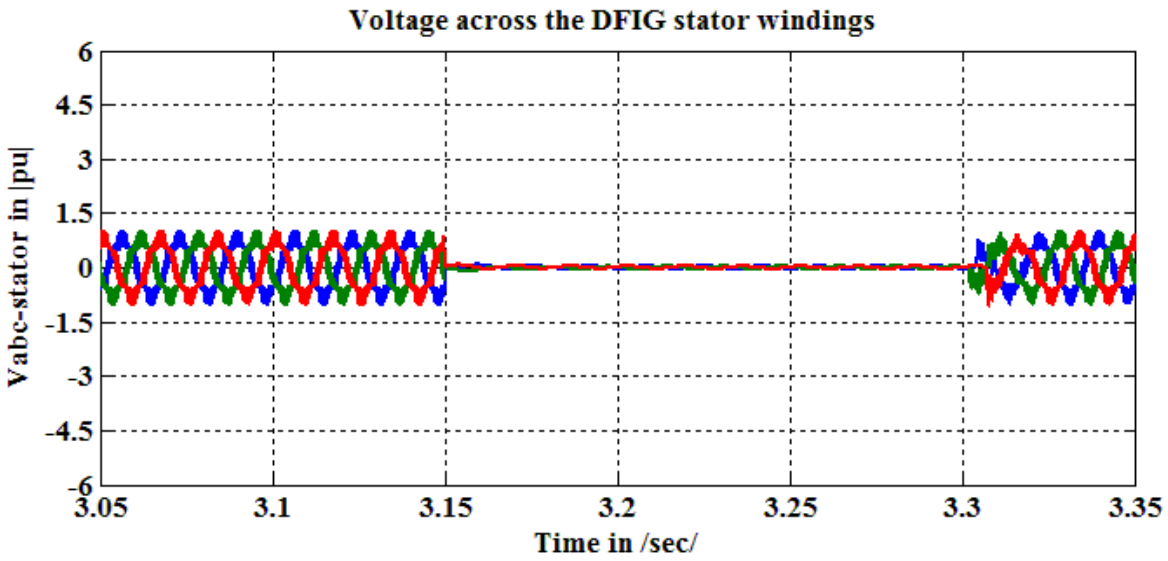

Figure 6.8. Voltage across the Stator Windings of the DFIG during Fault

Figure 6.9 shows the currents through the DFIG stator windings during fault. As shown in Figure 6.9, the stator current amplitude increases to about 4.15 times the rated value and to about 3.25 times after the fault has been cleared due to voltage dip of 100% at the stator

terminals as shown in Figure 6.9. Figure 6.9 is similar to the Figures 5.6-5.8 on pages (92-93) obtained through the transient analysis done in Chapter 5 of this thesis.

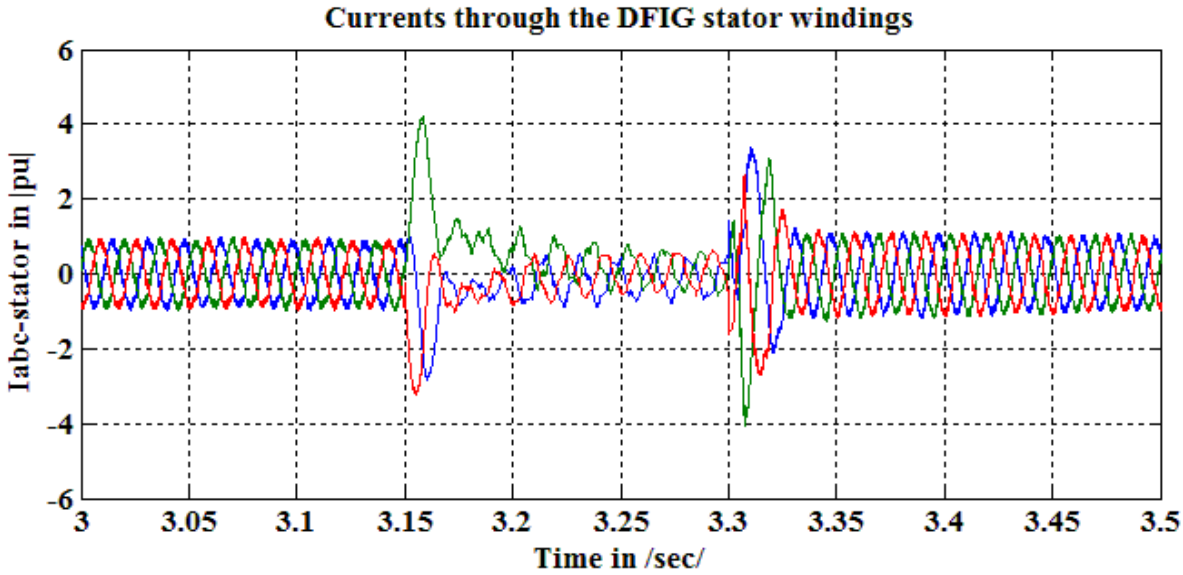

Figure 6.9. Currents through the Stator Windings of the DFIG during Fault

Figure 6.10 shows the currents through the DFIG rotor windings during fault. As shown in Figure 6.10, the rotor current amplitude increases to about 6.15 times the rated value and due to voltage dip of 100% at the stator terminals as shown in Figure 6.16. It can be observed in Figure 6.10, the current amplitude of the rotor currents is higher than that of the stator currents. The currents through the Rotor Side Converter (RSC) are same as the currents through rotor windings of the DFIG. Since the power electronic equipment cannot handle such high currents and expensive, they need to be protected.

Figure 6.10 is similar to the Figures 5.9-5.11 in pages (93-94) obtained through the transient analysis done in Chapter 5 of this thesis.

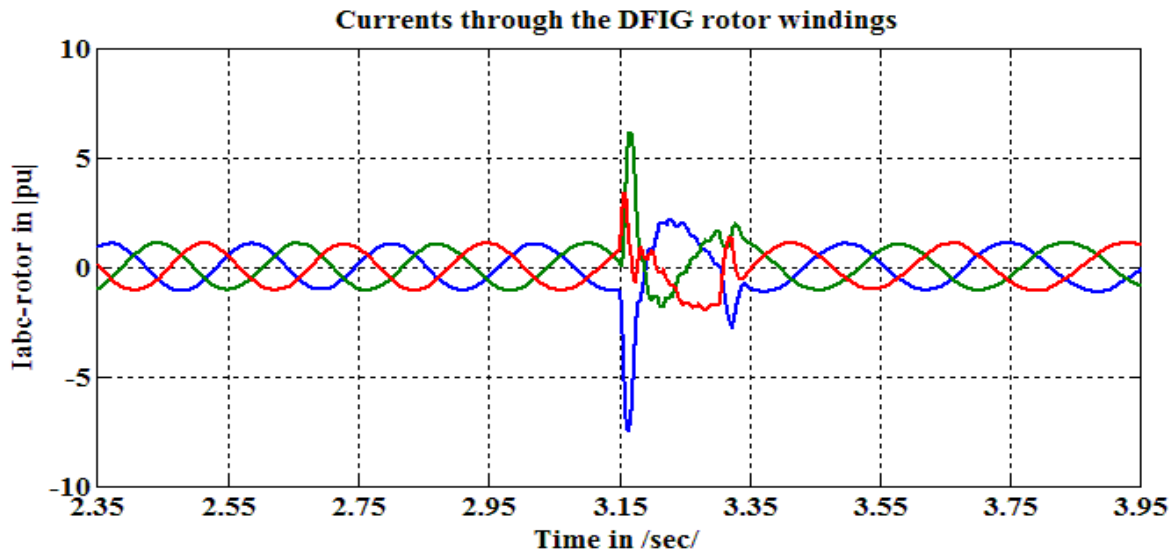

Figure 6.10. Currents through the Rotor Windings of the DFIG during Fault

Figure 6.11 shows the electromagnetic torque of the DIFG during fault. As shown on Figure 6.11, the electromagnetic torque approximately goes to zero during the fault and after the fault is cleared at 3.3 |sec|, the electromagnetic torque settles down at a slightly different value from its steady state. Figure 6.11 is similar to the Figure 5.12 shown in Chapter 5, page 95 of this thesis.

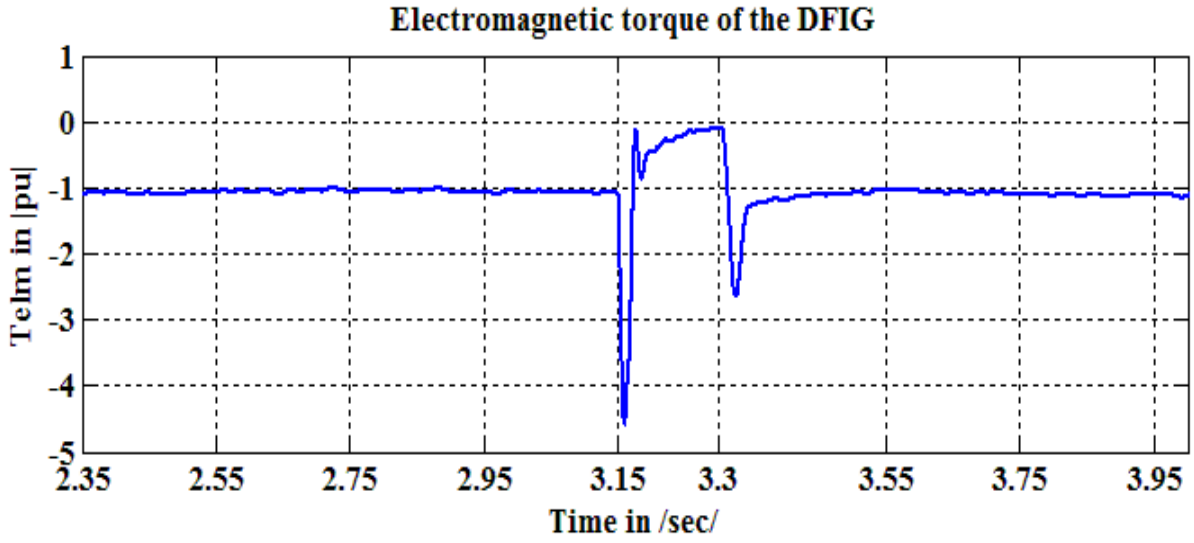

Figure 6.11. Electromagnetic Torque of the DFIG during Fault

6.4. Summary

Grid-connected Doubly Fed Induction Generators (DFIGs) are sensitive to dips in supply voltage, so-called “grid faults”. Fault ride through systems must be designed to manage the large and potentially dangerous fault currents in both stator and rotor circuits. However, DFIG fault response has been only partially or summarily treated in contemporary literature. A detailed analytical analysis of DFIG wind turbine grid-fault response was discussed in the thesis.

In order to study the physical behavior of the machine during the time of a fault, the DFIG model was built analytically using the flux linkage equations. The behavior of the DFIG currents, variations of flux linkages of the DFIG on d and q-axes, electromagnetic torque and angular frequency of the rotor during the occurrence of a three phase fault on the stator terminals of the DFIG were analyzed in detail.

To validate the results obtained using the analytical equations, the DFIG model was implemented using the Simpowersystems toolbox of Matlab Simulink. The voltage across the stator windings of the DFIG, currents through the DFIG stator windings and rotor windings and the electromagnetic torque of the DFIG were obtained for a three phase fault on the stator terminals of the DFIG. The results of the analytical model and the Simulink model are presented and several conclusions were drawn from this study.

6.5. Conclusions

The study of steady state and transient characteristics of the Doubly Fed Induction Generator (DFIG) resulted in the following conclusions:

Decoupled control of the active and reactive powers of the DFIG is possible as the d-axis and q-axis components of the rotor voltage component have significant individual effects.

The applied voltage across the rotor windings of the DFIG can shift the DFIG in generating mode from over-synchronous to under-synchronous speed range.

From the stator phase current (i_{sa}, i_{sb}, i_{sc}) graphs, the current amplitudes during the transient period are about 6 times higher than the corresponding steady state value.

From the rotor three phase current (i_{ra}, i_{rb}, i_{rc}) graphs, the current amplitudes during the transient period are about 8 times higher than corresponding steady state value. Such high rotor currents can damage the power electronic converters if not disconnected during the occurrence of a fault.

6.6. Future Work

New grid code requirements as shown in Figure 1.9 are in progress. This means that new wind turbine installations have to stay connected to the grid for voltage sags above certain reference sag, i.e. wind turbines have to ride through these voltage sags. Based on the analysis done, it can be concluded that the only method for improving the capability of grid Fault Ride Through (FRT) capability is to suppress the changes in the stator flux linkage. There are two methods to restrain the changes in stator flux, i.e either to implement the crowbar or to compensate the changes in the stator flux using the proposed methodology.

The crowbar solution is a bypass resistance connected to the rotor windings of the DFIG through the thyristor. The crowbar firing is triggered by the dc-link voltage which rises due to the first rotor current peak. When the crowbar is switched on, the converter is separated

from the rotor circuits, and the system goes to an asynchronous operating mode and consumes reactive power from the grid.

To suppress the changes in the stator flux during the fault, the following methodology is proposed:

A reactance with switches across it, i.e., in parallel is included in series with the stator windings of the DFIG. During the steady state operation of the DFIG, the switches connected in parallel to the reactance are closed. At the instant when a fault occurs, the rotor side converter is disconnected from the rotor of the DFIG and is connected to the crowbar, rotor windings of the DFIG are short circuited and the switches parallel to the reactance are opened simultaneously. At the moment when the fault has been cleared, switches that short circuit the rotor winding are turned off, crowbar is disconnected and the rotor side converter is connected to the rotor of the DFIG, but the switches parallel to the series reactance still remain open. After a time corresponding to the transient after the fault, the series reactances are short circuited, i.e., the switches across it are closed. The reactance parameter and the reactance operation time scenario should be selected such that along the fault duration and the post fault transient, the over currents magnitude and transient process to be limited, specifically to be optimized.

REFERENCES

[1] "Monthly Energy Review May 2010," *U.S. Energy Information Administration* (EIA), http://www.eia.gov/

[2] "U.S. Renewable Energy Consumption," *Center for Sustainable System* (CSS), http://css.snre.umich.edu/css_doc/CSS03-12.pdf

[3] Mark Z. Jacobson, "Review of solutions to global warming, air pollution, and energy security," *Energy and Environmental Science*, pp 148-173, December 2008.

[4] http://en.wikipedia.org/wiki/Wind_power

[5] "Third Quarter 2010 Market Report," *American Wind Energy Association* http://www.awea.org/learabout/publications/upload/2010_third_quarter report.pdf

[6] "Main Components of a Wind Turbine," *Avionex USA* http://www.avionexusa.com/pdf/Main_Components_of_a_Wind Turbine.pdf

[7] T.Sharpe, D.Jenkins, and T.Burton, "Wind Energy Handbook," *John Wiley & Son,* Ltd Chichester, ISBN 10:0471489972, June 2001.

[8] "Comparison with field data for Vestas V80 and V90 large wind turbines," http://www.wind-power-program.com/large_turbines.htm

[9] D.K.Jain, K.S.Sandhu, and M.Rajveer, "An overview of some important issues related to Wind Energy Conversion Systems (WECS)," *International Journal of Environmental Science and Development,* Vol. No. 1, Issue 4, pp. 352-363, October 2010.

[10] "An Wind Turbine Technology Overview," *Nyserda* http://www.powernaturally.org/programs/wind/toolkit/9_windturbinen etech.pdf

[11] A.Olimpo, N.Jenkins, and P.Cartwright "Wind energy modeling and control," Wiley, ISBN 9780470714331.

[12] H.Li and Z.Chen, "Overview of different wind generator systems and their comparisons," *IET Renewable Power Generation*, Vol. No.2, Issue 2, pp. 123-138, August 2007.

[13] L.Holdsworth, X.Ekananyake, and N.Jenkins, " Comparison of fixed speed and doubly-fed induction wind turbines during power system disturbances," *IEE Proceedings-Generation, Transmission, Distribution,* Volume 150, Issue 3, pp 345-350, May 2003.

[14] S.Heier, "Grid Integration of Wind Energy Conversion Systems," J*ohn Wiley & Sons, Ltd, Chichester*, 2006, ISBN 0470868996.

[15] J.G.Slootweg, "*Wind Power: Modelling and impacts on power system dynamics,"* PhD thesis, Technical Univesity of Delft, December 2003.

[16] A.Lipo, A.Rockhill, P.Tenca, "Low Voltage Ride Through Capability for Wind Turbines based on Current Source Inverter Topologies," *Research Report,* Department of Electrical and Computer Engineering, University of Wisconsin-Madison, December 2007.

[17] "Principles of Doubly Fed Induction Generators," Courseware Sample by the staff of Lab-Volt Ltd, May 2011.

[18] A.D.Hansen, F.Iov, P.Sorensen and F.Blaabjerg, "Overall control strategy of variable speed doubly-fed induction generator wind turbine," *NORDIC WIND POWER* CONFERENCE, pp. 1-7, Denmark, 1-2 March 2004.

[19] Professor, Dr. Ovidiu Crisan notes on "Modeling Doubly Fed Induction Generator," ECE 7381.

[20] A. Abedini, "Integration of Permanent Magnetic Synchronous Generator Wind Turbines into the Power Grid," *Dissertation for PhD,* University of Wisconsin-Madison, Milwaukee, December 2008.

[21] J.Morren and W.H.Haan, "Short-Circuit Current of Wind Turbines with Doubly Fed Induction Generator," *IEEE Transactions on Energy Conversion,* Vol 22, Issue 1, pp. 174-180, March 2007.

[22] Lopez and Sanchis, Roboam, "Dynamic behavior of Doubly Fed Induction Generator during three phase voltage dips," *IEEE Transactions on Energy Conversion*, Vol 22, Issue 3, pp. 709-717, September 2007.

[23] S.Li and S.Sinha, "A Simulation analysis of Double-Fed Induction Generator for Wind Energy Conversion Using PSpice," *International Journal of Power and EnergySystems*, Vol.29, No.2, pp 1-8, October 2009.

[24] http://www.thewindpower.net/windfarm_en_3169_synder-wind-project.php

[25] http://www.gov.pe.ca/photos/sites/envengfor/file/950010R1_V90-GeneralSpecification.pdf

[26] www.noaa.com

[27] A.Petterson, "*Analysis, Modeling and Control of Doubly Fed Induction Generators for Wind Turbines*," Thesis for the degree of Doctor of Philosophy, Chalmers University of Technology, Sweden 2005.

[28] Beltz limit Values http://www.reuk.co.uk/Betz-Limit.htm

[29] Faculty of Physics, University of Technology, Eindhoven, "Rotors for Wind Power," Revised edition, January 2004.

[30] A.Abedini, "*Integration of Permanent Magnet Synchronous Generator Wind Turbines into Power Grid*," Dissertation for the degree of Doctor of Philosophy, University of Wisconsin-Milwaukee, December 2008.

[31] A.B.Gonzalo, "Predective Directive Control (PDC) techniques of the Doubly fed induction machine for wind energy generation applications," *Thesis,* Mondragon University, July 2008.

[32] J.L. Rodriguez-Amenedl, S.Amalte, and J.C.Burgo, " Automation generation control of a wind farm with variable speed wind turbines," *IEEE Transactions on Energy Conversion,* Vol No 17, pp 279-284, June 2002.

[33] A.D.Hanse, F.Iov, and F.Blaabjerg, "Centralised power control of wind farm with doubly fed induction generators," *Renewable Energy,* Vol. No 31, pp. 935-951, June 2006.

[34] S.Muller, M.Deicke, and R.W. De Doncker, "Double fed induction generator systems for wind turbines," *IEEE Industry Applications Magazine,* Vol No 8, Issue 3, May/June 2002, pp. 26-33.

[35] F.M. Hughes, and O.Anaya-Lara, "Control of DFIG-based wind generation for power network support," *IEEE Transactions on Power System,* Vol No 20, Issue 4, pp 1958-1966, November 2005.

[36] "Description of the Controls used for Variable Speed DFIG Wind Turbine," Matlab/Simulink.

[37] List of Moments of Inertia, http://en.wikipedia.org/wiki/List_of_moments_of_inertia

[38] www.mathworks.com

APPENDIX A

The Total Installed Wind Capacity across the United States by the End of the Year 2010

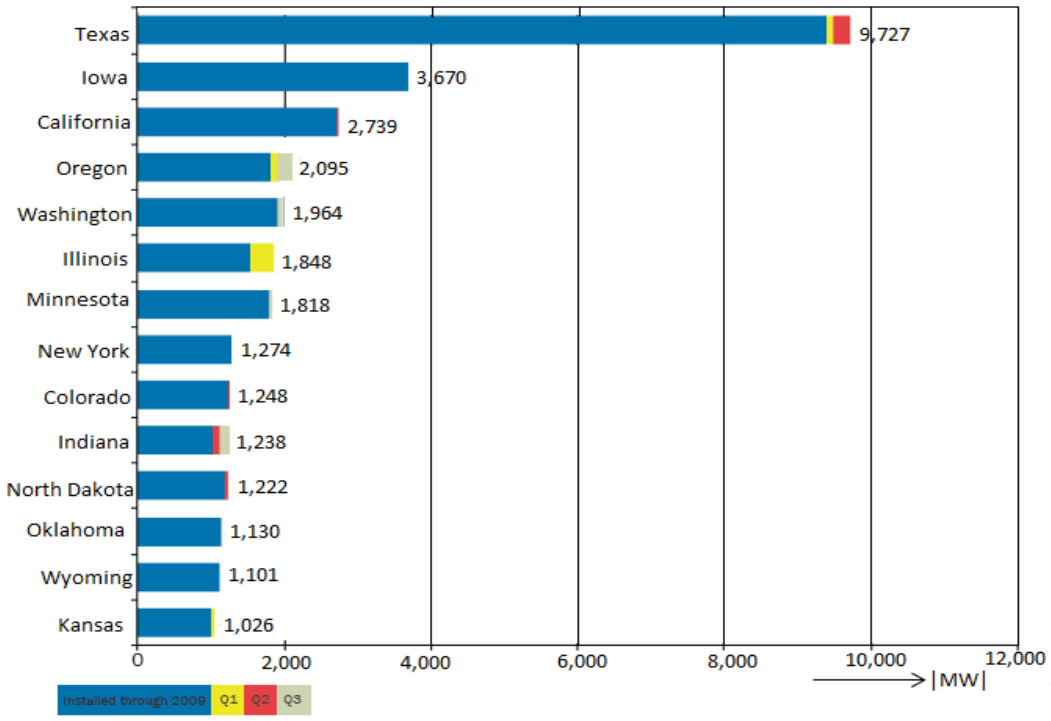

Figure A.1. Installed Wind Capacity in different States by 2010

The bar graph shows the wind energy installed in three quarters of 2010 and also the total installed wind capacity until 2010.

- From the graph it results that by the end of third quarter of 2010, there were 14 states with over 1,000 |MW| of wind installed and 37 states with some utility-scale wind installed.
- Oregon took the lead in adding the most capacity in the third quarter, a spot historically filled by Texas, where the industry now awaits investments in more electric transmission lines.
- With 111 |MW| added in the third quarter of 2010, Indiana moved into the top ten wind power states.

APPENDIX B

DFIG Machine Model Derivations

B.1 Detailed Explanation of Winding Terminal Voltage and Flux Linkage Equations in Phase Reference

Winding Terminal Voltage Equations in Phase Reference

$$[v]_{\text{sph}}^{|\text{V}|} = -[\text{R}]_{\text{sph}}^{|\frac{\text{V}}{\text{A}}|} * [i]_{\text{sph}}^{|\text{A}|} - \frac{\text{d}}{\text{dt}^{|\text{s}|}}[\Psi]_{\text{sph}}^{|\text{Vs}|}, \text{ and}$$

$$[v]_{\text{rph}}^{|\text{V}|} = [\text{R}]_{\text{rph}}^{|\frac{\text{V}}{\text{A}}|} * [i]_{\text{rph}}^{|\text{A}|} + \frac{\text{d}}{\text{dt}^{|\text{s}|}}[\Psi]_{\text{rph}}^{|\text{Vs}|}.$$

Where

$$[v]_{\text{sph}}^{|\text{V}|} = \begin{bmatrix} v_{\text{sa}} \\ v_{\text{sb}} \\ v_{\text{sc}} \end{bmatrix}^{|\text{V}|}, \; [v]_{\text{rph}}^{|\text{V}|} = \begin{bmatrix} v_{\text{ra}} \\ v_{\text{rb}} \\ v_{\text{rc}} \end{bmatrix}^{|\text{V}|}, [i]_{\text{sph}}^{|\text{A}|} = \begin{bmatrix} i_{\text{sa}} \\ i_{\text{sb}} \\ i_{\text{sc}} \end{bmatrix}^{|\text{A}|}, [i]_{\text{rph}}^{|\text{A}|} = \begin{bmatrix} i_{\text{ra}} \\ i_{\text{rb}} \\ i_{\text{rc}} \end{bmatrix}^{|\text{A}|},$$

$$[\text{R}]_{\text{sph}}^{|\frac{\text{V}}{\text{A}}|} = \begin{bmatrix} \text{R}_{\text{s}} & & \\ & \text{R}_{\text{s}} & \\ & & \text{R}_{\text{s}} \end{bmatrix}^{|\Omega|}, [\text{R}]_{\text{rph}}^{|\frac{\text{V}}{\text{A}}|} = \begin{bmatrix} \text{R}_{\text{r}} & & \\ & \text{R}_{\text{r}} & \\ & & \text{R}_{\text{r}} \end{bmatrix}^{|\Omega|}, [\Psi]_{\text{sph}}^{|\text{Vs}|} = \begin{bmatrix} \Psi_{\text{sa}} \\ \Psi_{\text{sb}} \\ \Psi_{\text{sc}} \end{bmatrix}^{|\text{Vs}|}, \text{and } [\Psi]_{\text{rph}}^{|\text{Vs}|} = \begin{bmatrix} \Psi_{\text{ra}} \\ \Psi_{\text{rb}} \\ \Psi_{\text{rc}} \end{bmatrix}^{|\text{Vs}|}.$$

Flux Linkage Equations in Phase Reference

$$[\Psi]_{\text{sph}}^{|\text{Vs}|} = [\text{L}]_{\text{ssph}}^{|\frac{\text{Vs}}{\text{A}}|} * [i]_{\text{sph}}^{|\text{A}|} + [\text{L}]_{\text{srph}}^{|\frac{\text{Vs}}{\text{A}}|} * [i]_{\text{rph}}^{|\text{A}|}, \text{ and}$$

$$[\Psi]_{\text{rph}}^{|\text{Vs}|} = [\text{L}]_{\text{rsph}}^{|\frac{\text{Vs}}{\text{A}}|} * [i]_{\text{sph}}^{|\text{A}|} + [\text{L}]_{\text{rrph}}^{|\frac{\text{Vs}}{\text{A}}|} * [i]_{\text{rph}}^{|\text{A}|}.$$

Where

$$[\text{L}]_{\text{ssph}}^{|\frac{\text{Vs}}{\text{A}}|} = \begin{bmatrix} (\text{L}_{\text{sl}} + \text{L}_{\text{ssm}}) & -0.5 * \text{L}_{\text{ssm}} & -0.5 * \text{L}_{\text{ssm}} \\ -0.5 * \text{L}_{\text{ssm}} & (\text{L}_{\text{sl}} + \text{L}_{\text{ssm}}) & -0.5 * \text{L}_{\text{ssm}} \\ -0.5 * \text{L}_{\text{ssm}} & -0.5 * \text{L}_{\text{ssm}} & (\text{L}_{\text{sl}} + \text{L}_{\text{ssm}}) \end{bmatrix}^{|\frac{\text{Vs}}{\text{A}}|},$$

$$[L]_{rrph}^{|\frac{Vs}{A}|} = \begin{bmatrix} (L_{rl} + L_{rrm}) & -0.5 * L_{rrm} & -0.5 * L_{rrm} \\ -0.5 * L_{rrm} & (L_{sl} + L_{rrm}) & -0.5 * L_{rrm} \\ -0.5 * L_{rrm} & -0.5 * L_{rrm} & (L_{rl} + L_{rrm}) \end{bmatrix}^{|\frac{Vs}{A}|},$$

$$[L]_{rsph}^{|\frac{Vs}{A}|} = -L_{rs}^{|\frac{Vs}{A}|} * [T]_{rs},$$

$$[L]_{rsph}^{|\frac{Vs}{A}|} = -L_{rs}^{|\frac{Vs}{A}|} * \begin{bmatrix} \cos\theta_{rel}{}^{0} & \cos(\theta_{rel} - 120)^{0} & \cos(\theta_{rel} - 240)^{0} \\ \cos(\theta_{rel} - 240)^{0} & \cos\theta_{rel}{}^{0} & \cos(\theta_{rel} - 120)^{0} \\ \cos(\theta_{rel} - 120)^{0} & \cos(\theta_{rel} - 240)^{0} & \cos\theta_{rel}{}^{0} \end{bmatrix}, \text{ and}$$

$$[L]_{srph}^{|\frac{Vs}{A}|} = [L]_{rsph}^{T|\frac{Vs}{A}|}.$$

Where the stator leakage, rotor leakage, stator and rotor mutual inductances are defined below, with $\mathcal{P}$ representing the magnetic permeance of the corresponding path.

$$L_{sl}^{|\frac{Vs}{A}|} = N_s^2 * \mathcal{P}_{msl}^{|\frac{Vs}{A}|}, L_{rl}^{|\frac{Vs}{A}|} = N_r^2 * \mathcal{P}_{mrl}^{|\frac{Vs}{A}|}, L_{ssm}^{|\frac{Vs}{A}|} = N_s^2 * \mathcal{P}_{mm}^{|\frac{Vs}{A}|}, L_{rrm}^{|\frac{Vs}{A}|} = N_r^2 * \mathcal{P}_{mm}^{|\frac{Vs}{A}|}$$

$$L_{rs}^{|\frac{Vs}{A}|} = L_{sr}^{|\frac{Vs}{A}|} = N_s * N_r * \mathcal{P}_{mm}^{|\frac{Vs}{A}|}.$$

B.2 Derivation of Windings Terminal Voltage and Flux Linkage Equations in dqo Reference Frame

DFIG should have the same instantaneous terminal power, the same magnetic energy, and the same magnetomotive force before and after the transformation. These three conditions are applied for transforming both stator and rotor phases to dqo reference frame.

Stator

$[T]_{sv}$,$[T]_{si}$, $[T]_{s\Psi}$ be the transformation matrices for transforming the stator voltages, currents and flux linkages from stator phase to dqo reference frame respectively, i.e.,

$$[v]_{sdq} = [T]_{sv} * [v]_{sph}, \quad (B.1)$$

$$[i]_{sdq} = [T]_{si} * [i]_{sph}, \text{ and} \quad (B.2)$$

$$[\Psi]_{sdq} = [T]_{s\Psi} * [\Psi]_{sph}. \quad (B.3)$$

The conservative rules stated above are now imposed.

a) The instantaneous terminal power of the stator windings before and after the transformation should remain the same, that is

$$[v]_{\mathrm{sdq}}^{\mathrm{T}} * [i]_{\mathrm{sdq}} = [v]_{\mathrm{sph}}^{\mathrm{T}} * [i]_{\mathrm{sph}}. \quad \text{(B.4)}$$

Substituting equation (B.1) and (B.2) into equation (B.4), it results

$$[v]_{\mathrm{sph}}^{\mathrm{T}} * [\mathrm{T}]_{\mathrm{sv}}^{\mathrm{T}} * [\mathrm{T}]_{\mathrm{si}} * [i]_{\mathrm{sph}} = [v]_{\mathrm{sph}}^{\mathrm{T}} * [i]_{\mathrm{sph}}, \text{ and} \quad \text{(B.5)}$$

$$[\mathrm{T}]_{\mathrm{sv}}^{\mathrm{T}} * [\mathrm{T}]_{\mathrm{si}} = [1]. \quad \text{(B.6)}$$

b) The magnetic energy of the stator windings before and after the transformation should remain the same, that is

$$\frac{1}{2}[\Psi]_{\mathrm{sdq}}^{\mathrm{T}} * [i]_{\mathrm{sdq}} = \frac{1}{2} * [\Psi]_{\mathrm{sph}}^{\mathrm{T}} * [i]_{\mathrm{sph}} \quad \text{(B.7)}$$

Substituting equation (B.2) and (B.3) into equation (B.7), it results

$$[\Psi]_{\mathrm{sph}}^{\mathrm{T}} * [\mathrm{T}]_{\mathrm{s}\Psi}^{\mathrm{T}} * [\mathrm{T}]_{\mathrm{si}} * [i]_{\mathrm{sph}} = [\Psi]_{\mathrm{sph}}^{\mathrm{T}} * [i]_{\mathrm{sph}}, \text{ and} \quad \text{(B.8)}$$

$$[\mathrm{T}]_{\mathrm{s}\Psi}^{\mathrm{T}} * \mathrm{N}_{\mathrm{sd}} = [1]. \quad \text{(B.9)}$$

c) The air gap magnetomotive force of the stator windings before and after transformation should remain the same, that is,

$$\begin{bmatrix} \mathrm{N}_{\mathrm{sd}} i_{\mathrm{sd}} \\ \mathrm{N}_{\mathrm{sq}} i_{\mathrm{sq}} \\ 3\mathrm{N}_{\mathrm{so}} i_{\mathrm{so}} \end{bmatrix} = \begin{bmatrix} \mathrm{N}_{\mathrm{s}} \cos\theta_{\mathrm{del}} & \mathrm{N}_{\mathrm{s}} \cos(\theta_{\mathrm{del}} - 120)^0 & \mathrm{N}_{\mathrm{s}} \cos(\theta_{\mathrm{del}} - 240)^0 \\ -\mathrm{N}_{\mathrm{s}} \sin\theta_{\mathrm{del}} & -\mathrm{N}_{\mathrm{s}} \sin(\theta_{\mathrm{del}} - 120)^0 & -\mathrm{N}_{\mathrm{s}} \sin(\theta_{\mathrm{del}} - 240)^0 \\ \mathrm{N}_{\mathrm{s}} & \mathrm{N}_{\mathrm{s}} & \mathrm{N}_{\mathrm{s}} \end{bmatrix} \begin{bmatrix} i_{\mathrm{sa}} \\ i_{\mathrm{sb}} \\ i_{\mathrm{sc}} \end{bmatrix}. \quad \text{(B.10)}$$

Rearranging the above matricial equation (B.10), it results

$$\begin{bmatrix} i_{\mathrm{sd}} \\ i_{\mathrm{sq}} \\ i_{\mathrm{so}} \end{bmatrix} = \begin{bmatrix} \left(\frac{\mathrm{N}_{\mathrm{s}}}{\mathrm{N}_{\mathrm{sd}}}\right) \cos(\theta_{\mathrm{del}})^0 & \left(\frac{\mathrm{N}_{\mathrm{s}}}{\mathrm{N}_{\mathrm{sd}}}\right) \cos(\theta_{\mathrm{del}} - 120)^0 & \left(\frac{\mathrm{N}_{\mathrm{s}}}{\mathrm{N}_{\mathrm{sd}}}\right) \cos(\theta_{\mathrm{del}} - 240)^0 \\ \left(\frac{\mathrm{N}_{\mathrm{s}}}{\mathrm{N}_{\mathrm{sq}}}\right) \sin(-\theta_{\mathrm{del}})^0 & -\left(\frac{\mathrm{N}_{\mathrm{s}}}{\mathrm{N}_{\mathrm{sq}}}\right) \sin(\theta_{\mathrm{del}} - 120)^0 & -\left(\frac{\mathrm{N}_{\mathrm{s}}}{\mathrm{N}_{\mathrm{sq}}}\right) \sin(\theta_{\mathrm{del}} - 240)^0 \\ \frac{1}{3}\left(\frac{\mathrm{N}_{\mathrm{s}}}{\mathrm{N}_{\mathrm{so}}}\right) & \frac{1}{3}\left(\frac{\mathrm{N}_{\mathrm{s}}}{\mathrm{N}_{\mathrm{so}}}\right) & \frac{1}{3}\left(\frac{\mathrm{N}_{\mathrm{s}}}{\mathrm{N}_{\mathrm{so}}}\right) \end{bmatrix} \begin{bmatrix} i_{\mathrm{sa}} \\ i_{\mathrm{sb}} \\ i_{\mathrm{sc}} \end{bmatrix}.$$

The number of turns of windings on d, q, o axes i.e, N_{sd}, N_{sq} and N_{so} are selected such that the transformation matrices should be equal, that is

$$[T]_{sv} = [T]_{si} = [T]_{s\Psi} = [T]_s. \quad \text{(B.10)}$$

Where

$$[T]_s = \sqrt{\frac{2}{3}} * \begin{bmatrix} \cos\theta_{del} & \cos(\theta_{del} - 120^0) & \cos(\theta_{del} - 240^0) \\ -\sin\theta_{del} & -\sin(\theta_{del} - 120^0) & -\sin(\theta_{del} - 240^0) \\ \frac{1}{\sqrt{2}} & \frac{1}{\sqrt{2}} & \frac{1}{\sqrt{2}} \end{bmatrix}, \quad \text{(B.11)}$$

$$[T]_s^{-1} = [T]_s^T, \quad \text{(B.12)}$$

$$\left(\frac{N_s}{N_{sd}}\right) = \left(\frac{N_s}{N_{sq}}\right) = \left(\frac{N_s}{N_{so}}\right) = \sqrt{3},$$

$$N_{sd} = N_{sq} = \sqrt{\frac{3}{2}} * N_s \quad \text{and} \quad N_{so} = \frac{1}{\sqrt{3}} * N_s. \quad \text{(B.13)}$$

By using set of equations (2.1), (B.1 - B.3), (B.10) and (B.11) it results

$$[T]_s[v]_{sph} = -[T]_s[R]_{sph}\,[T]_s^{-1}[i]_{sdq} - [T]_s\frac{d}{dt}\{[T]_s^{-1}\,[\Psi]_{sdq}\}, \text{ that is} \quad \text{(B.14)}$$

$$[v]_{sdq} = -\left([T]_s[R]_{sph}\,[T]_s^{-1}\right)[i]_{sdq} - [T]_s\quad [T]_s^{-1}\left(\frac{d}{dt}\,[\Psi]_{sdq}\right) - [T]_s\left(\frac{d}{dt}[T]_s^{-1}\right)[\Psi]_{sdq}.$$

(B.15)

With $[R]_{sdq} = [T]_s[R]_{sph}\,[T]_s^{-1}$, $[T]_s\left(\frac{d}{dt}[T]_s^{-1}\right) = [T]_{sw} = \begin{bmatrix} & -1 & \\ 1 & & \end{bmatrix}\omega_{del}$, and

$\omega_{del} = \frac{d\theta_{del}}{dt}$.

Substituting equation (B.15) in (B.14), it results as

$$[v]_{sdq} = -[R]_{sdq}[i]_{sdq} - \frac{d}{dt}\,[\Psi]_{sdq} - [T]_{sw}\,[\Psi]_{sdq}, \quad \text{(B.16)}$$

where $[T]_s[v]_{sph} = -[T]_s[R]_{sph}\,[T]_s^{-1}[i]_{sdq} - [T]_s\frac{d}{dt}\{[T]_s^{-1}\,[\Psi]_{sdq}\}$,

$$[T]_s[T]_s^{-1} = [T]_r[T]_r^{-1} = [I] = \begin{bmatrix} 1 & 0 & 0 \\ 0 & 1 & 0 \\ 0 & 0 & 1 \end{bmatrix},$$

$$[T]_{sw} = \begin{bmatrix} & -1 & \\ 1 & & \end{bmatrix}\omega_{del}. \quad \text{(B.17)}$$

Rotor

$[T]_{rv}$,$[T]_{ri}$, $[T]_{r\Psi}$ be the transformation matrices for transforming the rotor voltages, currents and flux linkages from phase to dqo reference respectively, i.e.,

$$[v]_{rdq} = [T]_{rv} * [v]_{rph}, \quad \text{(B.18)}$$

$$[i]_{rdq} = [T]_{ri} * [i]_{rph}, \quad \text{(B.19)}$$

$$[\Psi]_{rdq} = [T]_{r\Psi} * [\Psi]_{rph}. \quad \text{(B.20)}$$

By applying the same conservative requirements for the stator windings that are, a) the instantaneous terminal power of the rotor windings before and after the transformation should remain the same b) the magnetic energy of the rotor windings before and after the transformation should remain the same and c) the air gap magnetomotive force from the rotor windings before and after transformation should remain the same and imposing the following condition for the transformation matrices

$$[T]_{rv} = [T]_{ri} = [T]_{r\Psi} = [T]_r. \quad \text{(B.21)}$$

Where

$$[T]_r = \sqrt{\frac{2}{3}}\begin{bmatrix} \cos(\theta_{del} - \theta_{rel}) & \cos(\theta_{del} - \theta_{rel} - 120^0) & \cos(\theta_{del} - \theta_{rel} - 240^0) \\ -\sin(\theta_{del} - \theta_{rel}) & -\sin(\theta_{del} - \theta_{rel} - 120^0) & -\sin(\theta_{del} - \theta_{rel} - 240^0) \\ \frac{1}{\sqrt{2}} & \frac{1}{\sqrt{2}} & \frac{1}{\sqrt{2}} \end{bmatrix},$$

$$[T]_r^{-1} = [T]_r^T, \quad \text{(B.22)}$$

$$N_{rd} = N_{rq} = \sqrt{\frac{3}{2}} * N_r \text{ and } N_{ro} = \frac{1}{\sqrt{3}} * N_r = \sqrt{\frac{2}{3}} * \frac{1}{\sqrt{2}} N_r. \quad \text{(B.23)}$$

Using the set of equations (2.2), (B.21) and (B.22) it results

$$[T]_r[v]_{rph} = ([T]_r[R]_{rph}\,[T]_r^{-1})[i]_{rdq} + [T]_r \frac{d}{dt}\{[T]_r^{-1}\,[\Psi]_{rdq}\}, \text{ that is} \quad \text{(B.24)}$$

$$[v]_{rdq} = ([T]_r[R]_{rph}\,[T]_r^{-1})[i]_{rdq} + [T]_r[T]_r^{-1}\frac{d}{dt}[\Psi]_{rdq} + [T]_r\left(\frac{d}{dt}[T]_r^{-1}\right)[\Psi]_{rdq}. \quad \text{(B.25)}$$

With $[\mathrm{R}]_{\mathrm{rdq}} = [\mathrm{T}]_{\mathrm{r}}[\mathrm{R}]_{\mathrm{rph}}\,[\mathrm{T}]_{\mathrm{r}}^{-1}$,

$$[\mathrm{T}]_{\mathrm{r}}[\mathrm{T}]_{\mathrm{r}}^{-1} = [\mathrm{I}] = \begin{bmatrix} 1 & 0 & 0 \\ 0 & 1 & 0 \\ 0 & 0 & 1 \end{bmatrix}, [\mathrm{T}]_{\mathrm{rw}} = \begin{bmatrix} & -1 & \\ 1 & & \end{bmatrix}(\omega_{del} - \omega_{rel}). \tag{B.26}$$

Where the electrical angular frequencies of the d-axis and the rotor are defined as

$\omega_{\mathrm{del}} = \frac{\mathrm{d}\theta_{\mathrm{del}}}{\mathrm{dt}}$,

$\omega_{\mathrm{rel}} = \frac{\mathrm{d}\theta_{\mathrm{rel}}}{\mathrm{dt}}$. $\theta_{\mathrm{del}}, \theta_{\mathrm{rel}}$ are the angles shown in Figure 2.3, Chapter 2, page 32.

The rotor winding terminal voltage equation becomes

$$[v]_{\mathrm{rdq}} = -[\mathrm{R}]_{\mathrm{rdq}}[i]_{\mathrm{rdq}} - \frac{\mathrm{d}}{\mathrm{dt}}[\Psi]_{\mathrm{rdq}} - [\mathrm{T}]_{\mathrm{rw}}\Psi_{\mathrm{rdq}}. \tag{B.27}$$

By applying the derived transformation matrices to flux linkage equations in (B.10) and (B.20), it is obtained,

$$[\Psi]_{\mathrm{sdq}}^{|\mathrm{Vs}|} = [\mathrm{L}]_{\mathrm{ssdq}}^{|\frac{\mathrm{Vs}}{\mathrm{A}}|} * [i]_{\mathrm{sdq}}^{|\mathrm{A}|} + [\mathrm{L}]_{\mathrm{srdq}}^{|\frac{\mathrm{Vs}}{\mathrm{A}}|} * [i]_{\mathrm{rdq}}^{|\mathrm{A}|}, \tag{B.28}$$

$$[\Psi]_{\mathrm{rdq}}^{|\mathrm{Vs}|} = [\mathrm{L}]_{\mathrm{rsdq}}^{|\frac{\mathrm{Vs}}{\mathrm{A}}|} * [i]_{\mathrm{sdq}}^{|\mathrm{A}|} + [\mathrm{L}]_{\mathrm{rrdq}}^{|\frac{\mathrm{Vs}}{\mathrm{A}}|} * [i]_{\mathrm{rdq}}^{|\mathrm{A}|}. \tag{B.29}$$

Where

$$[\mathrm{R}]_{\mathrm{sdq}}^{|\Omega|} = \begin{bmatrix} \mathrm{R_s} & & \\ & \mathrm{R_s} & \\ & & \mathrm{R_s} \end{bmatrix}^{|\Omega|}, [\mathrm{R}]_{\mathrm{rdq}}^{|\Omega|} = \begin{bmatrix} \mathrm{R_r} & & \\ & \mathrm{R_r} & \\ & & \mathrm{R_r} \end{bmatrix}^{|\Omega|},$$

$$[\mathrm{T}]_{\mathrm{sw}}^{|\frac{1}{\mathrm{s}}|} = \begin{bmatrix} & -1 & \\ 1 & & \end{bmatrix}\omega_{\mathrm{del}}^{|\frac{1}{\mathrm{s}}|}, [\mathrm{T}]_{\mathrm{rw}}^{|\frac{1}{\mathrm{s}}|} = \begin{bmatrix} & -1 & \\ 1 & & \end{bmatrix}(\omega_{\mathrm{del}} - \omega_{\mathrm{rel}})^{|\frac{1}{\mathrm{s}}|},$$

$$[\mathrm{L}]_{\mathrm{ssdq}}^{|\frac{\mathrm{Vs}}{\mathrm{A}}|} = \begin{bmatrix} (\mathrm{L_{sl}} + 1.5\mathrm{L_{ssm}}) & & \\ & (\mathrm{L_{sl}} + 1.5\mathrm{L_{ssm}}) & \\ & & \mathrm{L_{sl}} \end{bmatrix}^{|\frac{\mathrm{Vs}}{\mathrm{A}}|},$$

$$[\mathrm{L}]_{\mathrm{rrdq}}^{|\frac{\mathrm{Vs}}{\mathrm{A}}|} = \begin{bmatrix} (\mathrm{L_{rl}} + 1.5\mathrm{L_{rrm}}) & & \\ & (\mathrm{L_{rl}} + 1.5\mathrm{L_{rrm}}) & \\ & & \mathrm{L_{rl}} \end{bmatrix}^{|\frac{\mathrm{Vs}}{\mathrm{A}}|},$$

$$[L]_{srdq}^{|\frac{Vs}{A}|} = \begin{bmatrix} -\frac{3}{2}L_{sr} & & \\ & -\frac{3}{2}L_{sr} & \\ & & 0 \end{bmatrix}^{|\frac{Vs}{A}|}, \quad [L]_{srdq}^{|\frac{Vs}{A}|} = [L]_{srdq}^{T|\frac{Vs}{A}|}.$$

It can be observed that the inductances obtained after the transformation are constant values.

B.3 Derivation of Windings Terminal Voltage and Flux Linkage Equations with Rotor Quantities Referred to the Stator

Rotor quantities on rotor dqo axes are referred to the stator dqo axes such to satisfy the following requirements:

a) The mmf of the new rotor currents referred to the stator must be the same as the actual mmf

b) The rotor's terminal instantaneous power to remain unchanged

c) The rotor's winding magnetic energy to remain the same

The new rotor quantities referred to the stator are temporarily marked with prime. On what follows are imposed the above requirements

a) $$\begin{bmatrix} N_{sd} & & \\ & N_{sq} & \\ & & 3N_{so} \end{bmatrix} \begin{bmatrix} i'_{rd} \\ i'_{rq} \\ i'_{ro} \end{bmatrix} = \begin{bmatrix} N_{rd} & & \\ & N_{rq} & \\ & & 3N_{ro} \end{bmatrix} \begin{bmatrix} i_{rd} \\ i_{rq} \\ i_{ro} \end{bmatrix}, \tag{B.30}$$

$$\begin{bmatrix} i'_{rd} \\ i'_{rq} \\ i'_{ro} \end{bmatrix} = \begin{bmatrix} \frac{N_{rd}}{N_{sd}} & & \\ & \frac{N_{rq}}{N_{sq}} & \\ & & \frac{N_{ro}}{N_{so}} \end{bmatrix} \begin{bmatrix} i_{rd} \\ i_{rq} \\ i_{ro} \end{bmatrix}, \tag{B.31}$$

$$[i]'_{rdq} = [T]_{Nsr}\,[i]_{rdq}, \tag{B.32}$$

$$[T]_{Nsr} = \begin{bmatrix} \frac{N_{rd}}{N_{sd}} & & \\ & \frac{N_{rq}}{N_{sq}} & \\ & & \frac{N_{ro}}{N_{so}} \end{bmatrix}. \tag{B.33}$$

b) $[v]'^{\mathrm{T}}_{\mathrm{rdq}}\,[i]'_{\mathrm{rdq}} = [v]^{\mathrm{T}}_{\mathrm{rdq}}\,[i]_{\mathrm{rdq}}$. (B.34)

With equations (B.32) and (B.34), it results

$[v]'^{\mathrm{T}}_{\mathrm{rdq}}[\mathrm{T}]_{\mathrm{Nsr}}\,[i]_{\mathrm{rdq}} = [v]^{\mathrm{T}}_{\mathrm{rdq}}\,[i]_{\mathrm{rdq}}$, (B.35)

$[v]'^{\mathrm{T}}_{\mathrm{rdq}} = [\mathrm{T}]^{-1}_{\mathrm{Nsr}}\,[v]_{\mathrm{rdq}}$. (B.36)

c) $\frac{1}{2}\,[\Psi]'^{\mathrm{T}}_{\mathrm{rdq}}[i]'_{\mathrm{rdq}} = \frac{1}{2}\,[\Psi]^{\mathrm{T}}_{\mathrm{rdq}}\,[i]_{\mathrm{rdq}}$, (B.37)

Similarly to condition b), it results as

$[\Psi]'_{\mathrm{rdq}} = [\mathrm{T}]^{-1}_{\mathrm{Nsr}}\,[\Psi]_{\mathrm{rdq}}$. (B.38)

Where $[\mathrm{T}]^{-1}_{\mathrm{Nsr}} = \begin{bmatrix} \frac{\mathrm{N_{sd}}}{\mathrm{N_{rd}}} & & \\ & \frac{\mathrm{N_{sq}}}{\mathrm{N_{rq}}} & \\ & & \frac{\mathrm{N_{so}}}{\mathrm{N_{ro}}} \end{bmatrix}$. (B.39)

For the new rotor quantities referred to the stator, the terminal voltage and flux linkage equations are defined on what follows:

Using equations (B.27) and (B.39), results as

$[\mathrm{T}]^{-1}_{\mathrm{Nsr}}\,[v]_{\mathrm{rdq}} = [\mathrm{T}]^{-1}_{\mathrm{Nsr}}\,[\mathrm{R}]_{\mathrm{rdq}}\,[\mathrm{T}]_{\mathrm{Nsr}}[i]'_{\mathrm{rdq}} + [\mathrm{T}]^{-1}_{\mathrm{Nsr}}\,[\mathrm{T}]_{\mathrm{rw}}[\mathrm{T}]_{\mathrm{Nsr}}\,[\Psi]'_{\mathrm{rdq}} +$

$[\mathrm{T}]^{-1}_{\mathrm{Nsr}}\,\frac{\mathrm{d}}{\mathrm{dt}}\,\{[\mathrm{T}]_{\mathrm{Nsr}}\}[\Psi]'_{\mathrm{rdq}}$. (B.40)

Where

$[\mathrm{R}]'_{\mathrm{rdq}} = \mathrm{R_r}\,[\mathrm{T}]^{-1}_{\mathrm{Nsr}}\,[1][\mathrm{T}]^{-1}_{\mathrm{Nsr}} = \mathrm{R_r}\,\{[\mathrm{T}]^{-1}_{\mathrm{Nsr}}\}^2 = \mathrm{R_r}\begin{bmatrix} \left(\frac{\mathrm{N_{sd}}}{\mathrm{N_{rd}}}\right)^2 & & \\ & \left(\frac{\mathrm{N_{sq}}}{\mathrm{N_{rq}}}\right)^2 & \\ & & \left(\frac{\mathrm{N_{so}}}{\mathrm{N_{ro}}}\right)^2 \end{bmatrix}$, (B.41)

$[\mathrm{T}]'_{\mathrm{rw}} = \begin{bmatrix} \frac{\mathrm{N_{sd}}}{\mathrm{N_{rd}}} & & \\ & \frac{\mathrm{N_{sq}}}{\mathrm{N_{rq}}} & \\ & & \frac{\mathrm{N_{so}}}{\mathrm{N_{ro}}} \end{bmatrix}\begin{bmatrix} 0 & -1 & 0 \\ 1 & 0 & 0 \\ 0 & 0 & 0 \end{bmatrix}\begin{bmatrix} \frac{\mathrm{N_{rd}}}{\mathrm{N_{sd}}} & & \\ & \frac{\mathrm{N_{rq}}}{\mathrm{N_{sq}}} & \\ & & \frac{\mathrm{N_{ro}}}{\mathrm{N_{so}}} \end{bmatrix}(\omega_{\mathrm{del}} - \omega_{\mathrm{rel}})$, and

$$= \begin{bmatrix} 0 & -\frac{N_{sd}N_{rq}}{N_{rd}N_{sq}} & 0 \\ \frac{N_{sd}N_{rd}}{N_{rq}N_{sd}} & 0 & 0 \\ 0 & 0 & 0 \end{bmatrix}. \quad \text{(B.42)}$$

Since $N_{sd} = N_{sq}$ and $N_{rd} = N_{rq}$, it results

$$[T]'_{rw} = \begin{bmatrix} 0 & -1 & 0 \\ 1 & 0 & 0 \\ 0 & 0 & 0 \end{bmatrix} (\omega_{del} - \omega_{rel}) = [T]_{rw}. \quad \text{(B.43)}$$

By using the set of equations (2.12), (B.40), (B.46) and (B.47), it results

$$[\Psi]_{sdq} = [L]_{ssdq}\,[i]_{sdq} + [L]_{srdq}\,[T]^{-1}_{Nsr}\,[i]'_{rdq}, \text{ and} \quad \text{(B.44)}$$

$$[T]^{-1}_{Nsr}\,[\Psi]_{rdq} = [T]^{-1}_{Nsr}\,[L]_{rsdq}[i]_{sdq} + [T]^{-1}_{Nsr}\,[L]_{rrdq}[T]^{-1}_{Nsr}\,[i]'_{rdq}. \quad \text{(B.45)}$$

Where

$$[L]'_{srdq} = [L]_{srdq}\,[T]^{-1}_{Nsr} = \begin{bmatrix} -\frac{3}{2}L_{sr} & & \\ & -\frac{3}{2}L_{sr} & \end{bmatrix} \begin{bmatrix} \frac{N_{sd}}{N_{rd}} & & \\ & \frac{N_{sq}}{N_{rq}} & \\ & & \frac{N_{so}}{N_{ro}} \end{bmatrix}$$

$$= \begin{bmatrix} -\frac{3}{2}\frac{N_{sd}}{N_{rd}}L_{sr} & & \\ & -\frac{3}{2}\frac{N_{sq}}{N_{rq}}L_{sr} & \\ & & 0 \end{bmatrix}, \quad \text{(B.46)}$$

$$[L]'_{rsdq} = [T]^{-1}_{Nsr}\,[L]_{rsdq} = \begin{bmatrix} \frac{N_{sd}}{N_{rd}} & & \\ & \frac{N_{sq}}{N_{rq}} & \\ & & \frac{N_{so}}{N_{ro}} \end{bmatrix} \begin{bmatrix} -\frac{3}{2}L_{sr} & & \\ & -\frac{3}{2}L_{sr} & \end{bmatrix}$$

$$= \begin{bmatrix} -\frac{3}{2}\frac{N_{sd}}{N_{rd}}L_{sr} & & \\ & -\frac{3}{2}\frac{N_{sq}}{N_{rq}}L_{sr} & \\ & & 0 \end{bmatrix}, \text{ and} \quad \text{(B.47)}$$

$$[L]'_{rrdq} = [T]^{-1}_{Nsr}\,[L]_{rrdq}\,[T]^{-1}_{Nsr}$$

$$= \begin{bmatrix} \left(\frac{N_{sd}}{N_{rd}}\right)^2 + (L_{rl} + 1.5L_{rrm}) & & \\ & \left(\frac{N_{sq}}{N_{rq}}\right)^2 + (L_{rl} + 1.5L_{rrm}) & \\ & & \left(\frac{N_{so}}{N_{ro}}\right)^2 L_{rl} \end{bmatrix}. \quad \text{(B.48)}$$

Finally, matricial form of the flux linkage equations with quantities on dqo reference frame and the rotor quantities referred to the stator are

$$[\Psi]_{sdq} = [L]_{ssdq}\,[i]_{sdq} + [L]'_{srdq}[i]'_{rdq}, \text{ and} \quad \text{(B.49)}$$

$$[\Psi]'_{rdq} = [L]'_{rsdq}[i]_{sdq} + [L]'_{rrdq}[i]'_{rdq}. \quad \text{(B.50)}$$

Comments

The rotor winding's leakage reactance referred to the stator with the ratio $\left(\frac{N_s}{N_r}\right)^2$, is not affected by the dqo transformation. This can be proved as shown below.

$$L_{sl} + 1.5L_{ssm} = N_s^2\,\mathcal{P}_{msl} + \frac{3}{2}N_s^2\mathcal{P}_{mm} = N_s^2\mathcal{P}_{msl} + \left(\sqrt{\frac{3}{2}}\,N_s\right)^2 \mathcal{P}_{mm}$$

$$= N_s^2\mathcal{P}_{msl} + N_{sd}^2\mathcal{P}_{mm}.$$

$$\text{So, } L_{sl} + 1.5L_{ssm} = (L_{sl} + L_m).$$

$$\frac{3}{2}\frac{N_{sd}}{N_{rd}}L_{sr} = \frac{3}{2}\frac{\sqrt{\frac{3}{2}}\,N_s}{\sqrt{\frac{3}{2}}\,N_r}\,N_s N_r \mathcal{P}_{mm} = \frac{3}{2}N_s^2\mathcal{P}_{mm} = \left(\sqrt{\frac{3}{2}}\,N_s\right)^2 \mathcal{P}_{mm} = N_{sd}^2\mathcal{P}_{mm} = L_m$$

$$\left(\frac{N_{sd}}{N_{rd}}\right)^2 + (L_{rl} + 1.5L_{rrm}) = \frac{N_s^2}{N_r^2}\left(N_r^2\mathcal{P}_{mrl} + \frac{3}{2}N_r^2\mathcal{P}_{mm}\right) = N_s^2\mathcal{P}_{mrl} + \frac{3}{2}N_s^2\mathcal{P}_{mm}$$

$$= (N_s^2\mathcal{P}_{mrl}) + \left(N_{sd}^2\mathcal{P}_{mm}\right) = L'_{rl} + L_m.$$

B.4 Detailed Derivation of Movement Equations

$$\sum p_{absorbed} = \frac{d}{dt}W_{internal}, \quad \text{(B.51)}$$

$$(p_{\mathrm{mec}} - \Delta p_{\mathrm{mec}}) + \left\{[v]_{\mathrm{rdq}}^{\mathrm{T}}[i]_{\mathrm{rdq}} - \Delta \mathrm{p}_{\mathrm{el.r}}\right\} + \left\{-[v]_{\mathrm{sdq}}^{\mathrm{T}} i_{\mathrm{sdq}} - \Delta \mathrm{p}_{\mathrm{el.s}}\right\} = \frac{\mathrm{dW_{magn}}}{\mathrm{dt}} + \frac{\mathrm{dW_{mec.internal}}}{\mathrm{dt}}. \quad \text{(B.52)}$$

With

$$[v]_{\mathrm{rdq}}^{\mathrm{T}}[i]_{\mathrm{rdq}} - \Delta \mathrm{p}_{\mathrm{el.r}} = [\Psi]_{\mathrm{rdq}}^{\mathrm{T}}[\mathrm{T}]_{\mathrm{rw}}^{\mathrm{T}}[i]_{\mathrm{rdq}} + \left\{\frac{\mathrm{d}}{\mathrm{dt}}[\Psi]_{\mathrm{rdq}}\right\}^{\mathrm{T}}[i]_{\mathrm{rdq}}, \quad \text{(B.53)}$$

$$-[v]_{\mathrm{sdq}}^{\mathrm{T}} i_{\mathrm{sdq}} - \Delta \mathrm{p}_{\mathrm{el.s}} = [\Psi]_{\mathrm{sdq}}^{\mathrm{T}}[\mathrm{T}]_{\mathrm{sw}}^{\mathrm{T}}[i]_{\mathrm{sdq}} + \left\{\frac{\mathrm{d}}{\mathrm{dt}}[\Psi]_{\mathrm{sdq}}\right\}^{\mathrm{T}}[i]_{\mathrm{sdq}}, \quad \text{(B.54)}$$

$$\frac{\mathrm{dW_{magn}}}{\mathrm{dt}} = \frac{1}{2}\left\{\left(\frac{\mathrm{d}}{\mathrm{dt}}[\Psi]_{\mathrm{sdq}}^{\mathrm{T}}\right)[i]_{\mathrm{sdq}} + [\Psi]_{\mathrm{sdq}}^{\mathrm{T}}\left(\frac{\mathrm{d}}{\mathrm{dt}}[i]_{\mathrm{sdq}}\right) + \left(\frac{\mathrm{d}}{\mathrm{dt}}[\Psi]_{\mathrm{rdq}}\right)[i]_{\mathrm{rdq}} + [\Psi]_{\mathrm{rdq}}^{\mathrm{T}}\left(\frac{\mathrm{d}}{\mathrm{dt}}[i]_{\mathrm{rdq}}\right)\right\}, \text{ and} \quad \text{(B.55)}$$

$$\frac{\mathrm{dW_{mec.internal}}}{\mathrm{dt}} = \mathrm{J}^{|\mathrm{Kgm^2}|}\omega_{\mathrm{r}}\frac{\mathrm{d}\omega_{\mathrm{r}}^{|\frac{\mathrm{geomtrad}}{\mathrm{s}}|}}{\mathrm{dt}^{|\mathrm{s}|}}. \quad \text{(B.56)}$$

Substituting the equations (B.51 – B.56) into equation (B.52) and rearranging, it results

$$(p_{\mathrm{mec}} - \Delta p_{\mathrm{mec}})^{|\mathrm{W}|} + [\Psi]_{\mathrm{sdq}}^{\mathrm{T}\,|\mathrm{Vs}|}[\mathrm{T}]_{\mathrm{sw}}^{\mathrm{T}}{}^{|\frac{1}{\mathrm{s}}|}[i]_{\mathrm{sdq}}{}^{|\mathrm{A}|} + [\Psi]_{\mathrm{rdq}}^{\mathrm{T}}[\mathrm{T}]_{\mathrm{rw}}^{\mathrm{T}}[i]_{\mathrm{rdq}} =$$

$$\mathrm{J}^{|\mathrm{Kgm^2}|}\omega_{\mathrm{r}}\frac{\mathrm{d}\omega_{\mathrm{r}}^{|\frac{\mathrm{geomtrad}}{\mathrm{s}}|}}{\mathrm{dt}^{|\mathrm{s}|}}.$$

Where

$$\mathrm{P}_{\mathrm{elm}}^{|\mathrm{W}|} = [\Psi]_{\mathrm{sdq}}^{\mathrm{T}\,|\mathrm{Vs}|}[\mathrm{T}]_{\mathrm{sw}}^{\mathrm{T}}{}^{|\frac{1}{\mathrm{s}}|}[i]_{\mathrm{sdq}}{}^{|\mathrm{A}|} + [\Psi]_{\mathrm{rdq}}^{\mathrm{T}}[\mathrm{T}]_{\mathrm{rw}}^{\mathrm{T}}[i]_{\mathrm{rdq}}.$$

Substituting the matrices on the right hand side of the above equation using the definitions in Section B.2, the equations of electromagnetic power and torque ($\mathrm{P_{elm}}$ and $\mathrm{T_{elm}}$) in actual units are obtained as

$$\mathrm{P}_{\mathrm{elm}}^{|\mathrm{W}|} = (1-\mathrm{s})\omega_{\mathrm{del}}^{|\frac{\mathrm{elrad}}{\mathrm{s}}|}\mathrm{L}_{\mathrm{m}}^{|\frac{\mathrm{Vs}}{\mathrm{A}}|}\left(i_{\mathrm{sd}}i'_{\mathrm{rq}} - i_{\mathrm{sq}}i'_{\mathrm{rd}}\right)^{|\mathrm{A}|^2}, \text{ and}$$

$$\mathrm{T}_{\mathrm{elm}}^{|\mathrm{Nm}|} = \frac{(1-\mathrm{s})\omega_{\mathrm{del}}^{|\frac{\mathrm{elrad}}{\mathrm{s}}|}}{\omega_{\mathrm{r}}^{|\frac{\mathrm{geomrad}}{\mathrm{s}}|}}\mathrm{L}_{\mathrm{m}}^{|\frac{\mathrm{Vs}}{\mathrm{A}}|}\left(i_{\mathrm{sd}}i'_{\mathrm{rq}} - i_{\mathrm{sq}}i'_{\mathrm{rd}}\right)^{|\mathrm{A}|^2}.$$

Above equations are converted to |rpu| according to Section 2.3.6, Chapter 2, page 36 and are defined as below,

$$P_{elm}^{|rpu|} = (1 - s)\, \omega_{del}{}^{|rpu|}\, L_m^{|rpu|} \left(i_{sd}^{|rpu|}\, i_{rq}^{|rpu|} - i_{sq}^{|rpu|}\, i_{rd}^{|rpu|} \right), \text{ and}$$

$$T_{elm}^{|rpu|} = (1 - s) \frac{\omega_{del}{}^{|rpu|}}{\omega_r{}^{|rpu|}}\, L_m^{|rpu|} \left(i_{sd}^{|rpu|}\, i_{rq}^{|rpu|} - i_{sq}^{|rpu|}\, i_{rd}^{|rpu|} \right).$$

APPENDIX C

BACK-to-BACK CONVERTER MODEL DERIVATIONS

Detailed Explanation of the Matricial Equations

The expansion of the matricial equations of the rectifier and inverter of the back-back converter (4.1 – 4.4) on Chapter 4, Section 4.1.1, page 67 are as follows:

$$v_{ga} = R_{grec} i_{oa} + L_{grec} \frac{di_{oa}}{dt} + v_{oa}, \tag{C.1}$$

$$v_{gb} = R_{grec} i_{ob} + L_{grec} \frac{di_{ob}}{dt} + v_{ob}, \tag{C.2}$$

$$v_{gc} = R_{grec} i_{oc} + L_{grec} \frac{di_{oc}}{dt} + v_{oc}. \tag{C.3}$$

This can be combined as

$$\begin{bmatrix} v_{ga} \\ v_{gb} \\ v_{gc} \end{bmatrix} = \begin{bmatrix} R_{grec} & & \\ & R_{grec} & \\ & & R_{grec} \end{bmatrix} \begin{bmatrix} i_{oa} \\ i_{ob} \\ i_{oc} \end{bmatrix} + \begin{bmatrix} L_{grec} & & \\ & L_{grec} & \\ & & L_{grec} \end{bmatrix} \begin{bmatrix} \frac{di_{oa}}{dt} \\ \frac{di_{ob}}{dt} \\ \frac{di_{oc}}{dt} \end{bmatrix} + \begin{bmatrix} v_{oa} \\ v_{ob} \\ v_{oc} \end{bmatrix}, \tag{C.4}$$

where

$$\begin{bmatrix} v_{oa} \\ v_{ob} \\ v_{oc} \end{bmatrix} = \begin{bmatrix} \frac{1}{2} A_{mo} v_{dc} \sin(\omega_0 t + \alpha_0) \\ \frac{1}{2} A_{mo} v_{dc} \sin\left(\omega_0 t + \alpha_0 - \frac{2\pi}{3}\right) \\ \frac{1}{2} A_{mo} v_{dc} \sin\left(\omega_0 t + \alpha_0 + \frac{2\pi}{3}\right) \end{bmatrix}, \tag{C.5}$$

$$v_{ra} = -R_{rinv} i_{ia} - L_{rinv} \frac{di_{ia}}{dt} + v_{ia}, \tag{C.6}$$

$$v_{rb} = -R_{rinv} i_{ib} - L_{rinv} \frac{di_{ib}}{dt} + v_{ib}, \tag{C.7}$$

$$v_{rc} = -R_{rinv} i_{ic} - L_{rinv} \frac{di_{ic}}{dt} + v_{ic}, \tag{C.8}$$

$$\begin{bmatrix} v_{ra} \\ v_{rb} \\ v_{rc} \end{bmatrix} = \begin{bmatrix} -R_{rinv} & & \\ & -R_{rinv} & \\ & & -R_{rinv} \end{bmatrix} \begin{bmatrix} i_{ia} \\ i_{ib} \\ i_{ic} \end{bmatrix} + \begin{bmatrix} -L_{rinv} & & \\ & -L_{rinv} & \\ & & -L_{rinv} \end{bmatrix} \begin{bmatrix} \frac{di_{ia}}{dt} \\ \frac{di_{ib}}{dt} \\ \frac{di_{ic}}{dt} \end{bmatrix} + \begin{bmatrix} v_{ia} \\ v_{ib} \\ v_{ic} \end{bmatrix}. \tag{C.9}$$

Where

$$\begin{bmatrix} v_{ia} \\ v_{ib} \\ v_{ic} \end{bmatrix} = \begin{bmatrix} \frac{1}{2} A_{mi} v_{dc} \sin(\omega_i t + \alpha_i) \\ \frac{1}{2} A_{mi} v_{dc} \sin\left(\omega_i t + \alpha_i - \frac{2\pi}{3}\right) \\ \frac{1}{2} A_{mi} v_{dc} \sin\left(\omega_i t + \alpha_i + \frac{2\pi}{3}\right) \end{bmatrix}. \quad \text{(C.10)}$$

The voltage across the dc-link capacitor as explained in Chapter 4, Section 4.1.2 on page 68

$$C \frac{dv_{dc}}{dt} = (S_1 i_{oa} + S_2 i_{ob} + S_3 i_{oc}) - (S_4 i_{ia} + S_5 i_{ib} + S_6 i_{ic}). \quad \text{(C.11)}$$

Where $S_1, S_2, S_3, S_4, S_5, S_6$ symbolically describe the converters switching states.

Derivation of the Back-to-Back Converter Equations in dqo Reference Frame

Grid-Side Converter Equations

The Transformation matrices $[T]_{grecv}$, $[T]_{greci}$ are defined such that

$$[T]_{grecv} \begin{bmatrix} v_{ga} \\ v_{gb} \\ v_{gc} \end{bmatrix} = \begin{bmatrix} v_{gd} \\ v_{gq} \\ v_{go} \end{bmatrix}, \quad \text{(C.12)}$$

$$[T]_{grecv} \begin{bmatrix} v_{oa} \\ v_{ob} \\ v_{oc} \end{bmatrix} = \begin{bmatrix} v_{od} \\ v_{oq} \\ v_{oo} \end{bmatrix}, \quad \text{(C.13)}$$

And $[T]_{greci} \begin{bmatrix} i_{oa} \\ i_{ob} \\ i_{oc} \end{bmatrix} = \begin{bmatrix} i_{0d} \\ i_{oq} \\ i_{oo} \end{bmatrix}$. (C.14)

Taking into consideration for the model to be conservative, and applying the conditions mentioned in APPENDIX B, the transformation matrix results as

$$[T]_{grecv} = [T]_{greci} = [T]_{grec},$$

$$[T]_{grec} = \sqrt{\frac{2}{3}} * \begin{bmatrix} \cos(\theta_{drec}) & \cos(\theta_{drec} - 120^0) & \cos(\theta_{drec} - 240^0) \\ -\sin(\theta_{drec}) & -\sin(\theta_{drec} - 120^0) & -\sin(\theta_{drec} - 240^0) \\ \frac{1}{\sqrt{2}} & \frac{1}{\sqrt{2}} & \frac{1}{\sqrt{2}} \end{bmatrix}, \quad \text{(C.15)}$$

where

$$\theta_{drec} = \int \omega_{drec} + \alpha_{drec}. \tag{C.16}$$

Using equations (C12-C.16) it results

$$[T]_{grec}^{-1}\begin{bmatrix} v_{gd} \\ v_{gq} \\ v_{go} \end{bmatrix} =$$

$$\begin{bmatrix} R_{grec} & & \\ & R_{grec} & \\ & & R_{grec} \end{bmatrix}[T]_{grec}^{-1}\begin{bmatrix} i_{od} \\ i_{oq} \\ i_{oo} \end{bmatrix} +$$

$$\begin{bmatrix} L_{grec} & & \\ & L_{grec} & \\ & & L_{grec} \end{bmatrix}\frac{d}{dt}\left([T]_{grec}^{-1}\begin{bmatrix} i_{od} \\ i_{oq} \\ i_{oo} \end{bmatrix}\right)[T]_{grec}^{-1}\begin{bmatrix} v_{od} \\ v_{oq} \\ v_{oo} \end{bmatrix}, \tag{C.17}$$

where

$$\frac{d}{dt}\left([T]_{grec}^{-1}\begin{bmatrix} i_{od} \\ i_{oq} \\ i_{oo} \end{bmatrix}\right) = [T]_{grec}^{-1}\begin{bmatrix} \frac{di_{od}}{dt} \\ \frac{di_{oq}}{dt} \\ \frac{di_{oo}}{dt} \end{bmatrix} + [T]_{grec}\frac{d}{dt}\left([T]_{grec}^{-1}\right). \tag{C.18}$$

Considering $[T]_{grec}\frac{d}{dt}\left([T]_{grec}^{-1}\right) = \omega_{drec}\begin{bmatrix} & -1 & \\ 1 & & \\ & & \end{bmatrix}$ in equation (C.18) and substituting it in equation (C.17), the equation (4.5) shown on page 68, Section 4.1.2, Chapter 4, results as

$$\begin{bmatrix} v_{gd} \\ v_{gq} \\ v_{go} \end{bmatrix} = \begin{bmatrix} R_{grec} & & \\ & R_{grec} & \\ & & R_{grec} \end{bmatrix}\begin{bmatrix} i_{od} \\ i_{oq} \\ i_{oo} \end{bmatrix} + \begin{bmatrix} L_{grec} & & \\ & L_{grec} & \\ & & L_{grec} \end{bmatrix}\begin{bmatrix} \frac{di_{od}}{dt} \\ \frac{di_{oq}}{dt} \\ \frac{di_{oo}}{dt} \end{bmatrix} +$$

$$\begin{bmatrix} & -L_{grec}\omega_{drec} & \\ L_{grec}\omega_{drec} & & \\ & & \end{bmatrix}\begin{bmatrix} i_{od} \\ i_{oq} \\ i_{oo} \end{bmatrix} + \begin{bmatrix} v_{od} \\ v_{oq} \\ v_{oo} \end{bmatrix}. \tag{C.19}$$

Rotor-Side Converter Equations

The Transformation matrices $[T]_{rinvv}$, $[T]_{rinvi}$ are defined such that

$$[T]_{rinvv}\begin{bmatrix} v_{ra} \\ v_{rb} \\ v_{rc} \end{bmatrix} = \begin{bmatrix} v_{rd} \\ v_{rq} \\ v_{ro} \end{bmatrix}, \tag{C.20}$$

$$[T]_{rinvi}\begin{bmatrix} i_{ia} \\ i_{ib} \\ i_{ic} \end{bmatrix} = \begin{bmatrix} i_{id} \\ i_{iq} \\ i_{io} \end{bmatrix}, \tag{C.21}$$

$$[T]_{rinvv}\begin{bmatrix} v_{ia} \\ v_{ib} \\ v_{ic} \end{bmatrix} = \begin{bmatrix} v_{id} \\ v_{iq} \\ v_{io} \end{bmatrix}. \tag{C.22}$$

Taking into consideration for the model to be conservative, and by applying the conditions mentioned in APPENDIX B, the transformation matrix result as

$$[T]_{rinvv} = [T]_{rinvi} = [T]_{rinv},$$

$$[T]_{rinv} = \sqrt{\frac{2}{3}} * \begin{bmatrix} \cos(\theta_{dinv}) & \cos(\theta_{dinv} - 120^0) & \cos(\theta_{dinv} - 240^0) \\ -\sin(\theta_{dinv}) & -\sin(\theta_{dinv} - 120^0) & -\sin(\theta_{dinv} - 240^0) \\ \frac{1}{\sqrt{2}} & \frac{1}{\sqrt{2}} & \frac{1}{\sqrt{2}} \end{bmatrix}, \tag{C.23}$$

$$\theta_{dinv} = \int \omega_{dinv} + \alpha_{dinv}. \tag{C.24}$$

Hence,

$$[T]_{rinv}^{-1}\begin{bmatrix} v_{rd} \\ v_{rq} \\ v_{ro} \end{bmatrix} =$$

$$\begin{bmatrix} -R_{rinv} & & \\ & -R_{rinv} & \\ & & -R_{rinv} \end{bmatrix}[T]_{rinv}^{-1}\begin{bmatrix} i_{id} \\ i_{iq} \\ i_{io} \end{bmatrix} +$$

$$\begin{bmatrix} -L_{rinv} & & \\ & -L_{rinv} & \\ & & -L_{rinv} \end{bmatrix}\frac{d}{dt}\left([T]_{rinv}^{-1}\begin{bmatrix} i_{id} \\ i_{iq} \\ i_{io} \end{bmatrix}\right) + [T]_{rinv}^{-1}\begin{bmatrix} v_{id} \\ v_{iq} \\ v_{io} \end{bmatrix}, \tag{C.25}$$

$$\text{and } \frac{\mathrm{d}}{\mathrm{dt}}\left([\mathrm{T}]_{\mathrm{rinv}}^{-1}\begin{bmatrix} i_{\mathrm{id}} \\ i_{\mathrm{iq}} \\ i_{\mathrm{io}} \end{bmatrix}\right) = [\mathrm{T}]_{\mathrm{rinv}}^{-1}\begin{bmatrix} \frac{\mathrm{d}i_{\mathrm{id}}}{\mathrm{dt}} \\ \frac{\mathrm{d}i_{\mathrm{iq}}}{\mathrm{dt}} \\ \frac{\mathrm{d}i_{\mathrm{io}}}{\mathrm{dt}} \end{bmatrix} + [\mathrm{T}]_{\mathrm{rinv}}\begin{bmatrix} i_{\mathrm{id}} \\ i_{\mathrm{iq}} \\ i_{\mathrm{io}} \end{bmatrix}\frac{\mathrm{d}}{\mathrm{dt}}([\mathrm{T}]_{\mathrm{rinv}}^{-1}). \quad \text{(C.26)}$$

With $[\mathrm{T}]_{\mathrm{rinv}}\frac{\mathrm{d}}{\mathrm{dt}}([\mathrm{T}]_{\mathrm{rinv}}^{-1}) = \omega_{\mathrm{dinv}}\begin{bmatrix} & -1 & \\ 1 & & \end{bmatrix}$ in equation (C.26) and substituting in equation (C.25) explanation of the equation (4.6), shown on page 68, Section 4.1.12, Chapter 4, results as

$$\begin{bmatrix} v_{\mathrm{rd}} \\ v_{\mathrm{rq}} \\ v_{\mathrm{ro}} \end{bmatrix} =$$

$$-\begin{bmatrix} \mathrm{R}_{\mathrm{rinv}} & & \\ & \mathrm{R}_{\mathrm{rinv}} & \\ & & \mathrm{R}_{\mathrm{rinv}} \end{bmatrix}\begin{bmatrix} i_{\mathrm{id}} \\ i_{\mathrm{iq}} \\ i_{\mathrm{io}} \end{bmatrix} - \begin{bmatrix} \mathrm{L}_{\mathrm{rinv}} & & \\ & \mathrm{L}_{\mathrm{rinv}} & \\ & & \mathrm{L}_{\mathrm{rinv}} \end{bmatrix}\begin{bmatrix} \frac{\mathrm{d}i_{\mathrm{id}}}{\mathrm{dt}} \\ \frac{\mathrm{d}i_{\mathrm{iq}}}{\mathrm{dt}} \\ \frac{\mathrm{d}i_{\mathrm{io}}}{\mathrm{dt}} \end{bmatrix} -$$

$$\begin{bmatrix} & -\mathrm{L}_{\mathrm{rinv}}\omega_{\mathrm{dinv}} & \\ \mathrm{L}_{\mathrm{rinv}}\omega_{\mathrm{dinv}} & & \end{bmatrix}\begin{bmatrix} i_{\mathrm{id}} \\ i_{\mathrm{iq}} \\ i_{\mathrm{io}} \end{bmatrix} + \begin{bmatrix} v_{\mathrm{id}} \\ v_{\mathrm{iq}} \\ v_{\mathrm{io}} \end{bmatrix}. \quad \text{(C.27)}$$

DC-Link Capacitor

As stated on [30], the dc-link voltage across the capacitor in dqo reference frame results as

$$\mathrm{S}_1 i_{\mathrm{oa}} + \mathrm{S}_2 i_{\mathrm{ob}} + \mathrm{S}_3 i_{\mathrm{oc}} = \frac{3}{4}\mathrm{A}_{\mathrm{mo}}\left(i_{\mathrm{od}}\cos(\alpha_{\mathrm{mo}} - \alpha_{\mathrm{drec}}) + i_{\mathrm{oq}}\sin(\alpha_{\mathrm{mo}} - \alpha_{\mathrm{drec}})\right), \quad \text{(C.28)}$$

$$\mathrm{S}_4 i_{\mathrm{ia}} + \mathrm{S}_5 i_{\mathrm{ib}} + \mathrm{S}_6 i_{\mathrm{ic}} = \frac{3}{4}\mathrm{A}_{\mathrm{mi}}\left(i_{\mathrm{id}}\cos(\alpha_{\mathrm{mi}} - \alpha_{\mathrm{dinv}}) + i_{\mathrm{iq}}\sin(\alpha_{\mathrm{mi}} - \alpha_{\mathrm{dinv}})\right), \quad \text{(C.29)}$$

$$\mathrm{C}\frac{\mathrm{d}v_{\mathrm{dc}}}{\mathrm{dt}} = (\mathrm{S}_1 i_{\mathrm{oa}} + \mathrm{S}_2 i_{\mathrm{ob}} + \mathrm{S}_3 i_{\mathrm{oc}}) - (\mathrm{S}_4 i_{\mathrm{ia}} + \mathrm{S}_5 i_{\mathrm{ib}} + \mathrm{S}_6 i_{\mathrm{ic}}). \quad \text{(C.30)}$$

APPENDIX D

Range of Values attained by DFIG Variables

Table D.1. Range of Values Attained by the DFIG Variables

Pdelbys Qdelbys	Is	Ir	slip	Vr	Phivr	Pabsbyr	Qabsbr	Pdeltot	Qdeltot
Pdedbys>0 Qdelbys>0	Is< 1 For s < 0.75	Sim to Is 0.40 2.38	-0.2	0.2092 -- 0.2611	-178.5 -164.8	-0.2898 -0.00613	-0.5558 -0.08216	0.1061 1.7777	0.1822 2.0561
			-0.1	0.1022 0.1298	-177.8 -163.7	-0.1373 0.005236	-0.2779 -0.04108	0.09476 1.624	0.1411 1.778
			0	0.002016 0.01189	-86.87 -14.38	0.001264 0.02829	10^{-18}	0.08339 1.472	Qdelbys
			0.1	0.1053 0.1394	-3.619 12.35	0.0134 0.181	0.04108 0.2779	0.07202 1.323	0.01747 1.264
			0.2	0.2102 0.2725	-1.627 13.26	0.2914 0.3338	0.08216 0.5558	0.0605 1.176	-0.06505 1.027
Pdedbys>0 Qdelbys<0	Inc with mag 0.141 2.12	Less mag 0.10 1.97	-0.2	0.1519 0.2041	-178.9 -164.4	-0.2908 -0.01582	-0.1209 -0.0789	0.115 1.791	-1.689 0.02093
			-0.1	0.07267 0.1008	-178.4 -163.6	-0.1395 -0.003583	-0.06987 0.09447	0.1092 1.639	-1.594 -0.03954
			0	0.000521 2 0.009	0.591 85.13	0.0002252 0.01947	10^{-18}	0.997 1.488	Qdelbys
			0.1	0.07724 0.1128	0.5194 21.86	0.1024 0.1695	-0.09447 0.06046	0.08976 1.337	-1.447 -0.119
			0.2	0.1534 0.2184	0.7831 20.9	0.02025 0.3228	-0.1889 0.1209	0.0777 1.185	-1.394 -0.138
Pdedbys<0 Qdelbys>0	0.141 2.12	0.40 2.38	-0.2	0.2099 0.2695	170.1 179.9	0.02292 0.3228	-0.5536 -0.08201	-1.823 -0.1339	0.1082 2.054
			-0.1	0.1034 0.1378	172.2 179.8	0.01176 0.1755	-0.2768 -0.04101	-1.676 -0.1252	0.141 1.777
			0	0.002015 0.0118	-165.24 -93.29	0.0008122 0.02828	10^{-18}	-1.528 -0.1115	Qdelbys
			0.1	0.1004 0.1298	-16.92 -2.09	-0.1357 0.0797	0.04101 0.2768	-1.381 -0.108	0.01855 1.264
			0.2	0.2076 0.2594	-15.48 -1.695	-0.2637 -0.000651	0.08201 0.5536	-1.234 -0.08569	-0.06289 1.027
Pdedbys<0 Qdelbys<0	0.141 2.12	0.10 1.97	-0.2	0.1528 0.2147	159.8 179.3	0.0202 0.3140	-0.1188 0.1891	-1.809 -0.1202	-1.689 0.01877
			-0.1	0.07689 0.1111	158.8 179.5	0.0102 0.1667	-0.05938 0.09454	-1.664 -0.1102	-1.595 -0.04062
			0	0.000516 0.009864	179.2 95.49	0.00022 0.019	10^{-18}	-1.512 -0.1002	Qdelbys
			0.1	0.07035 0.1006	-16.66 4.062	-0.1367 -0.000842	-0.01891 0.05938	-1.363 -0.0924	-1.446 -0.1189
			0.2	0.1498 0.2018	-17.77 1.704	-0.2854 -0.00947	-0.1891 0.1188	-1.221 -0.08025	-1.392 -0.1379

Where

Is, Ir represent magnitude of phase currents through the DFIG stator and rotor windings respectively, and Vr is the magnitude of voltage across the DFIG rotor windings.

APPENDIX E

MATLAB/SIMULINK Block Parameters

Transmission Line Block

The transmission line block represented in Figure 6.2 is a π-equivalent circuit for transmission line of 30 |km|. The parameters of the block are as below,

Positive sequence resistance in Ohms/km	0.2145 |Ω/km	
Positive sequence inductance in H/km	0.0018067 |H/km	
Positive sequence capacitance in F/km	$3.399*10^{-7}$ |F/km	

Transformer at the DFIG Wind Turbine

Configuration	Delta, Yg
Nominal power and frequency [Sn(VA),fn(Hz)]	3*3.16e^6 |VA|, 60 |Hz|
Winding 1 parameters [V1, R1(pu), L1(pu)]	25e3 |V|, 0.025/30 |pu|, 0.025|pu|
Winding 2 parameters [V2, R2(pu), L2(pu)]	1000 |V|, 0.025/30 |pu|, 0.025 |pu|
Magnetization resistance Rm(pu)	500 |pu|
Magnetization inductance Lm(pu)	inf

Transformer at the Grid

Configuration	Yg, Delta
Nominal power and frequency [Sn(VA),fn(Hz)]	47e^6 |VA|, 60 |Hz|
Winding 1 parameters [V1,R1(pu), L1(pu)]	120e^3 |V|, 0.08/30 |pu|, 0.08 |pu|
Winding 2 parameters [V2, R2(pu), L2(pu)]	25e^3 |V|, 0.08/30 |pu|, 0.08 |pu|
Magnetization resistance Rm(pu)	500 |pu|
Magnetization inductance Lm(pu)	500 |pu|

DFIG Wind Turbine

Generator data for 1 wind turbine

Nom. power, L-L volt.[Pn (VA), Vs_nom, Vr_nom]	3e6|VA| 1000|V| 400|V|
Frequency fn (Hz)	60|Hz|
Stator [Rs,Lls] (p.u.)	0.006067|pu|,0.07034|pu|
Rotor [Rr', Llr'] (p.u.)	0.005 |pu|, 0.1034|pu|
Magnetization inductance Lm (p.u.)	3.4734 |pu|
Inertia constant, friction factor, and pairs of poles [H(s) F(p.u.) p]	1.35|s|, 0.01|pu|, 2
Initial conditions [s th ias ibs ics phaseas phasebs phasecs]	[0.0233,0 0,0,0 0,0,0]

Converters data for 1 wind turbine

Grid-side converter maximum current (pu of generator nominal current)	0.3 |pu|
Nominal DC bus voltage (V)	1,680 |V|
DC bus capacitor (F)	10000e^-6|F|
Line filter capacitor (Q=50) (var)	120e^3 |V|

Turbine data for 1 wind turbine

Nominal mechanical output power (W)	3e^6 |VA|
Wind speed at nominal speed and at Cp max (between 6 m/s and 30 m/s)	15|m/s|
Initial wind speed (m/s)	15|m/s|

Drive train data for 1 wind turbine

Wind turbine inertia constant H (s)	6.32|s|
Shaft spring constant refer to high-speed shaft (pu of nominal mechanical torque/rad)	1.11
Shaft mutual damping (pu of nominal mechanical torque/pu dw)	1.5

Turbine initial speed (pu of nominal speed	1|pu|
Initial output torque (pu of nominal mechanical torque)	1|pu|

Control parameters for 1 wind turbine

DC bus voltage regulator gains $[K_{pvdc}, K_{ivdc}]$	[8, 400]
Grid-side converter current regulator $[K_{pgsc}, K_{igsc}]$	[0.83, 5]
Speed regulator gains $[K_{pspeed}, K_{ispeed}]$	[3, 0.6]
Rotor-side converter current regulator gains $[K_{prsc}, K_{irsc}]$	[0.6, 8]
Var regulator gains $[K_{pQ}, K_{iQ}]$	[5, 0.1]
Pitch angle gain [Kp]	[150]
Active power compensation $[K_{pcomp}, K_{icomp}]$	[3, 30]